Protein markers of inflammation and ageing in a European multi-centre dementia cohort

Doctoral thesis

to obtain a doctorate (PhD)

from the Faculty of Medicine

of the University of Bonn

Kishore Aravind Ravichandran

from Chennai, India

2024

Written with authorization of

the Faculty of Medicine of the University of Bonn

First reviewer: Prof. Dr. Michael T. Heneka

Second reviewer: Prof. Dr. Michael Pankratz

Day of oral examination: 21.02.2024

For the Institute of Innate Immunity

Director: Prof. Dr. Eicke Latz

என் முத்துராமன் ஐயாவுக்கு...

To my grandfather Muthuraman…

Table of Contents

List of abbreviations

A+	Amyloid pathology positive
AD	Alzheimer's disease
AIM2	Absent in melanoma-2
APOE4	Apolipoprotein E4
APP	Amyloid precursor protein
ASC	Apoptosis-associated speck-like protein
ATP	Adenosine triphosphate
AxlOE	Axl-overexpressing human THP-1 cells
Aβ	Amyloid β (1-42)
BCA	Bicinchoninic acid assay
BMI	Body mass index
BSA	Bovine serum albumin
C/EBP	CCAAT/enhancer-binding proteins
C1q; C3; C4	Complement components 1q; 3; 4
CARD	Caspase activation and recruitment domain
cDNA	Complementary Deoxyribonucleic acid
CMV	Cytomegalovirus
CN	Healthy controls
CRP	C-Reactive protein
CSF	Cerebrospinal fluid
DAMP	Damage-associated molecular patterns
DAT	Dementia of Alzheimer's type
Gas6	TAM ligand: Growth arrest specific 6
h	Hour(s)
HRP	Horseradish peroxide
ICAM1	Intercellular adhesion molecule 1
IFNAR	Interferon Alpha And Beta Receptor Subunit 1
IL	Interleukin
JAK1	Janus kinase-1
JPND	Joint-programme Neurodegenerative disease research

LPS	Lipopolysaccharide from Escherichia coli K12
MAPT	Microtubule-associated protein tau
MCI	Mild cognitive impairment
MerTK	TAM receptor
MIF	Macrophage migration inhibitory factor
min	Minute(s)
mRNA	Messenger ribonucleic acid
NFT	Neurofibrillary tau tangles
NF-κB	Nuclear factor kappa -chain-enhancer of activated B cells
Nig	Nigericin
NLR	Nod-like receptors
NLRC4	NLR family CARD-domain containing 4
NLRP3	NLR family pyrin domain containing 3
NPX	Normalized Protein eXpression
PAMP	Pathogen-associated molecular patterns
PBS	Phosphate-buffered saline
PBS-TX	Phosphate-buffered saline + 0.01% Triton®-X 100
PET	Positron emission tomography
PKA	Protein kinase A
PLL	Poly-L-lysine hydrobromide
PMA	Phorbol 12-myristate 13-acetate
PREADAPT	JPND-EU-funded project supporting this thesis
PRR	Pattern recognition receptors
PSEN1	Presenilin-1
QC	Quality control
RNA	Ribonucleic acid
RT	Room temperature
RT-PCR	Reverse transcription polymerase chain reaction
Rux	Ruxolitinib
SCD	Subjective cognitive decline
SFM	Serum free medium
SOCS1	Suppressor Of Cytokine Signaling 1

STAT1	Signal transducer and activator of transcription 1
T+	Tau pathology positive
TAM	Tyro3, Axl, MerTK receptors
TBST	Tris-buffered saline + Tween 20
TLR	Toll-like receptor
TNFR1	Tumor necrosis factor receptor 1
TNFR2	Tumor necrosis factor receptor 2
TREM2	Triggering-Receptor expressed on myeloid cells 2
Tyro3OE	Tyro3-overexpressing human THP-1 cells
VCAM1	Vascular cell adhesion molecule 1 (CD106)
WT	Wild-type control human THP-1 cells
YKL-40	Chitinase-3-Like Protein 1

1. Introduction

1.1. Alzheimer's disease and Neuroinflammation

1.1.1. Alzheimer's disease

Alzheimer's disease (AD) is the predominant cause of dementia where individuals suffer from impaired memory and cognition (Knopman et al., 2021). As much as 22% of the 1.9 billion individuals aged 50 and above worldwide are estimated with having early, mid-, and late stages of AD (Gustavsson et al., 2023). With a constantly increasing aging population, these estimates emphasize the upcoming gigantic burden on the economy and healthcare system for addressing AD. The key hallmarks of this disease are the formation of endogenous and peptide-based aggregates called Amyloid-β ($A\beta_{42}$) plaques and neurofibrillary Tau tangles (NFTs) in the brains of AD patients. The diagnosis and confirmation of AD rely on $A\beta_{42}$ and tau levels in the brain and body fluids that mark the aftermath of significant neurodegeneration (Hanslik and Ulland, 2020). Specifically, these proteins are measured through biochemical analyses and positron emission tomography (PET) imaging on the cerebrospinal fluid and brain as an indicative of the AD staging (Knopman et al., 2021). Although $A\beta_{42}$ and tau are excellent biomarkers in diagnosing AD, their upstream and downstream mechanisms in AD are not fully understood.

Currently, the origin of AD is proposed to propagate through $A\beta_{42}$ and tau. The Amyloid cascade proposes that functionally altered enzymes β-secretase-1 and γ-secretase cleave amyloid precursor protein (*APP*) leading to the release of insoluble $A\beta_{42}$ peptides (Heneka et al., 2015; Müller et al., 2017). These insoluble $A\beta_{42}$ peptides are hydrophobic and attain stability through aggregation that results in $A\beta_{42}$ plaque formation in the brain. Mutations in the amyloid precursor protein (*APP*) gene and the γ-secretase subunit Presenelin-1 (*PSEN1*) gene are two of the many genes that are associated with high AD risk and these two mutations promote excessive $A\beta_{42}$ generation and plaque formation (Figure 1).

In the case of NFTs, mutations and excessive phosphorylation of the microtubule-associated protein tau (*MAPT*) leads to the formation of NFTs within the neurons. The majority of cell-signaling cascade relies on the activation of phosphorylating kinases like

protein kinase A (PKA), CamKII-α, and GSK3-β which are proposed to involve in tau hyperphosphorylation (Barbier et al., 2019; Ising et al., 2019). When hyperphosphorylated, tau undergoes a conformational change that leads to its dissociation from the microtubules and subsequent aggregation to form NFTs within the neurons (Xia et al., 2020). Hence, the presence of NFTs indicates an unstable neuronal cytoskeleton which decreases neuronal functioning and results in the death of the neuron. It is suggested that both $A\beta_{42}$ and tau hypotheses coexist and act synergistically in a feedback loop that worsens AD progression (Busche and Hyman, 2020). The propagation of AD pathology by $A\beta_{42}$ and tau is significantly worsened by the involvement of the CNS immune cells, microglia, which spread neuroinflammation in the brain (Chen et al., 2016; Felsky et al., 2019; Hughes et al., 2020; Leng and Edison, 2021) (**Figure 1**).

Neuroinflammation is the inflammatory process initiated by the innate immune cells of the CNS that results in the release of pro-inflammatory cytokines like IL-1β, IL-6, IL-18, and other detrimental factors (Leng and Edison, 2021). The predominant innate immune cells involved in neuroinflammation are microglia and astrocytes, but also other cells like endothelial cells and peripheral blood cells that enter the brain contribute to the inflammation. Like peripheral inflammation, neuroinflammation is a defense mechanism by the body to protect the cells within the brain against a threat (Broz and Dixit, 2016; Latz et al., 2013). In particular, the immune cells react to $A\beta_{42}$ plaques and NFTs and activate the inflammasome which is a critical function of the innate defense mechanism (X. He et al., 2020). Here, the immune cells undergo a two-step process to achieve a supra-molecular inflammasome assembly that activates executioner proteases resulting in the afore-mentioned pro-inflammatory response. Inflammasome activation is documented in AD patient brains where it facilitates a vicious loop of pro-inflammatory responses in chronically activated microglia that worsens the AD progression (Halle et al., 2008; Heneka et al., 2013). There is an urgent need to understand and devise therapeutic strategies that address inflammasome-mediated neuroinflammation in AD.

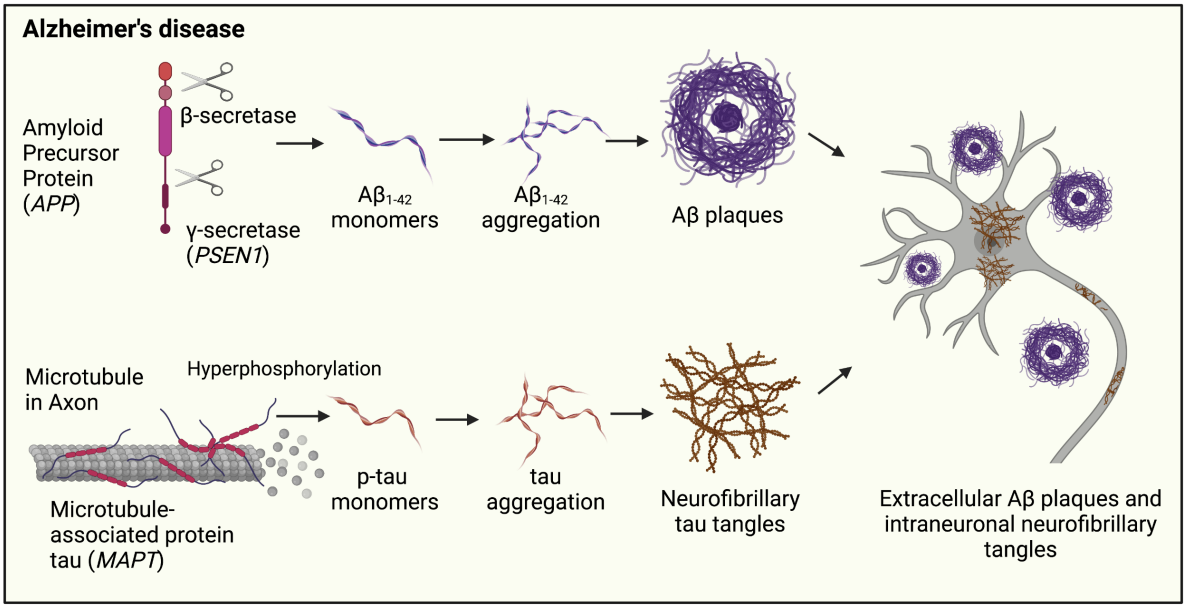

Figure 1: Amyloid plaques and Neurofibrillary tau tangles in Alzheimer's disease (AD)
In Alzheimer's disease (AD), the amyloid precursor protein (*APP*) in the cell membrane is cleaved by mutant β-secretase and γ-secretase (mutated *PSEN1*) to produce insoluble amyloid-β ($A\beta_{1-42}$) monomers. These $A\beta_{1-42}$ peptides accumulate in the extracellular matrix and form Aβ plaques outside the neurons. The microtubule-stabilizing protein tau (*MAPT*) in the neuronal axon dissociates from the structure when it is hyper-phosphorylated. Phosphorylated tau aggregates within the neurons to form neurofibrillary tau tangles (NFTs). Both $A\beta_{42}$ plaques and NFTs are documented in AD patients' brains. This figure was created with BioRender.com. Modified from (Ravichandran and Heneka, 2021)

1.1.2. Neuroinflammation and inflammasomes

Neuroinflammation is not only evident in neurodegenerative diseases, but also in physiological processes like aging (Andronie-Cioara et al., 2023). The immune cells of the body express intra- and extracellular receptors that identify their surrounding molecules and initiate an appropriate response against them (Latz et al., 2013). These intra- and extracellular receptors recognize signals called Damage-associated molecular patterns (DAMPs) and Pathogen-associated molecular patterns (PAMPs) using Pattern-recognition receptors (PRRs) (Zheng et al., 2020). The PRRs comprise five groups namely toll-like receptor (TLRs), absent in melanoma-2 (AIM2)-like receptors (ALRs), Nod-like receptor (NLRs), retinoic-acid-inducible gene-I (RIG-I)-like receptors (RLRs), and C-type lectin receptors (CLRs) family. Among these, the TLRs, ALRs, and NLRs are

involved in inflammasome complex formation (Davis et al., 2011; Ravichandran and Heneka, 2021; Schroder and Tschopp, 2010; Zheng et al., 2020).

The inflammasome complex is a supra-molecular scaffold structure that is assembled when through the downstream activation signals from PRRs (Martinon et al., 2002). From the NLR family of the inflammasome, the NLR and pyrin-domain containing 1 (NLRP1), NLRP3, NLRP6, NLRP7, NLRP12, and NLR and CARD-domain containing 4 (NLRC4) have formed inflammasome complexes (Latz et al., 2013; Zheng et al., 2020). The goal and consequence of an inflammasome assembly are to activate the inactive pro-inflammatory substrates to the activated forms.

NLRP3 inflammasome is one of the widely studied inflammasome and its activation is documented in several neurodegenerative diseases (Ravichandran and Heneka, 2021). It consists of an amino-terminal pyrin domain (PYD), a sensory NACHT (present in NLR family apoptosis inhibitor protein (NAIP), CIITA, HET-E, and TP-1) domain, and a carboxy-terminal leucine-rich repeats (LRR) (Hoffman et al., 2001; Swanson et al., 2019). It is generated in an auto-inhibited form where the LRR domain is folded and covers the NACHT domain for activation (Swanson et al., 2019; Xiao et al., 2023).

The NLRP3 assembly and activation is a two-step process (**Figure 2**). The immune cell exposed to the threat identifies the PAMPs and DAMPs through its TLRs and activates the MyD88-mediated NF-κB nuclear translocation. This first step called priming, results in the production of NLRP3, ASC, pro-IL-1β, pro-IL-18, gasdermin-D, and pro-caspase-1 which are essential for achieving the result of inflammasome activation (Swanson et al., 2019; Xing et al., 2017). The second step called activation is achieved through a wide variety of signals that include changes in the cellular ionic concentration and impaired mitochondria and lysosomes (Ravichandran and Heneka, 2021, 2023; Swanson et al., 2019). Specifically, NIMA-related kinase-7 (NEK7) activates NLRP3 when it senses the efflux of K^+ and Cl^- ions from the cell and the influx of Na^+ and Ca^{2+} into the cell (Y. He et al., 2016; Muñoz-Planillo et al., 2013; Shi et al., 2016; Y. Zhang et al., 2018).

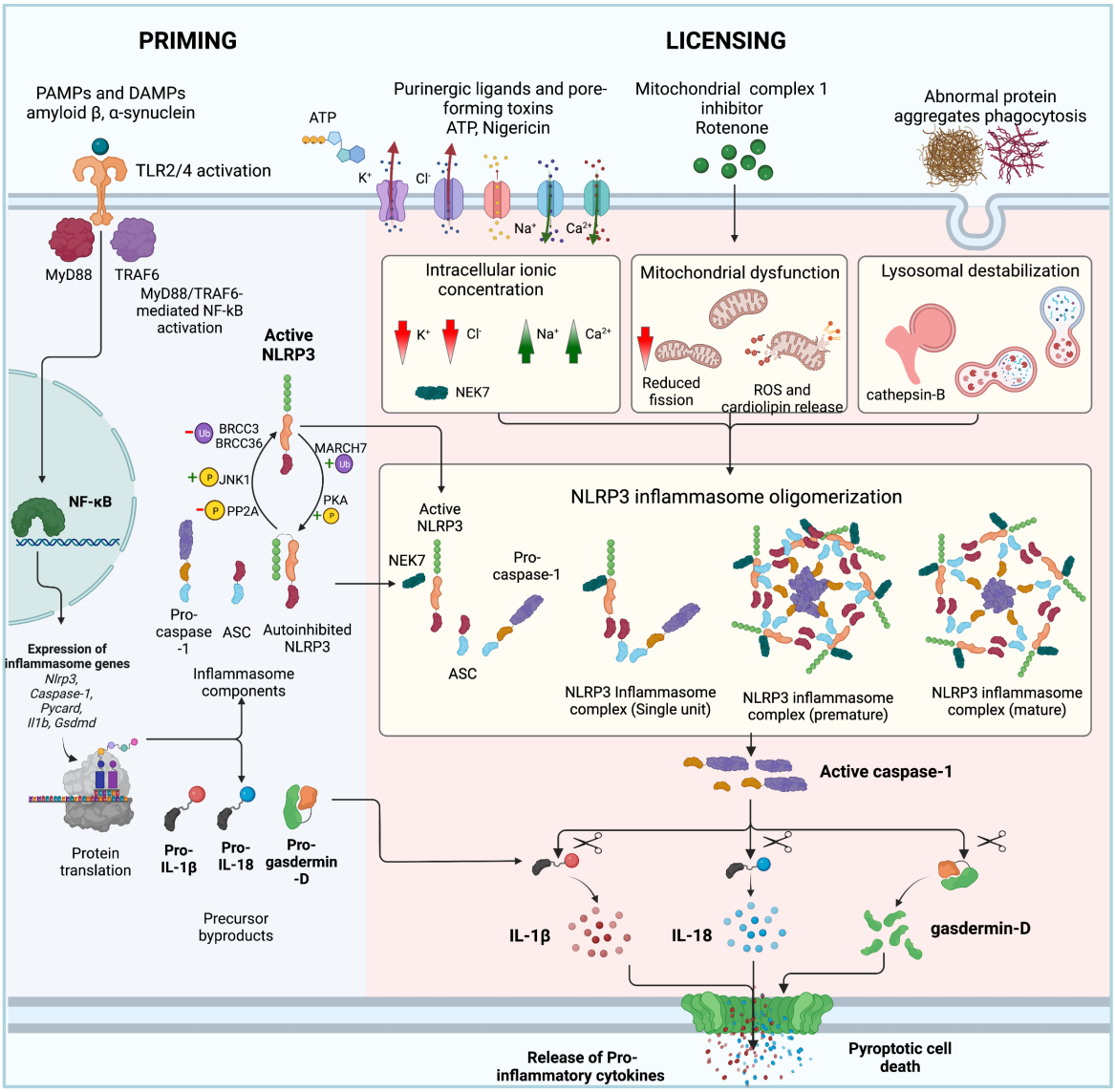

Figure 2: NLRP3 inflammasome activation.
The NLRP3 inflammasome is activated in a two-step process. The first step is priming, in which the PAMPs or DAMPs including amyloid-β, tau, α-synuclein, etc. are sensed by the Toll-like receptors (TLRs) in the membrane. TLR signalling leads to the activation of NF-κB through the MyD88/TRAF6 pathway, which causes its translocation to the nucleus. NF-κB binds to pro-inflammatory genes and results in the production of NLRP3, ASC, pro-caspase-1, and also the precursor forms of cytokines pro-IL-1β, pro-IL-18, and gasdermin-D. NLRP3 exists in auto-inhibited form when produced and is only activated through the second step, licensing or activation. Post-translational modification (PTMs) to NLRP3 by the phosphatase PP2A, the kinase JNK1, and the deubiquitinases BRCC2, and BRCC36 facilitate its activation, whereas the ubiquitinase MARCH7 and the kinase PKA inactivate it. The activation is achieved in three ways: (i) ionic imbalances by potassium and chloride ion efflux or sodium and calcium ion influx; (ii) mitochondrial dysfunction by reduced fission or abnormal electron transport chain leading to reactive oxygen species (ROS) build-up and cardiolipin release; (iii) lysosomal dysfunction by phagocytosis of abnormal protein aggregates of amyloid-β, tau, and α-synuclein leading to cathepsin-B release. These cues

are received by NLRP3 and initiate oligomerization of the inflammasome complex leading to the cleavage of caspase-1. Active caspase-1 cleaves the precursor forms of cytokines pro-IL-1β and pro-IL-18 into mature cytokines IL-1β, and IL-18 that are released by the pores formed on the membrane by cleaved gasdermin-D. This triggers a burst of pro-inflammatory cytokines that signal the surrounding cells, and they die by pyroptosis. This figure was created with BioRender.com. Modified from (Ravichandran and Heneka, 2023)

Synthetically, an ionophore called Nigericin induces potassium efflux in the cells leading to NLRP3 inflammasome. Other synthetic inhibitors for mitochondrial complex 1 (rotenone) and autophagy (3-methyladenine) induce NLRP3 activation by impairing the mitochondrial function in the cells (Wang et al., 2020; Won et al., 2015). Another distinct signal for NLRP3 activation is through the release of the lysosomal cathepsin-B due to an ineffective degradation of a phagocytosed molecule (Nakanishi, 2020; Swanson et al., 2019). In short, all these cues are a warning signal for the cell to react instantly in a pro-inflammatory manner to resolve the threats.

The activation step initiates the NLRP3 ATPase-mediated assembly of a molecular scaffold structure called the inflammasome complex (Duncan et al., 2007; Ravichandran and Heneka, 2021). The formation relies on the homotypic interaction between the PYD domains of NLRP3 and ASC and the CARD domains of ASC and pro-caspase-1 (Oroz et al., 2016). Free-floating ASC tends to oligomerize in the cytosol that attracts the pro-caspase-1 thereby facilitating instant formation of the inflammasome complex. Within the inflammasome complex, being in proximity with a neighboring pro-caspase-1 enables its protease activity to release the functional caspase-1 subunits p20 and p10 (Boucher et al., 2018; Ravichandran and Heneka, 2021; Swanson et al., 2019). The premature forms of the pro-inflammatory cytokines pro-IL-1β, pro-IL-18, and the pore-forming protein gasdermin-D are proteolytically activated into their mature forms. The cytokines are released through the gasdermin-D pores formed on the cell membrane that fuels further neuroinflammation in the neighbouring cells (Santa Cruz Garcia et al., 2022). This process is predominantly orchestrated by the microglia leading to a vicious loop of activation in neurodegenerative diseases.

1.1.3. Inflammasome activation in AD

Pathogenic forms of $A\beta_{42}$ and Tau are the key proteins that propagate the spread of AD in the patient's brain (Ravichandran and Heneka, 2023). Their aggregates $A\beta_{42}$ plaques and NFTs act as DAMPs and activates the TLR signalling leading to the priming of the microglia. Specifically, $A\beta_{42}$ monomers and aggregates have been documented to activate the TLR2 (Reed-Geaghan et al., 2009) and TLR4 signaling (De et al., 2019; Parajuli et al., 2013; Reed-Geaghan et al., 2009; Tahara et al., 2006) and tau has been shown to activate TLR2/8 (Jiang et al., 2021) and TLR4 (Meng et al., 2022) signalling in microglia. These microglia also phagocytose these aberrant protein aggregates resulting in lysosomal disruption and causing NLRP3 activation. Subsequently, this leads to the inflammasome formation and the release of IL-1β and IL-18 through the Gasdermin-D pores (Ravichandran and Heneka, 2023). These pro-inflammatory cytokines bind and activate the cytokine signaling cascade in an autocrine and paracrine manner leading to a vicious loop of neuroinflammatory reactions in the brain. In this way, $A\beta_{42}$ and tau involve the microglial inflammasomes and worsen AD progression.

Several studies have shown elevated levels of NLRP3, ASC, cleaved-caspase-1, IL-1β, cleaved-gasdermin-D, microgliosis, and astrogliosis in the brain tissues from human AD patients and mouse models of AD (**Figure 3**) (Heneka et al., 2013; Ising et al., 2019; Moonen et al., 2023; Stancu et al., 2022; Venegas et al., 2017). Hence, NLRP3 inflammasome is active in AD brains. Genetic deletion of NLRP3 inflammasome and its components like ASC were able to rescue the memory deficits in AD mice models (**Figure 3**) (Couturier et al., 2016; Heneka et al., 2013; Ising et al., 2019; Stancu et al., 2022; Venegas et al., 2017; Zhao et al., 2021). Similarly, pharmacological NLPR3-specific inhibitors including MCC950 (CRID3) restored the cognitive functions in AD mice by blocking NLRP3 and reducing neuroinflammation (**Figure 3**) (Han et al., 2022; Haseeb et al., 2022; Lonnemann et al., 2020; Yin et al., 2018). Other indirect means to suppress the NLRP3 activity include caspase-1 inhibitor VX-765 and Gasdermin-D inhibitor Disulfiram, which were also described to reduce IL-1β in the brain and improve the cognitive performance in AD mice (Flores et al., 2022; Rui et al., 2021; Tan et al., 2022). Hence, ameliorating IL-1β levels in the AD brain might be a novel strategy to address AD patients.

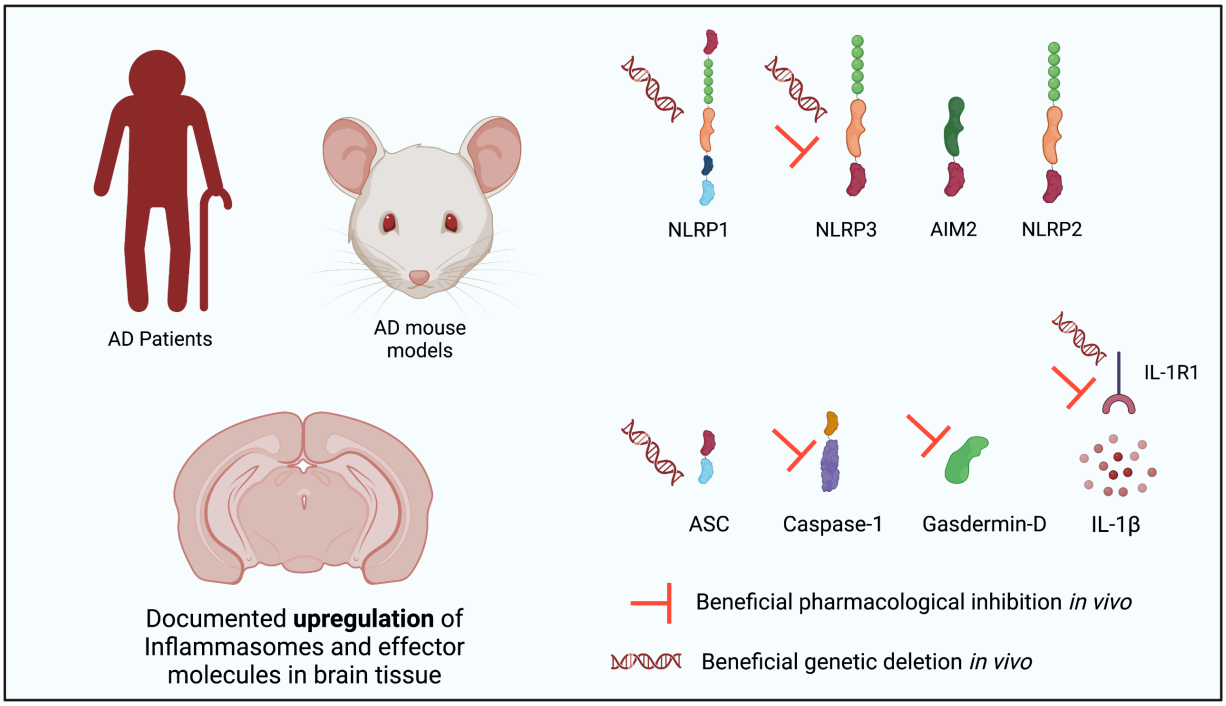

Figure 3: Inflammasome activation in Alzheimer's disease
In Alzheimer's disease (AD), the amyloid precursor protein (APP) in the cell membrane is cleaved by mutant β-secretase and γ-secretase to produce soluble amyloid-β ($A\beta_{42}$) monomers. The microtubule-stabilizing protein tau in the neuronal axon dissociates from the structure when it is hyper-phosphorylated. The inflammasomes and effector molecules upregulated in the AD brain are shown along with beneficial pharmacological or genetic deletion *in vivo*. This figure was created with BioRender.com. Modified from (Ravichandran and Heneka, 2023)

Neuroinflammation is evident in AD brain due to NLRP3 activation, which results in the release of cytokines, shedding of membrane receptors, and activation of the complement system of innate immunity by the cells in the central nervous system (Chatterjee et al., 2023; Hu et al., 2021; Rauchmann et al., 2020). Most of these released factors within the brain reach the cerebrospinal fluid (CSF) that circulates the brain. These factors in the CSF act as novel biomarkers to indicate the impact of the disease progression under neurodegenerative conditions. This thesis, being part of the PREADAPT project, primarily focuses on determining the levels of novel factors and byproducts released into the CSF due to neuroinflammation in the AD and dementia patients.

1.2. The PREADAPT project

The personalized profiles ageing dementia progression (PREADAPT) project is a JPND-EU-funded project that involves partners from multiple countries. Here, the goal was to identify personalized inflammatory profiles of aging and senescence which were modified specifically by risk factors in dementia patients. The work was divided into separate work packages, and the work package relevant to this thesis was to establish and measure 15 pre-selected inflammatory biomarkers in the CSF from different cohorts in Europe.

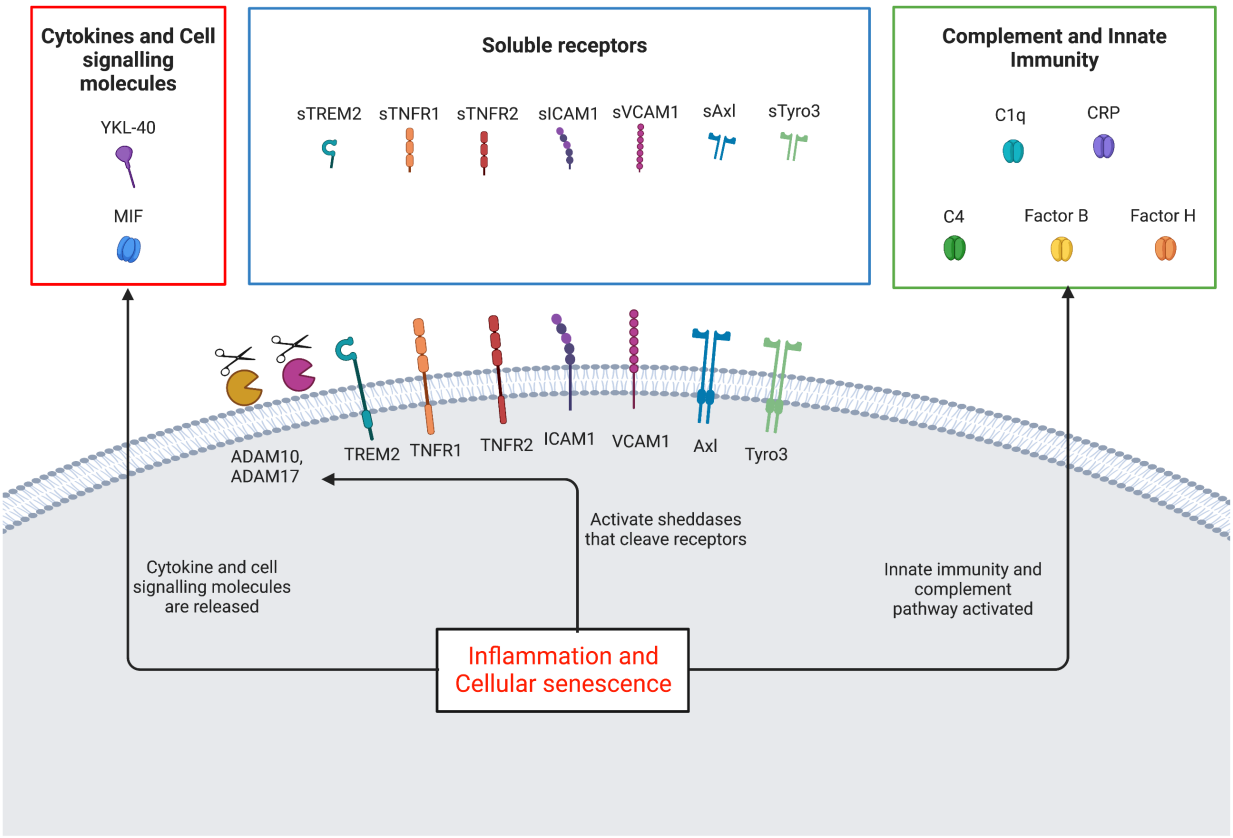

Figure 4: PREADAPT biomarkers measured in the CSF from the European cohorts The selected 15 biomarkers could be classified as cytokine and cell signaling molecules (YKL-40, MIF), soluble receptors (TREM2, TNFR1, TNFR2, ICAM1, VCAM1, Axl, Tyro3), and complement/innate immunity (C1q, C3, C4, Factor B, Factor H, and CRP). These proteins are released from an inflammatory microglia or astrocyte in a dementia brain and are accumulated in the CSF as biomarkers. All of these biomarkers could be reliably measured in the human CSF using the existing assay measurement platforms. This figure was created with BioRender.com. Adapted from (Brosseron et al., 2018, 2020, 2022)

The chosen 15 biomarkers were selected based on recently published studies on inflammatory biomarkers released in the CSF from dementia subjects (Brosseron et al., 2018, 2020). It was speculated that cellular senescence and inflammatory triggers can lead to the release of cytokine and cell signaling molecules like YKL40, and MIF. Secondly, it can activate sheddases like ADAM10 or ADAM 17 that cleave cell surface receptors leading to the release of soluble receptors like Tyro3, Axl, TREM2, VCAM1, ICAM1, TNFR1, and TNFR2, or can activate the complement and innate immunity leading to the release of complement and innate immunity factors C1q, C3, C4, Factor B, Factor H, and CRP **(Figure 4)**. A brief overview of the CNS sources and functions of these proteins is listed in **Table 1**.

Protein	Full-name	CNS source	Function
YKL-40	Chitinase-3-Like Protein 1	Astrocytes	Secreted glycoprotein, function unknown
MIF	Macrophage migration inhibitory factor	Microglia, astrocytes, neurons, endothelial cells	Secreted cytokine, released upon PAMPs/DAMPs signalling
Tyro3	TAM receptors	Neurons, Microglia, astrocytes, endothelial cells, oligodendrocytes	Phagocytic receptors, cell-cell interactions, homeostasis, anti-inflammatory
Axl			
TREM2	Triggering-Receptor expressed on myeloid cells 2	Cells of myeloid origin, microglia	Binds to PAMPs and DAMPs
VCAM1	Vascular cell adhesion molecule 1 (CD106)	Immune and vascular endothelial cells	Binds to $\alpha 4\beta 1$-integrin, Allow trans-endothelial cell migration of leukocytes
ICAM1	Intercellular adhesion molecule 1	Microglia, astrocytes, and vascular endothelial cells	Binds to $\beta 2$-integrin, Allow trans-endothelial cell migration of leukocytes
TNFR1	Receptors of TNF-α	Endothelial cells, oligodendrocytes, neurons, microglia, astrocytes	Binds to TNF-α, leads to pro-inflammatory signaling
TNFR2			
C1q; C3; C4	Complement components 1q; 3; 4; Factor B, H	Microglia, astrocytes, neurons	Infection defence, DAMPs/PAMPs binding
Factor B			
Factor H			

CRP	C-Reactive protein	Produced in liver	General inflammation marker

Table 1. List of 15 inflammatory biomarkers, their CNS sources, and functions

Although these biomarkers indicate the state of neuroinflammation in AD patients, the exact functional relevance of these biomarkers on the context of AD progression is poorly understood. Based on preliminary results suggesting protective effects of the TAM receptors and ligands in the context of AD (Herrera-Rivero et al., 2019), an *in vitro* study was designed for this thesis to investigate the role of Tyro3 and Axl receptors in AD-related neuroinflammation.

1.3. TAM receptors, a closer look

Tyro3, Axl, and MerTK are the receptors in the TAM receptor family. They are part of the receptor tyrosine kinases and play a role in phagocytosis and immune regulation (Lemke and Rothlin, 2008; Myers et al., 2019). Due to their negative feedback that causes immunosuppressive effects and proliferation, specific TAM inhibitors are used as targets to ameliorate cancer progression (Aehnlich et al., 2021). However, their role in the context of neurodegenerative diseases is not completely understood. In this thesis, it was hypothesized that TAM receptors might be playing a beneficial role in delaying the disease progression in neurodegenerative diseases.

Their predominant ligands Gas6 and Protein S, and the newly discovered ligands Galectin-3, Tubby, and tubby-like protein 1 were all having varied affinities to bind to these receptors (Caberoy et al., 2010, 2012; Lew et al., 2014). For instance, Gas6 and Tubby-like protein 1 binds with all three receptors, whereas Protein S binds primarily with Tyro3 and MerTK and Galectin-3 and Tubby with MerTK. Due to most studies performed on the primary ligands Gas6 and Protein S, this thesis will focus on these two ligands and the receptors Tyro3 and Axl. It is important that there is a gradient in the levels of these ligands produced and secreted into the extracellular matrix namely into the CSF. For instance, the ligand Protein S is found in abundant levels at the range of 150 pg/mL in CSF and 30 ng/mL in blood suggesting that TAM signaling in the human body is an ongoing process (Data from preliminary testing).

The exact function of these receptors is not elaborated. In brief, phagocytosis is assisted through a sandwich-like mechanism. A dying cell activates the enzyme flippase in its cell membrane that inverts and exposes the phosphatidylserine to the extracellular matrix (Kasikara et al., 2017). The ligand Gas6 is a Vitamin K-dependent protein and has a γ-carboxy butyric acid terminal which binds strongly with exposed phosphatidyl serine (Manfioletti et al., 1993). A phagocytic macrophage recognizes the ligands, dimerizes, and activates the tyrosine kinase downstream cascade. This eventually ends in the phosphorylation of key kinases that are involved in actin cytoskeleton rearrangement and the initiation of phagocytosis.

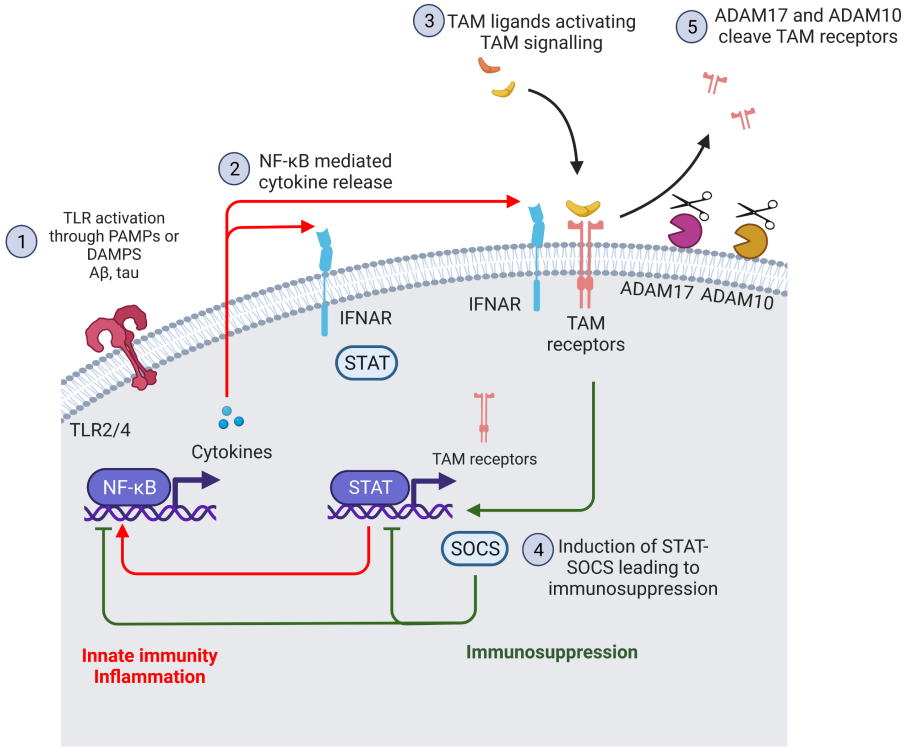

Figure 5: TAM receptors mechanism and relevance to Alzheimer's disease
(1) Any TLR signaling through DAMPs and PAMPs induce NF-κB-mediated cytokine production and release. **(2)** Cytokine binding to IFNAR induces STAT1 leading to the expression of TAM receptors on the surface to regulate inflammation. **(3-4)** TAM ligands bind to TAM receptors and over-induces STAT1 which activates the Suppressor of cytokine signaling 1 (SOCS1). SOCS1 impacts STAT1 and NF-κB-mediated pro-inflammatory gene expression thereby suppressing the ongoing inflammation. In this way, the TAM receptor system regulates inflammation. **(5)** Sheddases like ADAM10 and ADAM17 cleaves the receptors off the surface which are released into the CSF and are measured as biomarkers for AD (Lemke and Rothlin, 2008; Myers et al., 2019).

However, in normal conditions, the receptors are activated through ligand binding and dimerization **(Figure 5)**. This brings the kinase domains of the receptors closer which leads to their phosphorylation and activation. A cytokine released by an inflammatory cell activates a signaling cascade that induces the expression of TAM genes leading to their expression at the cell surface (Wium et al., 2018). Now, cytokine signaling together with TAM signaling induces the transcription factor STAT1, that in turn activates the expression of SOCS1 (Suppressor of cytokine signaling 1). SOCS1 is known to impair the production of cytokines leading to the regulation of inflammatory processes. In this way, the cell keeps inflammation under homeostasis and prevents it to enter a chronic inflammatory state. It is important to note that these mechanisms are proposed with caution, and the exact mechanism is unknown. Hence, understanding the role of these receptors in the context of AD might help in elucidating any protective mechanism that these receptors employ in the AD patient brains.

1.4. Aims of the study

Being part of the PREADAPT project, the primary aim of this thesis was to measure 15 selected factors and biomarkers released in the cerebrospinal fluid samples from multiple European dementia cohorts. The key biomarkers that were strongly influenced by Tau, Amyloid, and diagnosis were identified and utilized in the pipeline for PREADAPT to generate multi-dimensional data analysis and results. Partial results of these analyses revealed a beneficial role of soluble receptors Tyro3 and Axl in the CSF. In order to investigate the protective role of the TAM receptors Tyro3 and Axl in the context of Alzheimer's disease, *in vitro* over-expression systems of Tyro3 and Axl in THP-1 cells (human monocyte leukemia cells) were used. Here, these cells were exposed to AD patient brain microenvironment using $A\beta_{42}$ and tau proteins in order to check the phagocytic ability, NLRP3-mediated inflammatory response, and subsequent impact on the ongoing neuroinflammation. The results from this thesis describe for the first time an anti-inflammatory role of Tyro3 receptors and signalling in the context of AD.

2. Materials and methods

2.1. Materials

2.1.1. Instruments

Instrument	Company	Catalog Number
TECAN reader: Infinite M200 PRO	TECAN	Infinite M200 PRO
MESO QuickPlex SQ 120	Meso Scale Diagnostics, LLC	SQ 120
MAGPIX® System	Luminex™	MAGPIX®
FLEXMAP 3D™	Luminex™	APX1342
ODYSSEY CLx	LI-COR	ODYSSEY CLx
Pipet-Lite Adjustable Spacer LA8-300XLS	Mettler Toledo	17011843
Multipette® M4 · Repeater® M4	Eppendorf	EP4982000322
XCell4 SureLock™ Midi-Cell; Mini-Cell	Invitrogen™	WR0100; EI0001
Trans-Blot® Turbo™ Transfer System	BIO-RAD	1704150

Table 2: List of instruments

2.1.2. Substances

Compound name	Company	Catalog number
Phorbol 12-myristate 13-acetate (PMA)	Sigma-Aldrich	P1585
Nigericin (Nig)	InvivoGen	tlrl-nig
Ruxolitinib (Rux)	MedChemExpress	HY-50856
Lipopolysaccharide from Escherichia coli K12 (LPS)	InvivoGen	tlrl-eklps
Retinoic acid	Sigma-Aldrich	R2625
Poly-L-lysine hydrobromide (PLL)	Sigma-Aldrich	P1524

Corning® Matrigel®	Corning	354230
Halt Protease Phosphatase Inhibitor Cocktail	Thermo Fisher Scientific	78441

Table 3: List of substances

2.1.3. Commercial Kits

Kit name	Company	Catalog number
Human Chitinase-3-like-1 duoset ELISA	R&D systems	DY2599
Human Axl duoset ELISA	R&D systems	DY154
Human Tyro3/Dtk duoset ELISA	R&D systems	DY859
V-PLEX Vascular Injury Panel 2 Human Kit (CRP, VCAM-1, ICAM-1)	Mesoscale Discovery	K15198D
U-PLEX Custom Biomarker Group 1 Human Assays (MIF)	Mesoscale Discovery	K15067M
R-PLEX Human TNF-RI Antibody Set (TNF-R1)	Mesoscale Discovery	F210V
R-PLEX Human TNF-RII Antibody Set (TNF-R2)	Mesoscale Discovery	F21ZS
MILLIPLEX Human Complement Panel 2 - Immunology Multiplex Assay (C1q, C3, C4, Factor B, Factor H)	Merck Millipore	HCMP2MAG-19K
Human IL-1 beta/IL-1F2 DuoSet ELISA	R&D systems	DY201
Human TNF-α DuoSet ELISA	R&D systems	DY210
Pierce™ BCA Protein Assay Kit	Thermo Scientific™	23225
Mem-PER™ Plus Membrane Protein Extraction Kit	Thermo Scientific™	89842
NE-PER™ Nuclear and Cytoplasmic Extraction Reagents	Thermo Scientific™	78833
RNeasy Mini Kit	Qiagen	74104

Pierce™ Chromogenic Endotoxin Quant Kit	Thermo Scientific™	A39552

Table 4: List of commercial kits

2.1.4. Antibodies for Mesoscale TREM2 ELISA

Primary antibodies (Human antigens)			
Antibody (Host, antigen)	**Dilution**	**Company**	**Catalog no. (RRID)**
Goat anti-TREM2	1:800	R&D Systems	BAF1828 (AB_2208688)
Mouse anti-TREM2 (B-3)	1:200	Santa Cruz Biotechnology	sc-373828 (AB_10989941)
Secondary antibodies			
Mouse IgG with Sulpho-Tag	1:10000	Mesoscale Discovery	R32AC AB_2783819

Table 5: List of antibodies for TREM2 ELISA

2.1.5. Antibodies for Western blotting

Primary antibodies (Human antigens)			
Antibody (Host, antigen)	**Dilution**	**Company**	**Catalog no. (RRID)**
Rabbit anti-Tyro3 (D38C6)	1:1000	Cell signaling technologies	5585 (AB_10706782)
Rabbit anti-Axl (C89E7)	1:1000	Cell signaling technologies	8661 (AB_11217435)
Mouse anti-Caspase-1 (Bally-1)	1:2000	Adipogen	AG-20B-0048 (AB_2490257)
Mouse anti-IL-1β/IL-F2	1:1000	R&D systems	MAB201 (AB_358006)
Rabbit anti-Gasdermin-D	1:1000	Cell signaling technologies	97558 (AB_2864253)
Rabbit anti-NLRP3	1:1000	Abcam	ab263899 (AB_2889890)
Rabbit anti-ASC	1:1000	Adipogen	AG-25B-0006 (AB_2490440)
Mouse anti-β-Actin (BA3R)	1:5000	Invitrogen	MA5-15739 (AB_10979409)

Mouse anti-Lamin-B	1:1000	Proteintech	66095-1-Ig (AB_11232208)
Rabbit anti-NF-κB p65	1:1000	Cell signaling technologies	8242 (AB_10859369)
Rabbit anti-STAT1	1:1000	Cell signaling technologies	9172 (AB_2198300)
Rabbit anti-p-STAT1	1:1000	Cell signaling technologies	9167 (AB_561284)
Rabbit anti-SOCS1	1:500	Abcam	ab62584 (AB_956316)
Secondary antibodies			
Mouse IgG with IRDye 800CW	1:20000	LI-COR Biosciences	926-32210 AB_621842
Mouse IgG with IRDye 680RD	1:20000	LI-COR Biosciences	926-68070 AB_10956588
Rabbit IgG with IRDye 800CW	1:20000	LI-COR Biosciences	926-32211 AB_621843
Rabbit IgG with IRDye 680RD	1:20000	LI-COR Biosciences	926-68071 AB_10956166

Table 6: List of antibodies for Western blotting

2.1.6. Antibodies for Immunocytochemistry

Primary antibodies (Human antigens)			
Antibody (Host, antigen)	**Dilution**	**Company**	**Catalog no. (RRID)**
Mouse anti-Neuron-specific beta-III Tubulin (Tuj-1)	1:1000	R&D systems	MAB1195 (AB_357520)
Rabbit anti-NeuN	1:1000	Abcam	ab177487 (AB_2532109)
Secondary antibodies / Reagents			
Goat anti-mouse Alexa Fluor 488	1:500	Invitrogen	A-11017 (AB_2534084)
Goat anti-rabbit Alexa Fluor 647	1:500	Invitrogen	A-11017 (AB_2535813)

Table 7: List of antibodies for Immunocytochemistry

2.1.7. Solutions

R&D ELISA (YKL-40, Axl, Tyro3, IL-1β, TNF-α)

Solution/buffer	Composition	Company	Cat. No.
Phosphate-buffered saline (PBS), pH 7.4	Dulbecco's PBS powder (10L)	Applichem	APA0965.9010
Wash buffer	1 X PBS	Applichem	APA0965.9010
	0.05% Tween® 20	Carl Roth	9127.1
Reagent diluent	1% Bovine serum albumin (BSA)		
	1X PBS	Applichem	APA0965.9010
Stop solution	1M H_2SO_4		

Table 8: Solution composition for R&D ELISA

Western blotting

Solution/buffer	Composition	Company	Cat. No.
1X MES running buffer	NuPAGE™ MES SDS-Running buffer	Invitrogen™	NP0002
Tris-buffered saline + Tween 20 (TBST), pH 8	50 mM Tris	Carl Roth	5429.3
	150 mM NaCl	Carl Roth	3957.4
	0.1% Tween® 20	Carl Roth	9127.1
Blocking buffer	3% Bovine serum albumin (BSA)	Rockland	BSA-1000
	1X TBST	-	-

Table 9: Solution composition for Western blotting

Immunocytochemistry

Solution/buffer	Composition	Company	Cat. No.
PBS-TX	1X PBS	Merck	
	0.01% Triton®-X 100	Carl Roth	3051.3
4% PFA	4% Paraformaldehyde	Applichem	APA0965.9010

	1X PBS	Carl Roth	9127.1
Blocking buffer	3% Bovine serum albumin (BSA)	Rockland	BSA-1000
	5% Normal Goat serum	Abcam	ab7481
	PBS-TX	-	-

Table 10: Solution composition for Immunocytochemistry

2.2. Methods

2.2.1. Human CSF sample collection

This study included two dementia cohorts: DELCODE (Germany) and Fundacío ACE (F.ACE) (Spain). Sample collection and ethical approval for the DELCODE and Fundacío ACE (F.ACE) cohorts are described elaborately in the published study (Brosseron et al., 2022). For DELCODE, the registration number of the trial is 117/13 and was approved (No. 122/18) by the ethical committee of the medical faculty of the University of Bonn. This approval is for the use of data and biomaterial for the specific work described in this thesis and the publication (Brosseron et al., 2022). For F.ACE, the data and biomaterial usage were approved by the Ethical Committee of the Hospital Clínic I Provincial de Barcelona (HCB/2014/0494, HCB/2016/0571, HCB/2016/0835, HCB/2017/0125 and HCB/2018/0333). All study protocols were in agreement with the local and international regulations on clinical studies (Sociedad Española de Neurología (www.sen.es)). More information about the data can be found in **Table 11.**

Reagent or materials	Source	Identifier
DELCODE Cohort Data	German Center for Neurodegenerative Diseases (DZNE)	https://www.dzne.de/en/research/studies/clinical-studies/delcode/
F.ACE Cohort Data	F.ACE Alzheimer Center Barcelona	https://www.fundacioace.com/en

Table 11: Deposited data

2.2.2. Study design

DELCODE includes subjects at a minimum age of 60 years, recruited from German residents. CSF samples underwent biomarker measurement for the determination of the inflammatory marker panel. Additional data retrieved from the DELCODE study included demographic data (age, sex, APOE genotype, and body mass index (BMI), previously determined routine AD biomarker levels ($A\beta_{40}$, $A\beta_{42}$, and ratio $A\beta_{42}$/ $A\beta_{40}$, phospho-(p)-tau-181, total(t)-tau and the ratio $A\beta_{42}$/ p-tau-181) (Jessen et al., 2018). The subjects were classified into healthy controls (CN: 94), subjective cognitive decline (SCD: 94), mild cognitive impairment (MCI: 68), and Dementia of Alzheimer's type (DAT: 37) which are ordered in the increasing degree of cognitive dysfunctions (**Table 11**). Individuals classified in the SCD group have self-reported experiences with problems with cognitive function. MCI is a transitional stage between general aging deficits and dementia where subjects show cognitive impairment. DAT denotes individuals with dementia that are characteristic of Alzheimer's disease.

The second cohort Fundacío ACE (F.ACE) consists of 59 SCD and 723 MCI subjects (**Table 12**). Data obtained from F.ACE included age, sex, APOE genotype, BMI, CSF $A\beta_{42}$, p-tau, and t-tau. General information on the F.ACE cohort criteria and procedures has been described elsewhere (Boada et al., 2014)**.** Briefly, F.ACE includes subjects older than 49 years, who had subjective cognitive complaints defined as a score of ≥ 8 on MFE-30, the Spanish version of the Memory Failures in Everyday Life Questionnaire, and were Spanish literate residents.

Cohort	**DELCODE**		**F.ACE**
Country	Germany		Spain
Assays	Manual	Olink®	Manual
Sample size (N)	293	481	782
Groups	CN (94); SCD (94); MCI (68), DAT (37)	CN (126); SCD (194); MCI (105), DAT (60)	SCD (59), MCI (723)

Amyloid cutoff (A+)	Amyloid-β ratio $A\beta_{42}/A\beta_{40}$ < 0.08	Amyloid-β ratio $A\beta_{42}/A\beta_{40}$ < 0.08	Assay 1: $A\beta_{42}$ < 676 pg/mL; Assay 2, $A\beta_{42}$ < 796 pg/mL,
Total-Tau cutoff (T+)	t-tau > 510.9 pg/mL	t-tau > 510.9 pg/mL	Assay 1: t-tau > 367 pg/mL; Assay 2: t-tau > 412 pg/mL
Amyloid/Tau groups	A-T- (147); A-T+ (20); A+T- (45); A+T+ (80)	A-T- (245); A-T+ (24); A+T- (92); A+T+ (120)	A-T- (314); A-T+ (112); A+T- (152); A+T+ (204)
Diagnosis/ Tau groups	CN T- (76); CN T+ (18); SCD T- (73); SCD T+ (21); MCI T- (36); MCI T+ (31); DAT T- (7); DAT T+ (30)	CN T- (104); CN T+ (22); SCD T- (160); SCD T+ (34); MCI T- (56); MCI T+ (46); DAT T- (17); DAT T+ (42)	SCD T- (52); SCD T+ (7); MCI T- (414); MCI T+ (309)
Proteins measured	Tyro3, Axl, YKL40, TREM2, MIF, C1q, Factor H, TNFR1, TNFR2, ICAM1, VCAM1, C3, Factor B, C4, CRP	Tyro3, Axl, YKL40, TREM2, MIF, C1q, Factor H, TNFR1, TNFR2, ICAM1, VCAM1, C3, Factor B, MerTK, Protein S, Gas 6	Tyro3, Axl, YKL40, TREM2, MIF, C1q, Factor H, TNFR1, TNFR2, ICAM1, VCAM1, C3, Factor B, C4, CRP

*Healthy controls: CN, Subjective cognitive decline: SCD, Amnestic mild cognitive impairment (MCI), Dementia of Alzheimer's Type (DAT)

Table 12: Cohorts used in this thesis

2.2.3. Sample processing:

In brief, samples were retrieved from the biorepository of the DELCODE study and F.ACE and initially underwent one additional freeze-thaw-cycle on ice to split samples into smaller aliquots of 10 to 60 µl, depending on the requirements of the respective immunoassays. Samples were pipetted into 96 well V-bottom storage plates (Greiner Bio-One, ref. 651101), sealed using a freezing-resistant aluminum foil (Greiner Bio-One, ref. 676090), placed on dry ice for fast re-freezing and finally stored at −80 °C until analysis. This ensures only two freeze-thaw cycles until measurement. All samples were randomized and pseudonymized before aliquoting and the measuring personnel was blinded to any group indications that influence statistical analysis. All samples were

measured in duplicates to ensure precision. The maximum allowed coefficient of variance (CV) was 20 %. The measurements for samples exceeding 20 % CV were repeated. A reference CSF sample was pooled and aliquoted which was used in each immunoassay plate to account for inter-plate differences during the measurements.

2.2.4. CSF dilution factors and assay specifications for measurements

	CSF dilution	Assay type	Assay Method	Highest standard (pg/mL)	Lowest standard Detection limit (pg/mL)
YKL-40	2000	Singleplex	Colorimetric	2000	31.3
Axl	5	Singleplex	Colorimetric	4000	62.5
Tyro3	40	Singleplex	Colorimetric	4000	62.5
TREM2	4	Singleplex	Electrochemiluminescence	8000	125
MIF, TNFR1, TNFR2	15	Multiplex	Electrochemiluminescence	22300	5.44
				8192	2
				8192	2
CRP, ICAM1, VCAM1	20	Multiplex	Electrochemiluminescence	188000	12.03
				49900	3.19
				49700	3.19
C1q, C3, C4, Factor B, Factor H	80	Multiplex	Bead-based	60000	80
				200000	270
				400000	550
				60000	80
				300000	410

Table 13: CSF dilution factors and assay specifications for measurements

2.2.5. Colorimetric ELISA

The R&D assays for YKL-40, Axl, and Tyro3 employ a colorimetric-based quantification. Here, a polystyrene plate is coated with a capture antibody that captures the target proteins in the CSF. A biotinylated detection antibody is added to sandwich the analytes which can be quantified through an HRP-mediated blue-colored product formation. The reaction is stopped with an acid to convert the product to yellow color which could be measured at 450 nm absorbance. This method does not allow multiplexing for samples at the same time. It also requires more sample volume.

The quantification of biomarkers in the CSF was measured according to the manufacturer's protocol. Briefly, for all the assays, the ELISA plates were coated with capture antibody diluted in PBS overnight at RT. The following day, the wells are washed with PBST (0.05 % Tween-20 in PBS) three times and were blocked with reagent diluent (1 % BSA in PBS, sterile filtered) for 1 h at RT. Samples and standards diluted in reagent diluent were loaded on to the plate and incubated for 2 h at RT. After washing, the biotinylated detection antibody diluted in reagent diluent was added and incubated for 2 h. Following detection, the HRP-streptavidin conjugate was added to the well, and incubated in the dark for 20 min, followed by washing and the addition of the colorless substrate TMB. TMB reacts with the horse radish peroxidase present in each well and converts it to a blue product. The reaction is stopped using the stop solution which is 2 N H_2SO_4. The intensity of the product is directly correlated with the amount of protein present in the wells. This was measured in the plate reader with the absorption wavelength set at 450 nm and reference correction set at 540 nm. The absorption values were extrapolated with the corresponding standard values.

2.2.6. Electro-chemiluminescence ELISA

The Mesoscale assays for TREM2, TNFR1, TNFR2, MIF, CRP, VCAM1, and ICAM1 use the electro-chemiluminescence principle. Briefly, a similar sandwich ELISA is used, except the detection is through a sulpho-TAG detection antibody. This can convert the substrate to a luminescent product when electricity is passed on the plate through the specialized reader. This method allows multiplexing by enabling multiple spots within each well that are distinct for each analyte.

2.2.6.1. TREM2

TREM2 in CSF was measured through a home-brew assay (Suárez-Calvet et al., 2016). MSD GOLD 96-well Streptavidin SECTOR Plates (Mesoscale Discovery) were blocked using 250 µL blocking buffer (3 % BSA in PBS + 0.05 % Tween-20) overnight at 4 °C with 300 rpm shaking. The wells were then coated with 25 µL biotinylated capture antibody, goat anti-TREM2 (1:800; R&D systems), diluted in blocking buffer for 90 min at RT with 300 rpm shaking. After washing three times, 50 µL samples and standards diluted in sample buffer (1 % BSA in PBS + 0.05 % Tween-20) were loaded onto the wells and incubated for 2 h at RT with 300 rpm shaking standards (**Table 13**). The wells were washed three times and 50 µL mouse anti-TREM2 (1:200; Santa Cruz Biotechnology) diluted in blocking buffer was added and incubated for 1 h at RT with 300 rpm shaking. After washing three times, the wells were incubated in 25 µL secondary antibody, goat anti-mouse IgG with Sulfo-Tag (1:10000; Mesoscale Discovery) diluted in blocking buffer for 1 h at RT with 300 rpm shaking. After the last wash, 150 µL 1X Read buffer T diluted with water was added to the wells and immediately read at MESO QuickPlex SQ 120 instrument. The concentration for the samples was determined by interpolation from the standard curve in the Mesoscale Diagnostics software.

2.2.6.2. MIF, TNFR1, and TNFR2 multiplex

A custom U-PLEX Development Pack for 3-Assay (Mesoscale Discovery), U-PLEX human MIF assay (Mesoscale Discovery), R-PLEX human TNF-R1 assay (Mesoscale Discovery), and R-PLEX human TNF-R2 assay (Mesoscale Discovery) were used for the measurements. The following linker: antibody combinations were maintained throughout the study - Linker 1: TNF-R1, Linker 3: TNF-R2, and Linker 10: MIF. 200 µL of biotinylated capture antibody was incubated with 300 µL corresponding linkers (1, 3, or 10) for 30 min at RT. Then, 300 µL of U-PLEX stop solution was added and incubated for 30 min at RT. After mixing, the prepared 100X capture antibody was diluted in UPLEX-stop solution, 50 µL was added to each well and incubated overnight at 4 °C with 600 rpm shaking. The wells were washed with PBS + 0.05 % Tween 20 (PBST) and 25 µL Diluent 43 was added. Following the diluent, 25 µL of samples and standards standards (**Table 13**) diluted in Diluent 43 were added and incubated for 1 h at RT with 600 rpm shaking. After washing, 50 µL detection antibody solution (1X detection antibody for MIF, TNF-R1, and TNF-R2 in

Diluent 3) was added to the wells which were loaded onto the wells and incubated for 1 h at RT with 600 rpm shaking. After the last wash, 150 µL of Read buffer B was to the wells, and the plates were read immediately at the MESO QuickPlex SQ 120 instrument. The concentration for the samples was determined by interpolation from the standard curve in the Mesoscale Diagnostics software.

2.2.6.3. CRP, ICAM1, VCAM1 multiplex

For CRP, ICAM1, and VCAM1 measurements, the V-PLEX Vascular Injury Panel 2 Human Kit (Mesoscale Discovery) was used. Briefly, 25 µL samples and standards (**Table 2.9**) diluted in Diluent 101 were added to the pre-coated plates and incubated for 2 h at RT with 600 rpm shaking. After washing, 25 µL of antibody solution containing 1X detection antibody against CRP, ICAM1, and VCAM1 with a Sulfo-Tag diluted in Diluent 101 was added to the wells. The plates were incubated for 1 h at RT with 600 rpm shaking after which the plates were washed and 150 µL 1X Read buffer T was added. The plates were read immediately at the MESO QuickPlex SQ 120 instrument. The concentration for the samples was determined by interpolation from the standard curve in the Mesoscale Diagnostics software.

2.2.7. Bead-based complement multiplex ELISA

The Luminex bead-based assays for the Complement factor C1q, C3, C4, Factor B, and Factor H were done using magnetic beads that are coated with specific antibodies. The beads interact with the analytes and bind the analytes from the samples. The detection antibody targets the analytes that were bound to these beads which can be visualized using Phycoerythrin, a red pigment. The reading of the plate occurs in the FlexMap 3D system, which functions similarly to a flow cytometer. Briefly, it passes all the beads present in each well through a fluidics system to identify the analyte and its intensity. This method allows multiplexing of several analytes at the same time.

For C1Q, C3, C4, Factor B, and Factor H measurements, the MILLIPLEX Human Complement Panel 2 - Immunology Multiplex Assay (Merck Millipore) was used. The assay was performed according to the manufacturer's protocol. Briefly, the antibody-tagged beads for each marker were mixed and diluted in the bead diluent. The samples

and standards were prepared according to the dilutions in the assay buffer standards (**Table 2.9**). To the well, 25 µL of assay buffer, 25 µL of the mixed antibody-bead solution, and 25 µL of prepared samples and standards were added and the plates were incubated for 2 h in dark at RT with 600 rpm shaking. The magnetic beads were washed three times in wash buffer using a magnetic platform and then 50 µL of detection antibody was added to each well. The beads were incubated for 1 h at RT in the dark with 600 rpm shaking after which 50 µL of Streptavidin-Phycoerythrin was added to the wells. The beads were incubated for 30 min at RT in the dark with 600 rpm shaking and then were washed three times. Lastly, the beads were resuspended in 150 µL FlexMAP Sheath fluid before being loaded onto the FLEXMAP 3D™ system for quantification. The sample concentration was calculated by interpolating from the standards through the Luminex™ software for FLEXMAP 3D™.

2.2.8. Data analysis and Statistics: Manual biomarker measurements

The cut-off values for A/T biomarkers were adapted from the published article **(Table 2.8)** (Brosseron et al., 2022). Briefly, the cut-offs were derived using Gaussian mixture modeling data in the R package flexmix (version 2.3-15). Non-parametric Kruskal-Wallis tests with Bonferroni correction for multiple testing were performed to evaluate group-wise differences. Furthermore, biomarker data were used for ANCOVA to determine the influential covariates in these comparisons. All statistical analyses for clinical datasets were performed and visualized in R software (R Foundation). The source codes will be made available on request.

2.2.9. Olink® proteomics and analysis

In the case of Olink®, the protein measurements were outsourced to the Olink® company. Olink® is a novel biomarker measurement platform that uses Proximity Extension Assay (PEA) technology combined with Next generation sequencing readout on Illumina instruments (Olink®). Of particular interest, this was the first time that 3072 proteins were measured in large dementia cohorts of human CSF. Hence, this thesis is part of a pioneer study in investigating novel CSF biomarkers. Olink® used specific antibodies for the markers that are proprietary to the company. In brief, 10 µL of the sample was used for every 384 proteins. The mechanism employed was that the antibodies have a specific

DNA fragment that has a barcode. The higher the analyte in the sample, the more the antibodies were bound to it leading to multiple DNA-tags coming in proximity. This proximal interaction was supported by a polymerase chain reaction leading to the amplification of the signal for the specific analyte. In this way, Olink® was able to measure multiple targets in a single well with high throughput.

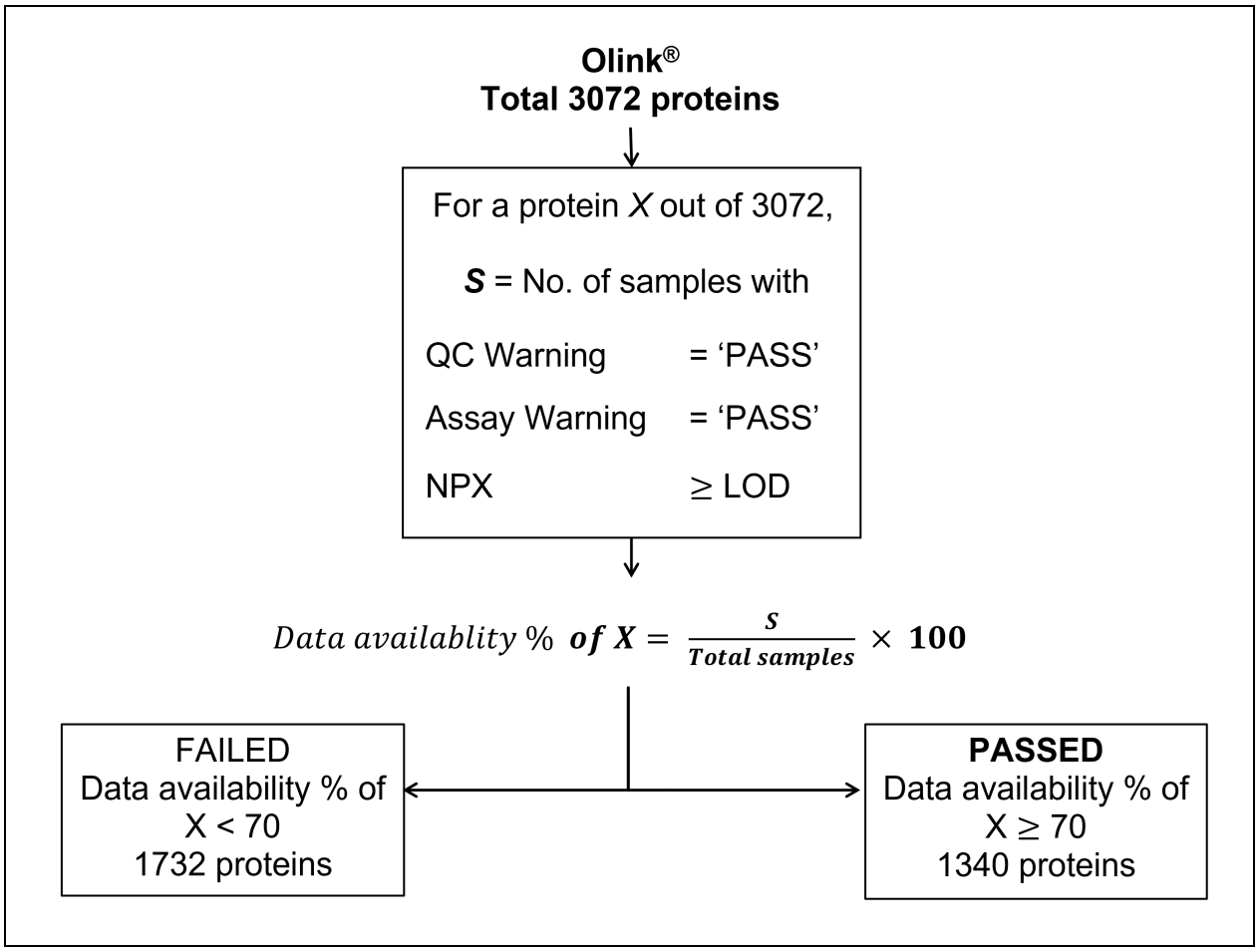

Figure 6: Olink® quality control (QC) pipeline.
Every assay is subjected through the quality control pipeline and only the assays that pass these criteria were used for subsequent analysis in this thesis. The missing percentage of any included assay should be less than or equal to 30%. LOD: Limit of detection

Data obtained by this assay is provided as Normalized Protein eXpression (NPX), with each protein in the assay having its own detection limit value in NPX. Every assay out of the 3072 proteins was passed through a QC pipeline as depicted in (**Figure 6)**. Only assays with a data availability percentage more than or equal to 70% were included for further analysis in this study. Out of the 3072 proteins, 1340 proteins survived this QC

pipeline. All the Olink® analyses performed in this thesis were conducted on these passed protein assays. In this thesis, all data were processed, compared, and the key biomarkers were validated in both manual and Olink® platforms. Subsequently, the Non-parametric Kruskal-Wallis tests with Bonferroni correction for multiple testing were conducted for the A/T and Diagnosis/T schemes. Also, key co-variates were identified using ANCOVA analysis to correct for co-variate-influenced effects. All the analyses were performed in R software (R Foundation). The source codes are available at GitHub (https://github.com/KishorearavindAbi/Olink-RScripts-Kishore-Thesis.git)

2.2.10. THP-1 cell culture

Wild-type THP-1 cells (human monocytic leukemia cells) and TAM over-expressing THP-1 cells were kindly provided by Dr. Susanne Schmidt from the institute of innate immunity, University Hospital Bonn. Briefly, the plasmids containing the *TYRO3* and *AXL* genes with a high expression promoter CMV were packaged into a lentiviral vector. Viral transduction on THP-1 cells generated TAM over-expressing cells, which were plated as single cells for subsequent selection based on TAM expression levels, morphology, and proliferation. Successful colonies were chosen for monoclonal expansion and the best clone was selected for all the subsequent experiments. All cells were maintained in RPMI 1640 Medium, GlutaMAX™ Supplement (Gibco™) supplemented with 10% heat-inactivated Fetal bovine serum (FBS) (Gibco™) and 1% Penicillin/Streptomycin (Gibco™) at 37°C in 5% CO_2 and humidified atmosphere. The cells were split every 3-5 days. For all the experiments, the cells were stimulated with 50 nM phorbol 12-myristate 13-acetate (PMA, Sigma-Aldrich) in serum-free medium (SFM) (RPMI 1640 Medium, GlutaMAX™ Supplement (Gibco™) + 1% Penicillin/Streptomycin (Gibco™)) for 16 h to transform the monocytes to macrophages.

2.2.11. SH-SY5Y neuronal cell culture and differentiation

Human neuroblastoma cells (SH-SY5Y) were purchased from ATCC. The cells were maintained in growth medium DMEM GlutaMAX™ Supplement (Gibco™) fortified with 15% heat-inactivated FBS and 1 % Penicillin/Streptomycin (Gibco™) and grown for three-four days at 37°C in 5% CO_2 and humidified atmosphere. The differentiation medium is DMEM GlutaMAX™ Supplement (Gibco™) with 3% heat-inactivated FBS, 1 %

Penicillin/Streptomycin (Gibco™), and 10 µM Retinoic acid (Sigma), which transforms the cells into mature neurons. The cells were plated onto poly-L-Lysine and Matrigel-coated coverslips and maintained in the differentiation medium for 14 days with the medium replacement every second day. Lastly, the mature neurons were serum-starved overnight on serum-free DMEM GlutaMAX™ Supplement (Gibco™) with 1% Penicillin/Streptomycin (Gibco™) and were used for subsequent experiments.

2.2.12. Recombinant tau preparation

Plasmids containing human wild-type (2N4R) tau were kindly provided by Dr. Christina Ising (Ising et al., 2019). Briefly, the plasmids were transformed into BL21(DE3) E. coli (Agilent). Single colonies were scaled up to recommended growth density and tau expression was induced by IPTG (Merck) addition. The induced bacteria were harvested after 3 h, centrifuged, and the pellets were resuspended in BRB-80 (80 mM PIPES (Carl-Roth), 1 mM magnesium sulfate (Carl-Roth), 1 mM EGTA (Carl-Roth), pH 6.8) containing 0.1% 2-mercaptoethanol (Carl-Roth) and 1 mM PMSF (Thermo Scientific™). The resuspended bacterial pellets were sonicated, centrifuged, and the tau-containing supernatant was collected. This supernatant was boiled for 10 min at 95 °C and centrifuged at 3810 X g to remove contaminants. The recombinant tau in the supernatants was captured using a cation exchange chromatography column after which the column was washed with BRB-80 containing 0.1 % 2-mercaptoethanol. The captured tau was eluted from the column using BRB-80 with 0.1 % 2-mercaptoethanol containing an increasing concentration of sodium chloride. Each eluted fraction was tested for the presence of tau using a Coomassie gel stain. The buffer in the combined tau-containing fractions was replaced with 10 mM ammonium bicarbonate (Carl-Roth) using Amicon ultra centrifugal units (10-kDa molecular weight cut-off) (Merck). Multiple rounds of buffer replacement were done to ensure the efficient removal of all the endotoxins. The final concentrated tau was harvested from the columns, quantified using BCA assay (Thermo Fisher Scientific), aliquoted, dried using speed-vac, and stored at –80 °C until usage in experiments. Tau proteins were resuspended in SFM right before stimulation and each preparation was tested for endotoxin levels with an endotoxin quantification kit (Pierce) following the manufacturer’s instructions.

2.2.13. Amyloid β ($Aβ_{42}$) fibrilization for stimulation

Amyloid $β_{(1-42)}$ (HFIP-treated) was purchased from Bachem (Cat. No. 4090148). Briefly, $Aβ_{42}$ peptides were dissolved in DMSO (Carl-Roth) to get 5 mM stock. The $Aβ_{42}$ stock was further diluted to 100 µM in individual tubes, which were allowed to fibrilize in the incubator at 37 °C for 24 h. The fibrilized $Aβ_{42}$ was stored at –80 °C until use in stimulation experiments.

2.2.14. TAMRA-Amyloid β ($Aβ_{42}$) fibrilization for phagocytosis

TAMRA-labeled β-$Amyloid_{(1-42)}$ (Anaspec, AS-60476) were dissolved in 10 mM NaOH (Carl-Roth). The stock was diluted to 50 µM in 50 mM Tris (Carl-Roth) pH 7 in individual tubes and aged in the incubator at 37 °C for 24 h. The fibrilized TAMRA-$Aβ_{42}$ were stored at –80 °C until use in phagocytosis experiments.

2.2.15. Amyloid phagocytosis

WT, Tyro3OE, and AxlOE cells in RPMI 1640 Medium, GlutaMAX™ Supplement (Gibco™) with 1% Penicillin/Streptomycin (Gibco™) (serum-free medium, SFM) were seeded at 80000 cells/ well in Nunc™ MicroWell™ 96 wells black cell culture plates (Thermo Scientific™). After overnight 50 nM PMA stimulation, the cells were washed with warm DPBS (Gibco™) and treated with or without 2 µM Tau in SFM for 3 h. Afterward, the cells were exposed to 0.25 µM TAMRA-$Aβ_{42}$ for 4 h. Then the solution was discarded and replaced with 0.2 % Trypan blue solution (Sigma-Aldrich) and incubated for one min to quench the extracellular fluorescence. The solution was discarded and the plates containing the cells were read on a TECAN plate reader Infinite M200 PRO (TECAN) at 540 nm excitation and 585 nm emission. To account for deviations in cell seeding, the cells were incubated in 25 µg/mL Hoechst 33342 (Thermo Scientific™) in DPBS + 0.1 % Triton X-100 (Carl-Roth) for 15 min in the dark. The plates were then read at 360 nm excitation and 418 nm emission. The TAMRA reading was then normalized to the Hoescht reading for each well. The percentage of $Aβ_{42}$ phagocytosis was expressed relative to the control cells.

2.2.16. Tau + $A\beta_{42}$ -induced inflammasome activation

WT, Tyro3OE, and AxlOE cells in SFM were seeded at 1 X 10^5 cells/ well in 96-well, and 1 X 10^6 cells/ well in 12-well Cell Culture Multiwell Plates (Greiner Bio-One). After overnight 50 nM PMA stimulation, the cells were washed with warm DPBS (Gibco™) and treated with or without 0.1 µM tau monomers in SFM for 3 h. Following tau treatment, the cells were exposed to 5 µM $A\beta_{42}$ fibrils (Bachem) for 24 h. The supernatants and cells were further processed for ELISA, Western blotting, and RT-PCR.

2.2.17. Nigericin-induced inflammasome activation

WT, Tyro3OE, and AxlOE cells in SFM were seeded at 1 X 10^5 cells/ well in 96-well, 1 X 10^6 cells/ well in 12-well, and 2 X 10^6 cells/ well in 6-well Cell Culture Multiwell Plates (Greiner Bio-One). After overnight 50 nM PMA stimulation, the cells were washed with warm DPBS (Gibco™) and treated with or without 100 nM Lipopolysaccharide from Escherichia coli K12 (LPS) (InvivoGen) in SFM for 3 h. Pyroptotic cell death was induced by adding 10 µM Nigericin (InvivoGen) and incubating for 45 min. The supernatants and cells were further processed for ELISA, Western blotting, and RT-PCR.

2.2.18. JAK1/2 inhibitor and inflammasome activation

WT, Tyro3OE, and AxlOE cells in SFM were seeded at 2 X 10^6 cells/ well in 6-well Cell Culture Multiwell Plates (Greiner Bio-One). After overnight 50 nM PMA stimulation, the cells were washed with warm DPBS (Gibco™) and treated with or without 10 µM Ruxolitinib (MedChemExpress) in SFM for 24 h. The following day, the cells were washed with warm DPBS (Gibco™) and treated with or without 100 nM Lipopolysaccharide from Escherichia coli K12 (LPS) (InvivoGen) in SFM for 3 h. 10 µM Nigericin (InvivoGen) was used to induce inflammasome activation. The supernatants and cells were further processed for ELISA, Western blotting, and RT-PCR.

2.2.19. Quantification of cytokines and soluble receptors

Cytokines and soluble receptors release was determined using the human IL-1 beta/IL-1F2 DuoSet ELISA (DY201, R&D Systems), human TNF-α DuoSet ELISA (DY210, R&D Systems), human Tyro3 DuoSet ELISA (DY859, R&D Systems), human Axl DuoSet ELISA (DY154, R&D Systems). Quantification of the proteins in the cell culture

supernatants was performed according to the manufacturer's protocol. Colorimetric measurements were made at 450 nm using a microplate reader (Infinite M200, Tecan). Sample concentrations of cytokines and soluble receptors were determined by interpolation of the values from the corresponding standard curve.

2.2.20. RNA isolation and RT-PCR

RNA extraction and purification were performed according to the manufacturer's protocol for the RNeasy Micro kit (Qiagen). The yield of the purified RNA was measured using a Nanodrop (Thermo Scientific). For cDNA synthesis, 400 ng of RNA was incubated with cDNA master mix (10X RT buffer, 25X dNTP Mix (100 mM), 10X Random Primers, and 50 U Multiscribe Reverse Transcriptase) (Thermo Scientific) to a total volume of 40 µL in RNAse free PCR tubes (Thermo Scientific). The PCR tubes containing the sample mixture were loaded onto a thermal cycler (Eppendorf) and run according to a predefined program mentioned in **Table 14**:

Cycles	Temperature	Time (mm:ss)
1	25	10:00
1	37	120:00
1	85	5:00
1	4	infinity

Table 14: cDNA synthesis program

For quantitative RT-PCR, the TaqMan Gene Expression Assay kit was used. Briefly, 2 µL of cDNA was mixed with TaqMan master mix containing 2X TaqMan gene expression Mix, 1 µL 18S rRNA primer, and 1 µL Gene primer of interest in a 96-well PCR plate. The human TaqMan probes used for this assay are (ThermoFisher): NLRP3 Hs00918082_m1, PYCARD Hs01547324_gH, CASP1 Hs00354836_m1, IL1B Hs01555410_m1, IL18 Hs01038788_m1, GSDMD Hs00986748_g1, TLR4 Hs00152939_m1, REL Hs00968440_m1, RELA Hs00153294_m1, RELB Hs00232399_m1, NFKB1 Hs00765730_m1, NFKB2 Hs01028901_g1, SOCS3 Hs02330328_s1, and SOCS1 Hs00705164_s1. The plate was loaded into Applied Biosystems StepOne Real-Time PCR and the program described in **Table 15** was run:

Cycles	Temperature °C	Time (mm:ss)
1	50	2:00
1	95	10:00
40	95	0:15
	60	0:30

Run: Standard; 48-/96- well fast; Reaction volume: 20 µL; Ramp Speed: Standard

Table 15: TaqMan Gene expression Assay

Relative gene expression was calculated using the ΔΔCt method through the 18S ribosomal RNA as a constitutive gene. The gene expression of TAM overexpressing cells was then reported as a fold-change relative to the control THP-1 cells.

2.2.21. Western Blotting

After the stimulation experiment in a 6-well plate, the cells were washed with PBS and processed for lysis. Ice cold RIPA buffer (50 mM Tris-HCl, 1 % Triton X-100, 0.5 % sodium deoxycholate, 0.1 % sodium dodecyl sulfate (SDS), 150 mM sodium chloride, pH 8.0) containing 1X Halt's protease inhibitor (Thermo Scientific) was directly added onto the cells and the plates were incubated in a plate shaker for 20 min at 4 °C. The lysed cells were then scraped using a rubber policeman and collected into a centrifuge tube. The lysate was further incubated in ice for 10 min with intermittent mixing. Then, the lysates were centrifuged at 20,000 X g for 15 min at 4 °C and the clear supernatants were collected. The protein concentration was determined using the Pierce™ BCA Protein Assay Kit (Thermo Scientific). An equal amount of lysate protein was prepared, denatured at 95 °C, and loaded in a NuPAGE® 4 % – 12 % Bis-Tris Gel (Invitrogen, Thermo Fisher Scientific) for SDS gel electrophoresis-mediated separation.

Proteins from the cell culture supernatants were precipitated as described previously. Briefly, 500 µL supernatant was mixed with 500 µL of ice-cold methanol and 125 µL chloroform. After centrifugation at 13000 X g for 5 min at 4 °C, the aqueous phase was discarded, and the remaining phase was mixed with 500 µL ice-cold methanol. The mixture was centrifuged at 13000 X g for 5 min at 4 °C and the pellet was dried, dissolved in 2X loading buffer, and denatured at 95 °C before loading into the gel.

The separated proteins were transferred from the gel to a 0.2 µm Nitrocellulose membrane using the Trans-Blot Turbo system (BIO-RAD). The membranes were washed with Tris-buffered saline containing Tween-20 (TBST, 10 mM Tris-HCl, 150 mM NaCl, 0.05 % Tween-20, pH 8.0). The membranes were then blocked using 3 % BSA in TBST for 1 h at RT. Then, the membranes were incubated overnight at 4 °C in primary antibodies **(Table 8)** mouse anti-IL-1β (1:1000; R&D), mouse anti-Caspase-1 (1:1000; Bally-1, Adipogen), rabbit anti-NLRP3 (1:1000; Abcam), rabbit anti-ASC (1:1000; Abcam), rabbit anti-Gasdermin-D (1:1000; Cell Signaling Technologies), rabbit anti-STAT1 (1:1000; Cell Signaling Technologies), rabbit anti-phospho-STAT1 (1:1000; Cell Signaling Technologies), rabbit anti-SOCS1 (1:750; Abcam), rabbit anti-NF-κB (1:1000; Cell Signaling Technologies), rabbit anti-phospho-NF-κB (1:1000; Cell Signaling Technologies), mouse anti-Tyro3 antibody (1:1000; R&D), mouse anti-Axl antibody (1:1000; R&D), mouse anti-Lamin B1 (1:1000; Abcam), and mouse anti-β-actin (1:5000; Invitrogen). The membranes were then washed for 5 min; three times with TBST, and then incubated in secondary antibodies IRDye® 800CW Goat anti-Rabbit IgG (1:20,000 in 3 % BSA-TBST; LI-COR Biosciences), IRDye® 800CW Goat anti-Mouse IgG (1:20,000 in 3 % BSA-TBST; LI-COR Biosciences), IRDye® 680LT Goat anti-Rabbit IgG (1:20,000 in 3 % BSA-TBST; LI-COR Biosciences) and IRDye® 680LT Goat anti-Mouse IgG (1:20,000 in 3 % BSA-TBST; LI-COR Biosciences) for 1 h at RT. Membranes were washed and then visualized with the Odyssey CLx Imaging System (LI-COR Biosciences) and the intensity was quantified using Image Studio (LI-COR Biosciences).

2.2.22. Immunocytochemistry on differentiated neurons stimulated with conditioned medium from THP-1 cells

For this experiment, WT control, Tyro3OE, and AxlOE cells were stimulated using LPS (3 h) and Nigericin (45 min), harvested the conditioned medium, sterile-filtered, and frozen at -80 °C until the neuron stimulation experiments. Retinoic acid-differentiated SH-SY5Y neurons were used to check the effects of the conditioned medium on neurons. After 7 days of differentiation, the differentiation medium was replaced by the serum-free medium in DMEM overnight. The following day, the neurons were washed, and the conditioned medium from WT control, Tyro3OE, and AxlOE cells was applied to the neurons and left in the incubator for 45 min. Then, the neurons were washed and proceeded with

immunocytochemistry. Briefly, the cells were washed with PBS 3 times after which the cells were fixed in 4 % PFA for 10 min with gentle rocking. Then, the fixed cells were washed with PBS 3 times followed by blocking in the blocking buffer (3 % BSA/ 5 % Goat serum in PBS + 0.01 % Triton X 100) for 1 h at RT. After blocking the cells were exposed to the primary antibody in a blocking solution and incubated in a cold room at 4 °C with gentle rocking overnight. The following day the cells were washed three times with PBST and then the secondary antibody diluted in the blocking buffer was applied and incubated for 1 h at RT with gentle rocking. Afterward, the slides were washed with PBS-T 3 times, followed by a rinse in Milli-Q water. Then the coverslips were mounted onto a microscopic slide using the Prolong DAPI Gold mountant. The slides were incubated at RT at dark overnight for the mountant to dry and harden. The slides were then proceeded with confocal microscopy.

2.2.23. Statistics for *in vitro* experiments

All statistical analyses were performed in GraphPad Prism 9.0 (GraphPad software). All data were presented as Mean ± SEM in the figures. The data points shown were from individual experiments where N indicates the number of independent experiments performed. One-way ANOVA for column datasets and two-way ANOVA for grouped datasets were performed with Post-Hoc tests (Dunnet's for one-way and Tukey's for two-way ANOVA) in order to determine the multiple comparison effects. Outliers were removed based on the ROUT test (Q = 1 %). The significance level of the p-values were indicated as * $p < 0.05$, * $p < 0.01$, ***$p < 0.001$, ****$p < 0.0001$

3. Results

3.1. Inflammatory biomarkers are elevated in the cerebrospinal fluid samples from dementia subjects

3.1.1. A brief overview of the rationale

In this chapter, the effects of pathological amyloid-β levels, pathological total-tau levels, and clinical diagnosis of dementia subjects on the inflammatory biomarkers in the cerebrospinal fluid were investigated. Although in the recent study, pathological phospho-tau was used as the indicator for T+ subjects, in this thesis, total-tau was used to stratify the subjects (Brosseron et al., 2022). The reason is that phospho-Tau and total Tau correlate with each other and the presence of any form of tau (phosphorylated or not) is sufficient to cause an inflammatory response.

Here, the 15 biomarkers that were measured manually in the DELCODE and F.ACE cohort and also the measurements made through the Olink® panel for the DELCODE cohort were analyzed. First, the reliability of the Olink® panel as a biomarker platform was verified by correlating the DELCODE Olink® measurements with its manual measurements. Then, group-based analysis were performed for the A/T scheme and Diagnosis/T schemes including associations with the covariates age, sex, BMI, and *APOE4* for all the cohorts. Key covariates that influence these inflammatory biomarkers were identified and the covariate-adjusted ANCOVA analysis was performed for these markers in Tau+ subjects.

3.1.2. Verifying Olink® measurements

Before starting the proteomic analysis using Olink® measurement, the reliability of this platform had to be verified. For this purpose, the measurements of proteins that were measured on both platforms were correlated. Except for complement factor C4 and CRP, all other 13 biomarkers overlap in both panels and were used for this correlation. Spearman's correlation analysis was performed for this dataset which revealed a strong correlation between the manual and Olink® measurements for the DELCODE cohort (**Figure 7**). In particular, the correlation with the Amyloid and tau markers was similar in the case of manual and Olink® measurements, validating the application of this extensive

biomarker panel. This concludes that Olink® is a reliable platform for further analysis of proteins that were not measured through manual platforms.

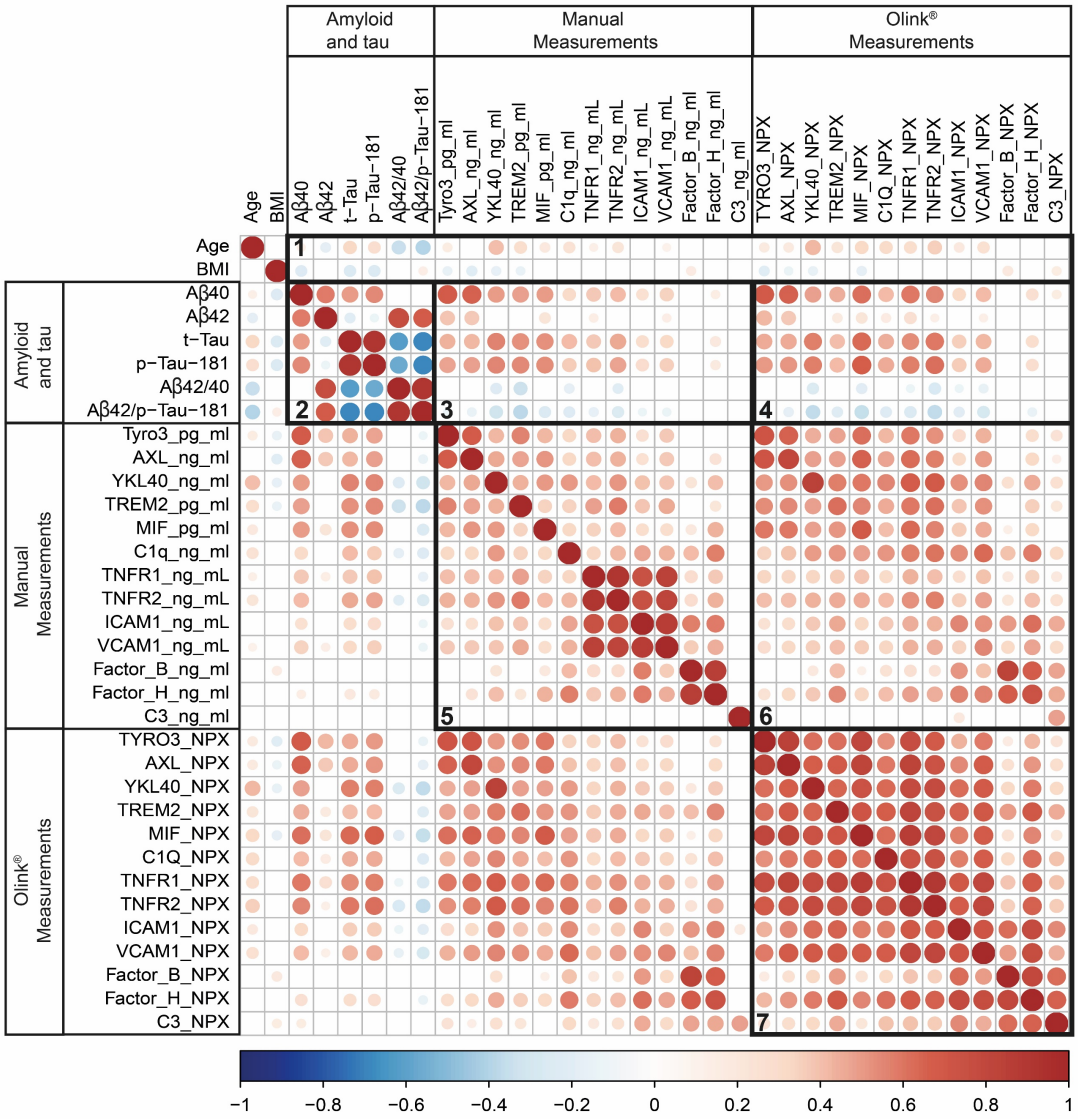

Figure 7: Correlation plot for DELCODE manual measurements vs Olink® measurements

13 overlapping proteins in manual and Olink® measurements were correlated with each other and Amyloid/Tau markers. The colour bar represents Spearman's R-value and only significant findings are reported in the figure. The correlations were (1) biomarkers with age, BMI; (2) Amyloid/Tau with Amyloid/Tau; (3) Manual measurements with Amyloid/Tau; (4) Olink measurements with Amyloid/Tau; (5) Manual measurements with manual measurements; (6) Manual measurements with Olink measurements; and (7) Olink measurements with Olink measurements. Panel 6 shows a strong correlation between manual and Olink® measurements (Diagonal).

3.1.3. Inflammatory biomarkers are elevated in the Tau-positive subjects irrespective of the amyloid status

Firstly, the effects on the biomarkers by pathological amyloid levels **(Table 12)** with pathological tau levels **(Table 12)** were examined in three measurements, (i) DELCODE manual, (ii) DELCODE Olink®, and (iii) F.ACE manual (A/T scheme). All analyses were performed in R software. The detailed results containing ANCOVA analysis and significant covariates are listed separately for the DELCODE manual **(Table 16)**, DELCODE Olink® **(Table 17)**, and F.ACE manual **(Table 18).** For the sake of simplicity and relevance for the thesis, only Tyro3 and Axl from each measurement platform were selected and visualized as boxplots using ggplot2 in R software **(Figure 8)**.

Briefly, in DELCODE manual measurements, the majority of the inflammatory biomarkers were significantly increased in the T+ subjects. All proteins except complement factor C3, factor B, and CRP showed significance after co-variate adjusted ANCOVA analysis for A/T scheme **(Table 16)**. Age was the predominant covariate that influenced MIF, C1q, YKL-40, TREM2, and TNFR2 levels in subjects. Other covariates like sex influenced C1q only, bmi influenced Factor B and CRP, and *APOE4* status influenced TREM2 only in these subjects.

In DELCODE Olink® measurements, the findings were completely reproduced that all proteins except complement factor C3 and factor B were significant for co-variate adjusted ANCOVA analysis for A/T scheme (C4 and CRP were not available in Olink® panel) **(Table 17)**. Interestingly, age was found to be a significant co-variate impacting all 13 proteins measured through the Olink® panel. Similarly, sex was found to be a significant co-variate in all proteins except Tyro3, MIF, and TREM2 whereas, BMI significantly influenced Tyro3, C3, Factor B, Factor H, and ICAM1. *APOE4* status showed no significant impact on the proteins measured through the Olink® panel in the DELCODE cohort.

Lastly, in F.ACE manual measurements, there was a significant p-value for co-variate adjusted ANCOVA analysis for all proteins including C3 and factor B, except for CRP **(Table 18)**. Similar to the DELCODE Olink® results, age was significantly influencing all proteins, except Tyro3 and Axl in the F.ACE cohort. Sex impacted C1q, C4, factor B, factor H, TNFR2, ICAM1, and VCAM1 significantly, whereas bmi impacted C4, factor B, factor

H, ICAM1, and CRP. *APOE4* status influenced only ICAM1, VCAM1, and CRP in the F.ACE cohort.

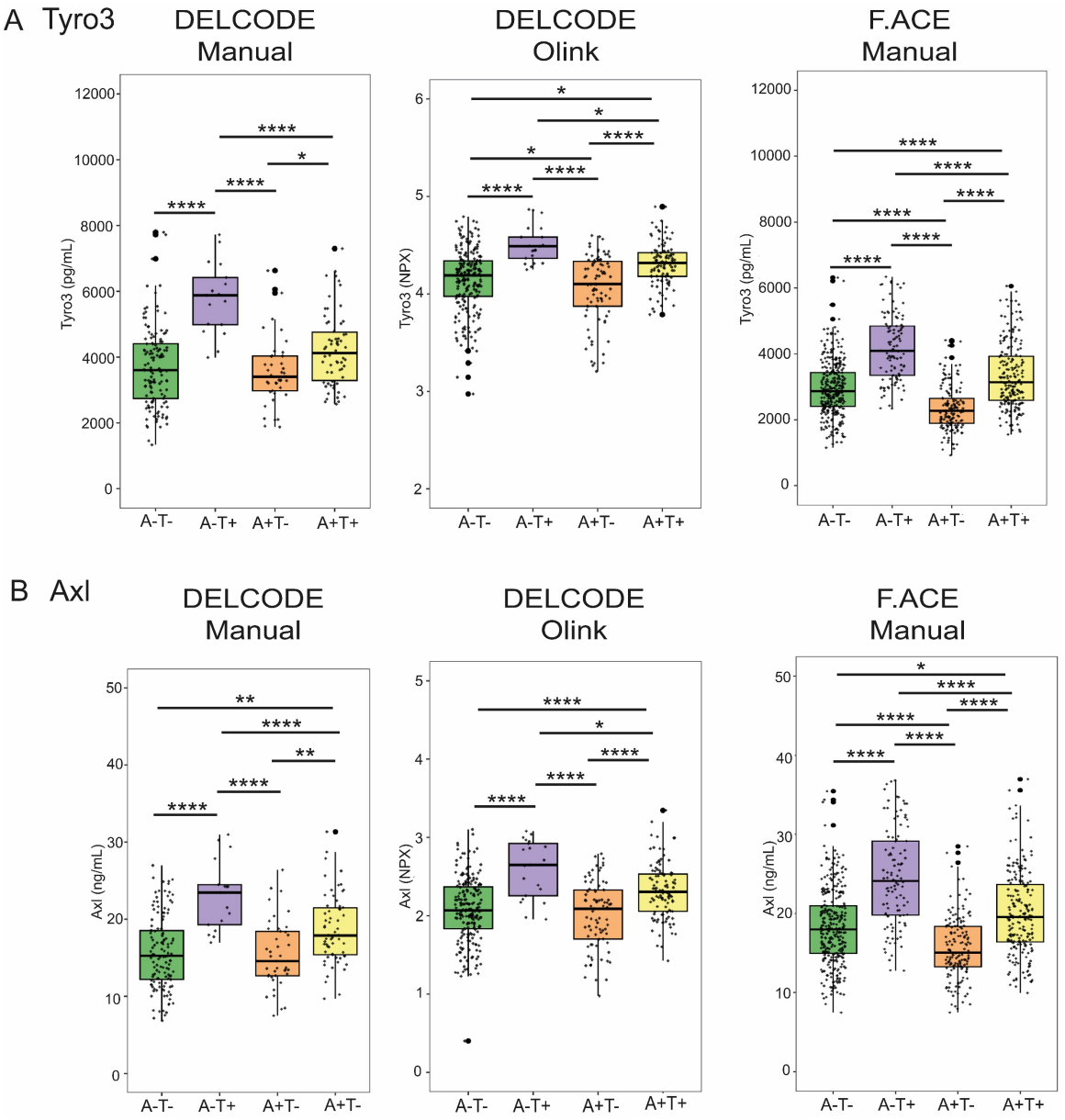

Figure 8: Inflammatory biomarkers stratified with A/T scheme
(A) Tyro3 and **(B)** Axl from DELCODE manual measurements (N= A-T- (147), A-T+ (20), A+T- (45), A+T+ (80), Kruskal-Wallis test, * $p < 0.05$, ** $p < 0.01$, *** $p < 0.001$, **** $p < 0.0001$), DELCODE Olink® measurements (N= A-T- (216), A-T+ (21), A+T- (83), A+T+ (106), Kruskal-Wallis test, * $p < 0.05$, ** $p < 0.01$, *** $p < 0.001$, **** $p < 0.0001$), and F.ACE manual measurements (N= A-T- (314), A-T+ (112), A+T- (152), A+T+ (204), Kruskal-Wallis test, * $p < 0.05$, ** $p < 0.01$, *** $p < 0.001$, **** $p < 0.0001$), stratified with A/T scheme. Most of the biomarkers are significantly elevated in the Tau+ subjects irrespective of Amyloid status.

. **Table 16. DELCODE manual – A/T scheme**

Marker	A-T-	A-T+	A+T-	A+T+	Kruskal-Wallis	Covariates	ANCOVA
N	147	20	45	80	*p*-value	*p*-value	*p*-value
Tyro3 (pg/mL)	3601.7 ± 1212.4, 7796.1 - 1334.5	5874.1 ± 1089.6, 7722.2 - 3986.6	3404.5 ± 1074.2, 6630.0 - 1874.8	4124.0 ± 1120.2, 7298.3 - 2568.9	A- T+ > A- T- < 0.0000001 A+ T- > A- T+ < 0.0000001 A+ T+ > A- T+ 0.0001263 A+ T+ > A+ T- 0.0436571	-	$p < 0.0000001$
Axl (ng/mL)	15.3 ± 4.7, 27.0 - 6.8	23.5 ± 4.5, 31.0 - 17.0	14.6 ± 4.4, 26.4 - 7.5	17.9 ± 4.5, 31.3 - 9.7	A- T+ > A- T- < 0.0000001 A+ T+ > A- T- 0.0018729 A+ T- > A- T+ 0.0000072 A+ T+ > A- T+ 0.020651 A+ T+ > A+ T- 0.009922	-	$p < 0.0000001$
MIF (pg/mL)	8987.4 ± 3227.4, 17800.4 - 2213.9	14078.2 ± 3474.8, 20223.5 - 7596.7	8373.4 ± 2432.3, 15127.3 - 4626.9	11467.4 ± 3383.9, 19807.8 - 5223.7	A- T+ > A- T- < 0.0000001 A+ T+ > A- T- 0.0008856 A+ T- > A- T+ <0 .0000001 A+ T+ > A- T+ 0.0211803 A+ T+ > A+ T- 0.0000241	Age 0.0421843	$p < 0.0000001$
C1q (ng/mL)	180.9 ± 53.8, 354.1 - 62.7	268.6 ± 70.6, 410.2 - 129.0	192.5 ± 71.0, 387.9 - 110.8	213.6 ± 56.7, 364.4 - 104.1	A- T+ > A- T- 0.0000274 A+ T- > A- T+ 0.0008508 A+ T+ > A- T+ 0.008851	Age 0.0064063, sex 0.0000701	$p = 0.0000550$
YKL-40 (ng/mL)	299.9 ± 104.1, 592.9 - 91.4	466.9 ± 104.9, 712.6 - 288.3	318.4 ± 120.2, 747.8 - 154.3	402.1 ± 146.4, 784.1 - 159.6	A- T+ > A- T- 0.0000729, A+ T+ > A- T- 0.0042834 A+ T- > A- T+ 0.0001562 A+ T+ > A+ T- 0.0012457	Age 0.0000001	$p = 0.0000003$
TREM2 (pg/mL)	5521.9 ± 1159.3, 8350.3 - 2736.9	7392.4 ± 945.3, 9091.2 - 5573.6	6403.7 ± 1161.8, 8665.0 - 3294.2	6742.6 ± 1391.8, 10348.4 - 3840.6	A- T+ > A- T- 3E-7 A+ T+ > A- T- 0.0085359 A+ T- > A- T+ 0.0001224 A+ T+ > A- T+ 0.0185517	Age 0.0202887, *APOE* 0.0000007	$p < 0.0000001$
C3 (ng/mL)	630.5 ± 593.7, 2565.4 - 140.6	505.8 ± 952.0, 3937.0 - 169.8	788.7 ± 775.1, 3698.6 - 171.5	605.7 ± 756.9, 4098.8 - 158.1	-	-	-
C4 (ng/mL)	512.4 ± 197.6, 1216.7 - 194.0	650.3 ± 201.2, 1034.9 - 349.0	566.9 ± 153.9, 990.3 - 240.3	576.9 ± 199.2, 1018.6 - 204.3	A+ T- > A- T+ 0.0427772	-	$p = 0.0260016$
Factor B (ng/mL)	476.9 ± 223.6, 1236.7 - 128.7	565.9 ± 225.5, 1043.2 - 246.5	468.7 ± 173.5, 862.1 - 153.9	472.1 ± 210.9, 1120.9 - 187.2	-	bmi 0.0049661	-

Factor H (ng/mL)	487.7 ± 176.2, 1109.9 - 200.8	649.1 ± 139.5, 814.3 - 408.2	513.7 ± 132.7, 766.5 - 265.3	545.1 ± 170.6, 904.5 - 204.8	A- T+ > A- T- 0.0225143 A+ T- > A- T+ 0.0053216	-	p = 0.0061891
TNFR1 (ng/mL)	0.7 ± 0.2, 1.7 - 0.3	1.0 ± 0.2, 1.3 - 0.8	0.7 ± 0.2, 1.4 - 0.5	0.9 ± 0.2, 1.5 - 0.5	A- T+ > A- T- 0.0000835 A+ T+ > A- T- 0.0004435 A+ T- > A- T+ 0.0004397 A+ T+ > A+ T- 0.0005625	-	p < 0.0000001
TNFR2 (ng/mL)	1.3 ± 0.4, 3.1 - 0.5	1.7 ± 0.3, 2.4 - 1.2	1.4 ± 0.3, 2.3 - 0.9	1.7 ± 0.5, 2.8 - 0.8	A- T+ > A- T- 0.0005768 A+ T+ > A- T- 0.0004104 A+ T- > A- T+ 0.0102221 A+ T+ > A+ T- 0.0064958	Age 0.0028220	p = 0.0000019
ICAM1 (ng/mL)	4.1 ± 1.6, 11.0 - 2.1	5.7 ± 1.3, 8.4 - 3.4	4.3 ± 1.3, 7.3 - 2.2	4.7 ± 1.7, 10.4 - 2.2	A- T+ > A- T- 0.0036816 A+ T- > A- T+ 0.0055263	-	p = 0.0010341
VCAM1 (ng/mL)	8.5 ± 3.1, 19.5 - 3.5	11.0 ± 2.2, 14.7 - 6.9	9.1 ± 2.5, 16.0 - 5.4	9.5 ± 3.2, 19.9 - 4.7	A- T+ > A- T- 0.0155252 A+ T- > A- T+ 0.0228538,	-	p = 0.0064751
CRP (ng/mL)	2738.4 ± 5764.2, 37843.6 - 279.2	2538.7 ± 6101.3, 21631.9 - 666.4	2627.2 ± 6629.7, 33836.9 - 290.5	1929.4 ± 5523.2, 28026.6 - 177.6	-	bmi 0.0083181	-

Table 16: DELCODE manual – A/T scheme

Inflammatory biomarkers measured in the manual panels were stratified with A/T ($A\beta_{42}$/ $A\beta_{40}$ ratio / t-tau) scheme groups of DELCODE subjects represented by median ± standard deviation, maximum and minimum value. Differences between subject groups were tested by the non-parametric Kruskal-Wallis test, followed by ANCOVA with all 4 covariates (age, sex, BMI, and *APOE4*). Significant covariates that influence the biomarkers were identified, and a co-variate adjusted ANCOVA *p*-values for the group comparisons were reported for each biomarker

.Table 17: DELCODE OLINK– A/T scheme

Marker	A-T-	A-T+	A+T-	A+T+	Kruskal-Wallis	Covariates	ANCOVA
N	216	21	83	106	*p*-value	*p*-value	*p*-value
Tyro3 (NPX)	4.2 ± 0.3, 4.8 - 3.0	4.5 ± 0.2, 4.9 - 4.2	4.1 ± 0.3, 4.6 - 3.2	4.3 ± 0.2, 4.9 - 3.8	A- T+ > A- T- 0.000008, A+ T- > A- T- 0.0297988, A+ T+ > A- T- 0.0139546, A+ T- > A- T+ < 0.0000001, A+ T+ > A- T+ 0.0248858, A+ T+ > A+ T- 2E-7	Age 0.0076702, bmi 0.0308007	*p* < 0.0000001
Axl (NPX)	2.1 ± 0.4, 3.1 - 0.4	2.6 ± 0.4, 3.1 - 2.0	2.1 ± 0.4, 2.8 - 1.0	2.3 ± 0.4, 3.3 - 1.4	A- T+ > A- T- 6E-7, A+ T+ > A- T- 0.0009651, A+ T- > A- T+ < 0.0000001, A+ T+ > A- T+ 0.0199348, A+ T+ > A+ T- 7E-7	Age 0.0188864, sex 0.0041862	*p* < 0.0000001
MIF (NPX)	4.1 ± 0.5, 5.2 - 2.3	4.8 ± 0.3, 5.3 - 4.3	4.1 ± 0.4, 4.8 - 3.1	4.6 ± 0.4, 6.0 - 3.6	A- T+ > A- T- < 0.0000001, A+ T+ > A- T- < 0.0000001, A+ T- > A- T+ < 0.0000001, A+ T+ > A+ T- < 0.0000001	Age 0.0000003	*p* < 0.0000001
C1q (NPX)	-2.1 ± 0.4, -0.9 - - 3.4	-1.7 ± 0.3, -1.1 - - 2.5	-2.0 ± 0.4, -1.0 - - 3.2	-1.8 ± 0.4, -1.1 - - 2.7	A- T+ > A- T- 0.0088867, A+ T+ > A- T- 0.0014244, A+ T- > A- T+ 0.0020608, A+ T+ > A+ T- 0.0000273	Age < 0.0000001, sex 0.0129744	*p* = 0.0000006
YKL-40 (NPX)	5.5 ± 0.4, 6.4 - 4.0	6.0 ± 0.3, 6.6 - 5.1	5.6 ± 0.4, 6.7 - 4.6	6.0 ± 0.5, 7.1 - 4.6	A- T+ > A- T- 0.0000435, A+ T+ > A- T- < 0.0000001, A+ T- > A- T+ 0.0012436, A+ T+ > A+ T- 2E-7	Age < 0.0000001, sex 0.0322281	*p* < 0.0000001
TREM2 (NPX)	2.6 ± 0.7, 4.4 - 0.6	3.5 ± 0.6, 4.6 - 1.6	2.8 ± 0.7, 4.1 - 0.3	3.1 ± 0.8, 4.8 - 1.0	A- T+ > A- T- 0.0000073, A+ T+ > A- T- 0.000042, A+ T- > A- T+ 0.0001882, A+ T+ > A+ T- 0.0011905	Age 0.0004477	*p* < 0.0000001

C3 (NPX)	1.2 ± 0.6, 2.9 - -0.4	1.2 ± 0.6, 2.6 - -0.5	1.3 ± 0.7, 3.3 - -0.4	1.3 ± 0.6, 2.8 - 0.0	-	Age 0.0147851, sex 0.0007470, bmi 0.0003843	-
Factor B (NPX)	1.9 ± 0.5, 3.4 - 0.3	2.0 ± 0.4, 2.5 - 1.0	2.0 ± 0.6, 2.9 - 0.3	1.9 ± 0.5, 3.0 - 0.8	-	sex 0.0207012, bmi 0.0000049	-
Factor H (NPX)	1.8 ± 0.4, 3.0 - 0.8	2.2 ± 0.4, 2.9 - 0.8	1.8 ± 0.5, 3.0 - 0.6	2.0 ± 0.4, 3.0 - 1.1	A- T+ > A- T- 0.00689, A+ T+ > A- T- 0.0084024, A+ T- > A- T+ 0.00359, A+ T+ > A+ T- 0.0009491	Age 0.0009513, sex 0.0000002, bmi 0.0004057	p = 0.0000129,
TNFR1 (NPX)	3.1 ± 0.4, 3.9 - 1.9	3.6 ± 0.3, 4.2 - 3.0	3.2 ± 0.4, 3.9 - 2.3	3.5 ± 0.4, 4.5 - 2.6	A- T+ > A- T- 3E-7, A+ T+ > A- T- 6E-7, A+ T- > A- T+ < 0.0000001 A+ T+ > A+ T- < 0.0000001	Age 0.0000023, sex 0.0082013	p < 0.0000001
TNFR2 (NPX)	1.0 ± 0.4, 1.8 - -0.2	1.4 ± 0.3, 1.9 - 0.9	1.1 ± 0.4, 1.9 - 0.0	1.5 ± 0.4, 2.5 - 0.6	A- T+ > A- T- 0.000005, A+ T+ > A- T- < 0.0000001 A+ T- > A- T+ 0.0000092, A+ T+ > A+ T- < 0.0000001	Age < 0.0000001, sex 0.0001911	p < 0.0000001
ICAM1 (NPX)	-3.6 ± 0.4, -2.6 - -4.7	-3.1 ± 0.4, -2.5 - -4.0	-3.5 ± 0.4, -2.5 - -4.5	-3.4 ± 0.4, -2.4 - -4.5	A- T+ > A- T- 0.000425, A+ T+ > A- T- 0.000695, A+ T- > A- T+ 0.0019748, A+ T+ > A+ T- 0.0025069	Age 0.0002438, sex 0.0059387, bmi 0.0309751	p = 0.0000010
VCAM1 (NPX)	-1.4 ± 0.4, -0.6 - -2.5	-1.1 ± 0.3, -0.5 - -1.6	-1.4 ± 0.4, -0.6 - -2.2	-1.2 ± 0.4, -0.3 - -2.0	A- T+ > A- T- 0.0000027, A+ T+ > A- T- 0.0000927, A+ T- > A- T+ 0.0000112, A+ T+ > A+ T- 0.0001	Age 0.0000019, sex 0.0000002	p < 0.0000001

.Table 17: DELCODE OLINK– A/T scheme

Inflammatory biomarkers measured in the OLINK panels were stratified with A/T ($A\beta_{42}$/ $A\beta_{40}$ ratio / t-tau) scheme groups of DELCODE subjects represented by median ± standard deviation, maximum and minimum value. Differences between subject groups were tested by the non-parametric Kruskal-Wallis test, followed by ANCOVA with all 4 covariates (age, sex, BMI, and *APOE4*). Significant covariates that influence the biomarkers were identified, and a co-variate adjusted ANCOVA *p*-values for the group comparisons were reported for each biomarker.

Table 18: F.ACE manual – A/T scheme

Marker	A-T-	A-T+	A+T-	A+T+	Kruskal-Wallis	Covariates	ANCOVA
N	314	112	152	204	*p*-value	*p*-value	*p*-value
Tyro3 (pg/mL)	2867.2 ± 821.5, 6315.3 - 1153.3	4091.7 ± 1004.2, 6341.8 - 2340.5	2270.1 ± 672.8, 4414.7 - 925.2	3138.0 ± 982.0, 6057.1 - 1555.3	A- T+ > A- T- < 0.0000001 A+ T- > A- T- 0.0000136, A+ T+ > A- T- 0.0007748, A+ T- > A- T+ < 0.0000001, A+ T+ > A- T+ 5E-7, A+ T+ > A+ T- < .0000001	-	*p* < 0.0000001
Axl (ng/mL)	18.0 ± 4.8, 35.5 - 7.5	24.1 ± 6.1, 36.8 - 12.8	15.0 ± 4.0 , 28.5 - 7.5	19.5 ± 5.2, 37.0 - 9.9	A- T+ > A- T- < 0.0000001 A+ T- > A- T- 0.0005506, A+ T+ > A- T- 0.0304666, A+ T- > A- T+ < 0.0000001 A+ T+ > A- T+ < 0.0000001 A+ T+ > A+ T- < 0.0000001	-	*p* < 0.0000001
MIF (pg/mL)	10016.3 ± 2738.7, 18353.5 - 1367.2	15171.1 ± 3234.7, 23049.4 - 8912.6	9372.5 ± 2569.5, 20884.5 - 2686.7	13482.8 ± 3424.7 , 23079.4 - 3768.3	A- T+ > A- T- < 0.0000001 A+ T+ > A- T- < 0.0000001, A+ T- > A- T+ < 0.0000001, A+ T+ > A- T+ 0.0005119, A+ T+ > A+ T- < 0.0000001	Age 0.0016475	*p* < 0.0000001
C1q (ng/mL)	208.8 ± 55.1, 405.9 - 87.2	283.0 ± 70.4, 441.2 - 163.6	192.8 ± 55.0, 369.7 - 94.4	226.1 ± 59.8, 429.9 - 93.1	A- T+ > A- T- < 0.0000001, A+ T- > A- T+ < 0.0000001 A+ T+ > A- T+ 0.0000011, A+ T+ > A+ T- 0.0000131	Age < 0.0000001, sex 0.0000002	*p* < 0.0000001
YKL-40 (ng/mL)	227.6 ± 80.5, 490.9 - 89.6	334.6 ± 100.2, 562.7 - 150.8	231.8 ± 86.4, 478.6 - 89.8	320.5 ± 94.1, 598.4 - 106.6	A- T+ > A- T- < .0000001, A+ T+ > A- T- < .0000001 A+ T- > A- T+ < .0000001 A+ T+ > A+ T- < .0000001	Age < 0.0000001	*p* < 0.0000001
TREM2 (pg/mL)	5061.8 ± 1504.0, 10577.8 - 1622.8	6472.1 ± 1973.4, 11108.2 - 2324.0	4794.9 ± 1651.2, 11153.3 - 0.0	5624.0 ± 1715.6, 10897.7 - 2402.0	A- T+ > A- T- 8E-7, A+ T- > A- T- 0.0112397, A+ T- > A- T+ < .0000001, A+ T+ > A- T+ 0.002544, A+ T+ > A+ T- 0.0000384	Age 0.0000006	*p* < 0.0000001
C3 (ng/mL)	3860.5 ± 2941.7, 16465.6 - 1186.5	5025.2 ± 3508.0, 16407.5 - 2035.7	3725.2 ± 3573.3, 16268.3 - 868.9	4204.5 ± 2924.2, 15863.0 - 1572.3	-	Age 0.0002188, sex 0.0003219	*p* = 0.0398646

C4 (ng/mL)	1183.5 ± 476.5, 2872.2 - 408.1	1379.1 ± 547.4, 3056.7 - 522.3	1078.6 ± 538.4, 2621.6 - 325.3	1219.8 ± 478.4, 2961.2 - 337.3	A- T+ > A- T- 0.0003293, A+ T- > A- T+ 0.0000574, A+ T+ > A- T+ 0.029905	Age 0.0006778, sex < 0.0000001 bmi 0.0015540	p = 0.0000455
Factor B (ng/mL)	538.0 ± 227.6, 1348.1 - 159.0	592.0 ± 224.7, 1383.2 - 186.9	505.0 ± 244.7, 1290.0 - 129.5	500.3 ± 222.9, 1329.4 - 172.9	A+ T- > A- T+ 0.0423001	Age 0.0709783, sex 0.0000023, bmi 0.0003197,	p = 0.0377293
Factor H (ng/mL)	520.3 ± 190.2, 1241.3 - 211.7	673.7 ± 201.2, 1250.7 - 305.1	485.0 ± 201.0, 1141.1 - 214.6	538.6 ± 192.9, 1184.2 - 190.6	A- T+ > A- T- 4E-7, A+ T- > A- T+ 3E-7, A+ T+ > A- T+ 0.0007338	Age 0.0000077, sex < 0.0000001 bmi 0.0008630	p < 0.0000001
TNFR1 (ng/mL)	0.5 ± 0.1, 1.0 - 0.2	0.8 ± 0.2, 1.1 - 0.4	0.5 ± 0.1, 0.9 - 0.3	0.6 ± 0.1, 1.1 - 0.3	A- T+ > A- T- < 0.0000001, A+ T+ > A- T- 0.0000471, A+ T+ > A- T+ < 0.0000001 A+ T+ > A+ T- < 0.0000001	Age < 0.0000001	p < 0.0000001
TNFR2 (ng/mL)	1.0 ± 0.3, 1.8 - 0.2	1.5 ± 0.3, 2.2 - 0.6	0.9 ± 0.3, 1.7 - 0.5	1.2 ± 0.3, 2.3 - 0.6	A- T+ > A- T- < 0.0000001, A+ T+ > A- T- 2E-7, A+ T+ > A- T+ 0.0000088, A+ T+ > A+ T- < 0.0000001	Age < 0.0000001, sex 0.0012741	p < 0.0000001
ICAM1 (ng/mL)	2.3 ± 0.7, 4.8 - 0.6	3.2 ± 0.9, 5.1 - 1.6	2.2 ± 0.8, 4.9 - 1.0	2.7 ± 0.8, 5.0 - 1.2	A- T+ > A- T- < 0.0000001, A+ T+ > A- T- 0.0000072, A+ T+ > A- T+ 0.0000718, A+ T+ > A+ T- 4E-7	Age 0.0000002, sex 0.0001967, bmi 0.0026366, *APOE4* 0.0445090	p < 0.0000001
VCAM1 (ng/mL)	6.0 ± 1.6, 12.7 - 1.7	8.4 ± 2.1, 12.8 - 4.3	5.8 ± 1.7, 10.9 - 2.0	6.6 ± 1.8, 11.9 - 2.7	A- T+ > A- T- < 0.0000001, A+ T- > A- T+ < 0.0000001 A+ T+ > A- T+ < 0.0000001 A+ T+ > A+ T- 0.0000871	Age < 0.0000001, sex 0.0000219, *APOE4* 0.0488053	p < 0.0000001
CRP (ng/mL)	4036.3 ± 7622.0, 52838.5 - 391.8	4692.5 ± 9448.2, 54967.9 - 340.5	3431.8 ± 8819.2, 57200.0 - 302.6	3459.0 ± 7178.0, 40199.4 - 163.0	-	Age 0.0622339, bmi 0.0000011, *APOE4* 0.0001354	-

Table 18: F.ACE manual – A/T scheme

Inflammatory biomarkers measured in the manual panels were stratified with A/T ($A\beta_{42}$/ $A\beta_{40}$ ratio / t-tau) scheme groups of F.ACE subjects represented by median ± standard deviation, maximum and minimum value. Differences between subject groups were tested by the non-parametric Kruskal-Wallis test, followed by ANCOVA with all 4 covariates (age, sex, BMI, and *APOE4*). Significant covariates that influence the biomarkers were identified, and a co-variate adjusted ANCOVA *p*-values for the group comparisons were reported for each biomarker.

3.1.4. Inflammatory biomarkers are elevated in the Tau-positive subjects irrespective of the clinical diagnosis

Here, the effects on the biomarkers by cognitive staging (**Table 12)** with pathological tau levels **(Table 12)** were examined in the two cohorts' measurements: (i) DELCODE Olink® and (ii) F.ACE manual (Diagnosis/T scheme). To minimize redundancy, the DELCODE manual measurements were not used for this analysis since there were similarities between these measurements in DELCODE. All analyses were performed in R software. The detailed results containing ANCOVA analysis and significant covariates are listed separately for DELCODE Olink® **(Table 19)** and F.ACE manual **(Table 20).** For the sake of simplicity and relevance for the thesis, only Tyro3 and AXL from each measurement platform were selected and visualized as boxplots using ggplot2 in R software **(Figure 9)**.

In DELCODE Olink® measurements, all proteins except complement factor C3 and Factor B were significant for co-variate adjusted ANCOVA analysis for the Diagnosis/T scheme (C4 and CRP were not available in Olink® panel) **(Table 19)**. Similarly, age was found to be a significant co-variate impacting all proteins except Factor B in the Olink® panel. Additionally, sex has significantly impacted all proteins except Tyro3, MIF, and TREM2 whereas, BMI significantly influenced Tyro3, C3, Factor B, Factor H, and ICAM1. However, *APOE4* status showed no significant impact on the proteins measured through the Olink® panel in the DELCODE cohort.

Lastly, in F.ACE manual measurements, there was a significant p-value for co-variate adjusted ANCOVA analysis for all proteins except C3, factor B, and CRP **(Table 20)**. Similar to the DELCODE Olink® results, age was significantly influencing all proteins, except Tyro3, Axl, Factor B, and CRP in the F.ACE cohort. Sex impacted C1q, C3, C4, factor B, factor H, TNFR2, ICAM1, and VCAM1 significantly, whereas bmi impacted TREM2, C4, factor B, factor H, ICAM1, and CRP. *APOE4* status influenced Axl, C1q, Factor B, TNFR1, ICAM1, VCAM1, and CRP in the F.ACE cohort.

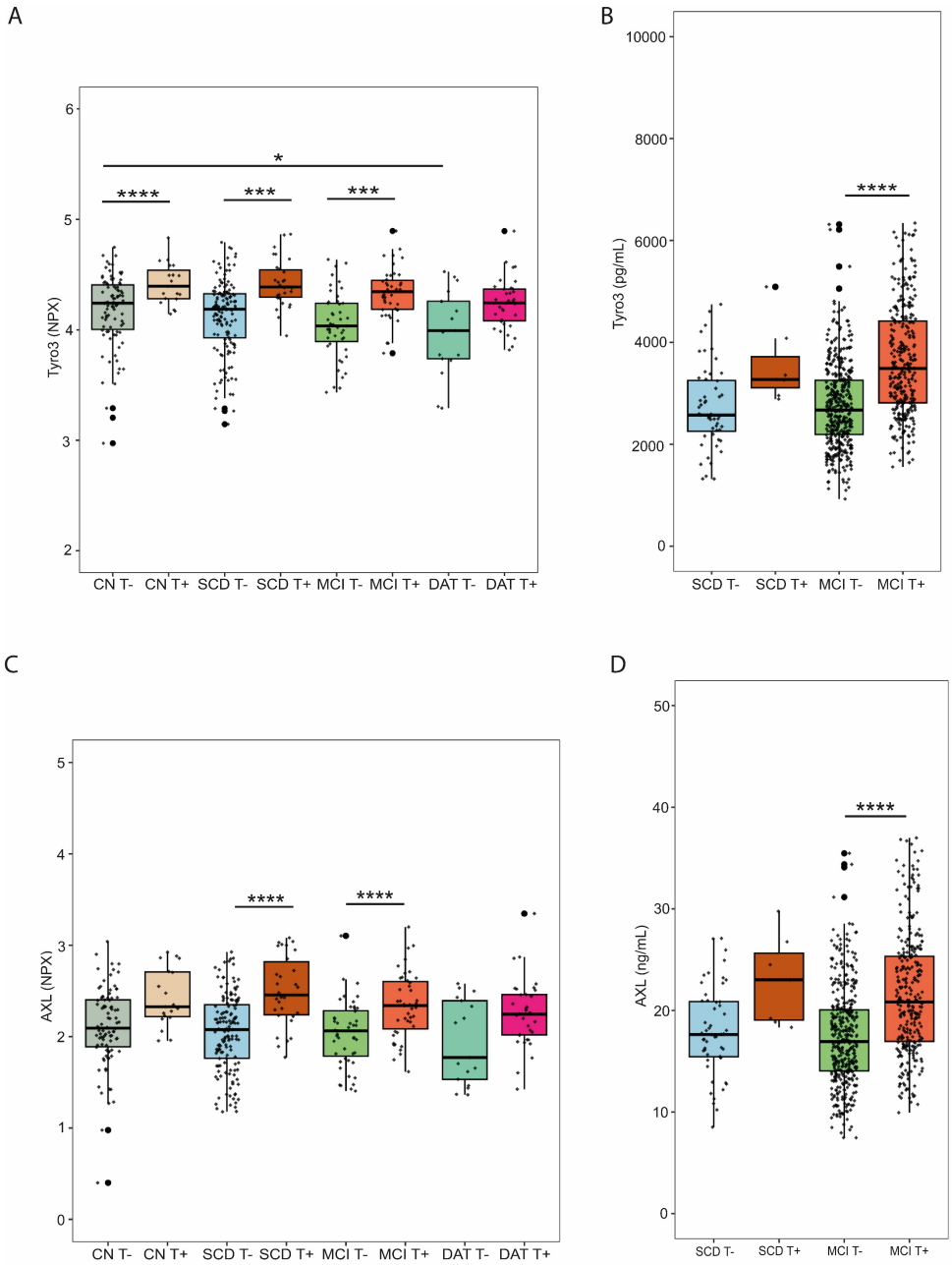

Figure 9. Inflammatory biomarkers stratified with Diagnosis + Tau scheme
Tyro3 **(A)** and Axl **(C)** from DELCODE Olink® measurements (N= CN T- (90), CN T+ (19), SCD T- (30), SCD T+ (30), MCI T- (47), MCI T+ (43), DAT T- (17), DAT T+ (35)) Kruskal-Wallis test, * $p < 0.05$, ** $p < 0.01$, *** $p < 0.001$, **** $p < 0.0001$), and Tyro3 **(B)** and Axl **(D)** from F.ACE manual measurements (N= SCD T- (52), SCD T+ (7), MCI T- (414), MCI T+ (309)) Kruskal-Wallis test, * $p < 0.05$, ** $p < 0.01$, *** $p < 0.001$, **** $p < 0.0001$), stratified with Diagnosis/T scheme. The majority of the biomarkers are significantly elevated in the Tau+ subjects irrespective of clinical diagnosis.

Table 19: DELCODE OLINK- Diagnosis/Tau scheme

Marker	CN T-	CN T+	SCD T-	SCD T+	MCI T-	MCI T+	DAT T-	DAT T+	Kruskal-Wallis	Covariates	ANCOVA
N	90	19	145	30	47	43	17	35	*p*-value	*p*-value	*p*-value
Tyro3 (NPX)	4.2 ± 0.3, 4.7 - 3.0	4.4 ± 0.2, 4.8 - 4.1	4.2 ± 0.3, 4.8 - 3.1	4.4 ± 0.2, 4.9 - 3.9	4.0 ± 0.3, 4.6 - 3.4	4.3 ± 0.2, 4.9 - 3.8	4.0 ± 0.4, 4.5 - 3.3	4.2 ± 0.2 4.9 - 3.8	DAT T- > CN T- 0.0263546, SCD T+ > SCD T- 0.0001096, MCI T+ > MCI T- 0.0003097, DAT T- > MCI T+ 0.0002529	Age 0.0012264, bmi 0.0312979	*p* < 0.0000001
Axl (NPX)	2.1 ± 0.4, 3.0 - 0.4	2.3 ± 0.3, 2.9 - 2.0	2.1 ± 0.4, 2.9 - 1.2	2.5 ± 0.4, 3.1 - 1.8	2.1 ± 0.4, 3.1 - 1.4	2.3 ± 0.4, 3.2 - 1.6	1.8 ± 0.5, 2.6 - 1.4	2.2 ± 0.4, 3.3 - 1.4	SCD T+ > SCD T- 0.0000052, MCI T+ > MCI T- 0.0076261,	Age 0.0075068, sex 0.0122803	*p* < 0.0000001
MIF (NPX)	4.2 ± 0.5, 4.9 - 2.3	4.7 ± 0.3, 5.3 - 4.0	4.1 ± 0.5, 5.2 - 2.7	4.7 ± 0.5, 5.4 - 3.6	4.1 ± 0.4, 5.1 - 2.8	4.6 ± 0.3, 5.4 - 3.9	4.1 ± 0.5, 5.1 - 3.0	4.7 ± 0.4, 6.0 - 4.0	CN T+ > CN T- 0.001482, SCD T+ > SCD T- < 0.0000001 MCI T+ > MCI T- 3E-7, DAT T+ > DAT T- 0.002348	Age < 0.0000001	*p* < 0.0000001
C1q (NPX)	-2.2 ± 0.4, -1.1 - -3.4	-1.8 ± 0.4, -1.4 - -2.6	-2.0 ± 0.4, -0.9 - -3.2	-1.7 ± 0.4, -1.1 - -2.6	-2.1 ± 0.4, -1.0 - -3.0	-1.8 ± 0.3, -1.1 - -2.7	-2.0 ± 0.4, -1.6 - -2.7	-1.7 ± 0.4, -1.2 - -2.5	SCD T+ > SCD T- 0.0111752, DAT T+ > DAT T- 0.0458432	Age 0.0000018, sex 0.0195042	*p* = 0.0000382
YKL-40 (NPX)	5.5 ± 0.4, 6.3 - 4.0	5.9 ± 0.5, 6.8 - 4.6	5.5 ± 0.4, 6.4 - 4.5	6.0 ± 0.4, 6.6 - 4.7	5.7 ± 0.4, 6.7 - 4.4	6.0 ± 0.4, 6.7 - 5.1	5.7 ± 0.5, 6.3 - 4.5	6.1 ± 0.5, 7.1 - 5.1	SCD T+ > SCD T- 0.0000115, MCI T- > MCI T- 0.0318225	Age < 0.0000001 sex 0.0219749	*p* < 0.0000001
TREM2 (NPX)	2.7 ± 0.8, 4.4 - 0.6	3.3 ± 0.7, 4.6 - 1.6	2.6 ± 0.7, 4.1 - 0.3	3.2 ± 0.8, 4.8 - 1.6	2.7 ± 0.7, 3.8 - 0.8	3.1 ± 0.7, 4.3 - 1.3	2.7 ± 0.7, 3.5 - 1.0	3.1 ± 0.8, 4.6 - 1.0	SCD T+ > SCD T- 0.0007996	Age 0.0000417	*p* = 0.0000008
C3 (NPX)	1.2 ± 0.6, 3.3 - -0.2	1.3 ± 0.7, 2.5 - -0.5	1.2 ± 0.6, 2.4 - -0.4	1.2 ± 0.6, 2.6 - 0.4	1.3 ± 0.5, 2.7 - 0.4	1.2 ± 0.6, 2.5 - 0.0	1.5 ± 0.6, 2.4 - 0.4	1.3 ± 0.6, 2.8 - 0.2	-	Age 0.0390980, sex 0.0004291, bmi 0.0005024	-

Factor B (NPX)	1.9 ± 0.5, 3.4 - 0.5	2.0 ± 0.5, 2.7 - 1.0	1.9 ± 0.6, 3.1 - 0.3	2.0 ± 0.4, 2.7 - 1.4	2.0 ± 0.4, 3.1 - 1.1	1.8 ± 0.5, 2.8 - 0.9	2.0 ± 0.6, 2.7 - 0.7	1.9 ± 0.5, 3.0 - 0.8	-	sex 0.0181219, bmi 0.0000075	-
Factor H (NPX)	1.8 ± 0.5, 3.0 - 0.8	2.1 ± 0.5, 2.8 - 0.8	1.7 ± 0.4, 2.8 - 0.6	2.0 ± 0.4, 2.9 - 1.3	2.0 ± 0.4, 2.8 - 1.1	2.0 ± 0.4, 2.7 - 1.2	2.0 ± 0.4, 2.5 - 1.2	2.1 ± 0.4, 3.0 - 1.3	SCD T+ > SCD T- 0.0272412	Age 0.0047250, sex 0.0000001, bmi 0.0006768	*p* = 0.0001303
TNFR1 (NPX)	3.2 ± 0.4, 3.9 - 1.9	3.5 ± 0.3, 4.2 - 3.0	3.1 ± 0.3, 3.9 - 2.3	3.6 ± 0.4, 4.3 - 2.6	3.2 ± 0.3, 3.8 - 2.3	3.5 ± 0.3, 4.0 - 2.6	3.0 ± 0.3, 3.7 - 2.5	3.4 ± 0.4, 4.5 - 2.6	SCD T+ > SCD T- 3E-7, MCI T- > MCI T- 0.0009708, DAT T+ > DAT T- 0.0328996	Age 0.0000005, sex 0.0149473	*p* < 0.0000001
TNFR2 (NPX)	1.0 ± 0.4, 1.9 - -0.2	1.4 ± 0.4, 2.5 - 0.9	1.0 ± 0.4, 1.8 - 0.0	1.6 ± 0.4, 2.5 - 0.6	1.1 ± 0.4, 1.8 - 0.1	1.5 ± 0.4, 2.1 - 0.6	1.1 ± 0.3, 1.6 - 0.4	1.5 ± 0.4, 2.4 - 0.6	CN T+ > CN T- 0.0285626, SCD T+ > SCD T- 3E-7, MCI T+ > MCI T- 0.0001387,	Age < .0000001, sex 0.0002341	*p* < 0.0000001
ICAM1 (NPX)	-3.6 ± 0.4, -2.6 - -4.6	-3.4 ± 0.5, -2.5 - -4.5	-3.6 ± 0.4, -2.7 - -4.7	-3.4 ± 0.4, -2.5 - -4.0	-3.4 ± 0.4, -2.5 - -4.3	-3.3 ± 0.4, -2.6 - -4.1	-3.4 ± 0.4, -2.7 - -3.9	-3.3 ± 0.4, -2.4 - -3.9	SCD T+ > SCD T- 0.0026486,	Age 0.0018623, sex 0.0062199, bmi 0.0478617	*p* = 0.0000061
VCAM1 (NPX)	-1.5 ± 0.4, -0.6 - -2.4	-1.3 ± 0.4, -0.3 - -2.0	-1.5 ± 0.4, -0.6 - -2.5	-1.1 ± 0.4, -0.3 - -1.9	-1.4 ± 0.3, -0.8 - -1.8	-1.2 ± 0.3, -0.6 - -2.0	-1.4 ± 0.3, -1.0 - -2.3	-1.1 ± 0.3, -0.5 - -1.9	SCD T+ > SCD T- 0.0000383	Age 0.0000047, sex 0.0000006	*p* = 0.0000002

Table 19: DELCODE OLINK- Diagnosis/Tau scheme

Inflammatory biomarkers measured in the OLINK panels were stratified with the cognitive staging of DELCODE subjects with pathological t-tau represented by median ± standard deviation, maximum and minimum value. Differences between subject groups were tested by the non-parametric Kruskal-Wallis test, followed by ANCOVA with all 4 covariates (age, sex, BMI, and *APOE4*). Significant covariates that influence the biomarkers were identified, and a co-variate adjusted ANCOVA *p*-values for the group comparisons were reported for each biomarker.

Table 20: F.ACE Manual- Diagnosis/Tau

Marker	SCD T-	SCD T+	MCI T-	MCI T+	Kruskal-Wallis	Covariates	ANCOVA
N	52	7	414	309	*p*-value	*p*-value	*p*-value
Tyro3 (pg/mL)	2570.7 ± 811.0, 4746.2 - 1320.9	3271.0 ± 779.2, 5089.8 - 2886.4	2672.2 ± 827.5, 6315.3 - 925.2	3487.6 ± 1072.7, 6341.8 - 1555.3	MCI T+ > MCI T- < 0.0000001	-	*p* < 0.0000001
Axl (ng/mL)	17.6 ± 4.3, 27.1 - 8.5	23.0 ± 4.4, 29.8 - 18.3	16.9 ± 4.8, 35.5 - 7.5	20.8 ± 6.0, 37.0 - 9.9	MCI T+ > MCI T- < 0.0000001	*APOE4* 0.0450472	*p* < 0.0000001
MIF (pg/mL)	9117.4 ± 2569.5, 16428.9 - 4583.5	16376.9 ± 2082.2, 17580.3 - 11782.7	9809.5 ± 2716.8, 20884.5 - 1367.2	13848.1 ± 3477.4, 23079.4 - 3768.3	SCD T+ > SCD T- 0.0006953, MCI T+ > MCI T- < 0.0000001	Age 0.0162671	*p* < 0.0000001
C1q (ng/mL)	196.0 ± 50.2, 322.2 - 105.3	245.3 ± 49.0, 322.0 - 192.4	201.2 ± 56.2, 405.9 - 87.2	239.4 ± 68.2, 441.2 - 93.1	MCI T+ > MCI T- < 0.0000001	Age 0.0000002, sex 0.0000003, *APOE4* 0.0493793	*p* < 0.0000001
YKL-40 (ng/mL)	229.2 ± 82.0, 438.5 - 90.6	322.1 ± 94.4, 475.8 - 224.1	229.3 ± 82.5, 490.9 - 89.6	327.9 ± 96.5, 598.4 - 106.6	MCI T+ > MCI T- < 0.0000001	Age < 0.0000001	*p* < 0.0000001
TREM2 (pg/mL)	5113.4 ± 1761.6, 9935.3 - 2534.1	5034.1 ± 1626.3, 7317.7 - 2324.0	5015.6 ± 1531.9, 11153.3 - 0.0	5954.0 ± 1829.5, 11108.2 - 2402.0	MCI T+ > MCI T- < 0.0000001	Age 0.0000362, bmi 0.0455952	*p* < 0.0000001
C3 (ng/mL)	3924.5 ± 2663.9, 16465.6 - 1204.9	4861.2 ± 1461.6, 5882.2 - 2723.4	3763.1 ± 3212.4, 16274.3 - 868.9	4453.7 ± 3203.5, 16407.5 - 1572.3	-	Age 0.0002601, sex 0.0002488	-
C4 (ng/mL)	1037.4 ± 525.4, 2583.3 - 497.4	1143.0 ± 270.7, 1640.4 - 833.0	1174.2 ± 493.9, 2872.2 - 325.3	1296.1 ± 513.6, 3056.7 - 337.3	MCI T+ > MCI T- 0.0005478	Age 0.0029194, sex < .0000001 bmi 0.0027312	*p* = 0.0012641,
Factor B (ng/mL)	524.4 ± 238.2, 1148.5 - 159.0	519.4 ± 131.7, 663.4 - 331.4	531.3 ± 232.8, 1348.1 - 129.5	529.2 ± 227.2, 1383.2 - 172.9	-	sex 0.0000018, bmi 0.0004575, *APOE4* 0.0459391	-

Factor H (ng/mL)	472.8 ± 190.5, 1241.3 - 214.6	590.0 ± 129.5, 759.1 - 384.1	517.2 ± 194.1, 1175.7 - 211.7	583.8 ± 203.2, 1250.7 - 190.6	MCI T+ > MCI T- 0.0000242	Age 0.0000701, sex < 0.0000001 bmi 0.0018325	p = 0.0000814,
TNFR1 (ng/mL)	0.5 ± 0.1, 0.7 - 0.3	0.7 ± 0.1, 0.8 - 0.5	0.5 ± 0.1, 1.0 - 0.2	0.7 ± 0.2, 1.1 - 0.3	SCD T+ > SCD T- 0.0324337, MCI T+ > MCI T- < 0.0000001	Age 0.0000038, *APOE4* 0.0015353	p < 0.0000001
TNFR2 (ng/mL)	0.9 ± 0.3, 1.4 - 0.5	1.5 ± 0.3, 1.8 - 0.9	1.0 ± 0.3, 1.8 - 0.2	1.3 ± 0.3, 2.3 - 0.6	SCD T+ > SCD T- 0.0178711, MCI T+ > MCI T- < 0.0000001	Age < 0.0000001 sex 0.0019236	p < 0.0000001
ICAM1 (ng/mL)	2.2 ± 0.7, 4.6 - 1.1	2.5 ± 0.7, 4.0 - 1.9	2.3 ± 0.7, 4.9 - 0.6	2.9 ± 0.8, 5.1 - 1.2	MCI T+ > MCI T- < 0.0000001	Age 0.0000052, sex 0.0001423, bmi 0.0046142, *APOE4* 0.0032012	p < 0.0000001
VCAM1 (ng/mL)	5.7 ± 1.4, 8.9 - 2.6	6.8 ± 2.1, 10.1 - 3.9	6.0 ± 1.7, 12.7 - 1.7	7.1 ± 2.0, 12.8 - 2.7	MCI T+ > MCI T- < 0.0000001	Age 0.0000011, sex 0.0000249 *APOE4* 0.0002712	p < 0.0000001
CRP (ng/mL)	4036.3 ± 5368.5, 21312.1 - 444.1	3459.0 ± 5614.6, 16582.7 - 547.6	3923.9 ± 8295.7, 57200.0 - 302.6	3902.9 ± 8133.2, 54967.9 - 163.0	-	bmi 0.0000013, *APOE4* 0.0000590	-

Table 20: F.ACE Manual- Diagnosis/Tau

Inflammatory biomarkers measured in the manual panels were stratified with the cognitive staging of F.ACE subjects with pathological t-tau represented by median ± standard deviation, maximum and minimum value. Differences between subject groups were tested by the non-parametric Kruskal-Wallis test, followed by ANCOVA with all 4 covariates (age, sex, BMI, and *APOE4*). Significant covariates that influence the biomarkers were identified, and a co-variate adjusted ANCOVA *p*-values for the group comparisons were reported for each biomarker.

3.2. Beneficial effects of increased TAM receptors *in vitro*

The biomarker measurements from the previous chapter were subjected to a multi-dimensional analysis in PREADAPT which revealed that subjects with higher Tyro3 and Axl in CSF performed cognitively better and were protected against AD progression (Brosseron et al., 2022). Hence, an *in vitro* overexpression system of the TAM receptors Tyro3 and Axl in THP-1 cells (human monocyte leukemia cells) were used to functionally characterize their role in the context of AD. These human monocyte cell lines transform into human macrophages upon PMA stimulation, which are the preliminary models for the microglia present in these subjects.

3.2.1. TAM-overexpressing THP-1 cells as a model for studying Tyro3 and Axl

Before proceeding with functional experiments, the overexpression of these receptors in these cells had to be validated. Cytosolic and membrane fractionation showed that intact Tyro3 and Axl proteins are overexpressed in these cells. The overexpressed proteins generated in the cytosol are also translocated to the membrane and expressed as functional receptors. **(Figure 10 A).** The overexpression of these receptors were also confirmed in the supernatants mimicking the physiological release of soluble TAMs in the CSF **(Figure 10 B-C)**.

3.2.2. Tyro3-overexpression improves Aβ_{42} phagocytosis in THP-1 macrophages

Tyro3 and Axl are phagocytic receptors, hence they might influence the phagocytosis of pathological Aβ_{42} fibrils and tau peptides. To check this, the cells were exposed to fluorescently labelled Aβ_{42} fibrils **(Figure 10 D)**. There was a significantly increased uptake of Aβ in the Tyro3OE cells when compared with WT THP-1 cells [One-way ANOVA, $F_{(2, 19)} = 5.458$, $p = 0.0134$] (WT: 100 ± 0 %, Tyro3OE: 150.47 ± 17.57 %, AxlOE: 95.25 ± 10.27 %, **Figure 10 E**). Furthermore, in order to check the influence of tau on the phagocytosis of Aβ fibrils by the THP-1 macrophages, the cells were exposed with tau for 3 h prior to phagocytosis **(Figure 10 D)**. When the control cells were exposed to tau pretreatment for 3 h, there was a trend toward reduced Aβ phagocytic capacity (WT

untreated: 100 ± 0 %, WT + tau: 57.77 ± 7.33 %, **Figure 10 F**). The tau-induced mild impairment in control cells was absent in Tyro3OE cells [Two-way ANOVA, Cell type x Tau $F_{(2, 30)}$ = 1.025, p = 0.3710; Cell type $F_{(2, 30)}$ = 7.374, p = 0.0025; Tau $F_{(1, 30)}$ = 2.630, p = 0.1154] (Tyro3OE untreated: 132.09 ± 18.02 %, Tyro3OE + tau: 124.72 ± 17.05 %, AxlOE untreated: 87.37 ± 14.06 %, AxlOE + tau: 80.62 ± 18.45 %, **Figure 10 F**)

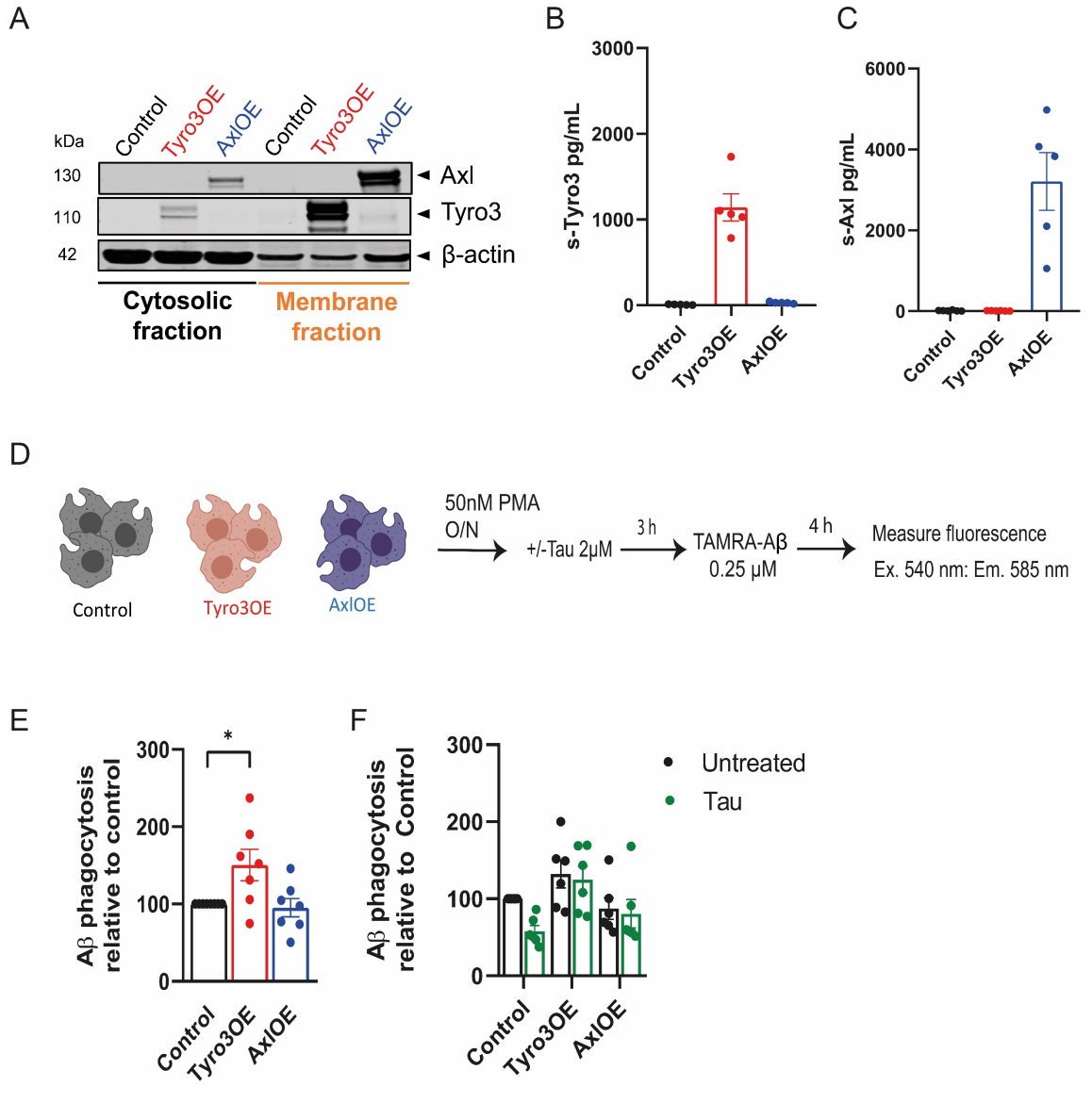

Figure 10: Tyro3 overexpression assists amyloid phagocytosis

(A) Confirmation of Tyro3 and Axl overexpression in the cytosolic and membrane fractions of THP-1 cell lysates. **(B, C)** Confirmation of Tyro3 and Axl overexpression in the supernatants of THP-1 cells (N=4-5 independent experiments). **(D)** Schematic for measuring $A\beta_{42}$ phagocytosis in WT control, Tyro3OE, and AxlOE cells. **(E)** Tyro3OE showed increased Aβ phagocytosis when compared with control (N= 7-8 independent

experiments, one-way ANOVA with Dunnet's post-hoc analysis, * $p < 0.05$). **(F)** Tau pre-treatment impairs $A\beta_{42}$ phagocytosis in WT control cells but not in Tyro3OE (N= 6 independent experiments, two-way ANOVA with Tukey's post-hoc analysis). All data presented as mean ± SEM.

3.2.3. Tyro3-overexpression reduced IL-1β during tau + $A\beta_{42}$-induced NLRP3 inflammasome activation in THP-1 macrophages

In order to check whether tau and $A\beta_{42}$ induced NLRP3 inflammasome activation in these cell types, the cells were exposed to these proteins according to the scheme **(Figure 11 A)**. Firstly, IL-1β release was significantly increased in the tau and tau + $A\beta_{42}$ group when compared with the untreated controls in the WT control cells [Two-way ANOVA with Tukey's post-hoc analysis, Cell type x Treatment $F_{(10, 36)} = 0.4679$, $p = 0.8997$; Cell type $F_{(2, 36)} = 24.82$, $p < 0.0001$; Treatment $F_{(5, 36)} = 6.268$, $p = 0.0003$] (WT untreated: 469.68 ± 73.14 pg/mL, WT + DMSO: 389.18 ± 22.99 pg/mL, WT + $A\beta_{42}$: 493.15 ± 25.54 pg/mL, WT + tau: 921.43 ± 98.92 pg/mL, WT + tau + DMSO: 922.76 ± 44.71 pg/mL, WT + tau + $A\beta_{42}$: 1151.98 ± 70.00 pg/mL, WT untreated vs. WT + tau : $p = 0.002$, two-way ANOVA with Tukey's post-hoc analysis, **Figure 11 C**).

Interestingly, IL-1β was significantly decreased in the Tyro3OE cells treated with tau + $A\beta_{42}$ stimulation, (Tyro3OE untreated: 44.35 ± 11.41 pg/mL, Tyro3OE + DMSO: 46.42 ± 14.05 pg/mL, Tyro3OE + $A\beta_{42}$: 43.15 ± 13.13 pg/mL, Tyro3OE + tau: 140.21 ± 18.87 pg/mL, Tyro3OE + tau + DMSO: 203.25 ± 43.03 pg/mL, Tyro3OE + tau + Aβ: 150.17 ± 25.70 pg/mL, WT + tau vs. Tyro3OE + tau : $p < 0.0001$, WT + tau + Aβ vs. Tyro3OE + tau + $A\beta_{42}$: $p < 0.0001$, two-way ANOVA with Tukey's post-hoc analysis, **Figure 11 C**). In contrast, AxlOE showed an increased IL-1β release with Tau + $A\beta_{42}$ stimulation (AxlOE untreated: 713.68 ± 29.26 pg/mL, AxlOE + DMSO: 730.47 ± 7.45 pg/mL, AxlOE + $A\beta_{42}$: 727.67 ± 12.07 pg/mL, AxlOE + tau: 1444.72 ± 90.42 pg/mL, AxlOE + tau + DMSO: 1436.72 ± 110.19 pg/mL, Tyro3OE + tau + $A\beta_{42}$: 1537.58 ± 124.21 pg/mL, WT + tau vs. AxlOE + tau : $p < 0.0001$, WT + tau + $A\beta_{42}$ vs. AxlOE + tau + $A\beta_{42}$: $p = 0.0031$, two-way ANOVA with Tukey's post-hoc analysis, **Figure 11 C**)

In a subsequent analysis, it was identified that other inflammasome components namely NLRP3, ASC, Caspase-1 were expressed at normal levels in Tyro3OE and that the

decrease in IL-1β is not due to reduced inflammasome activation in Tyro3OE **(Figure 11 D)**.

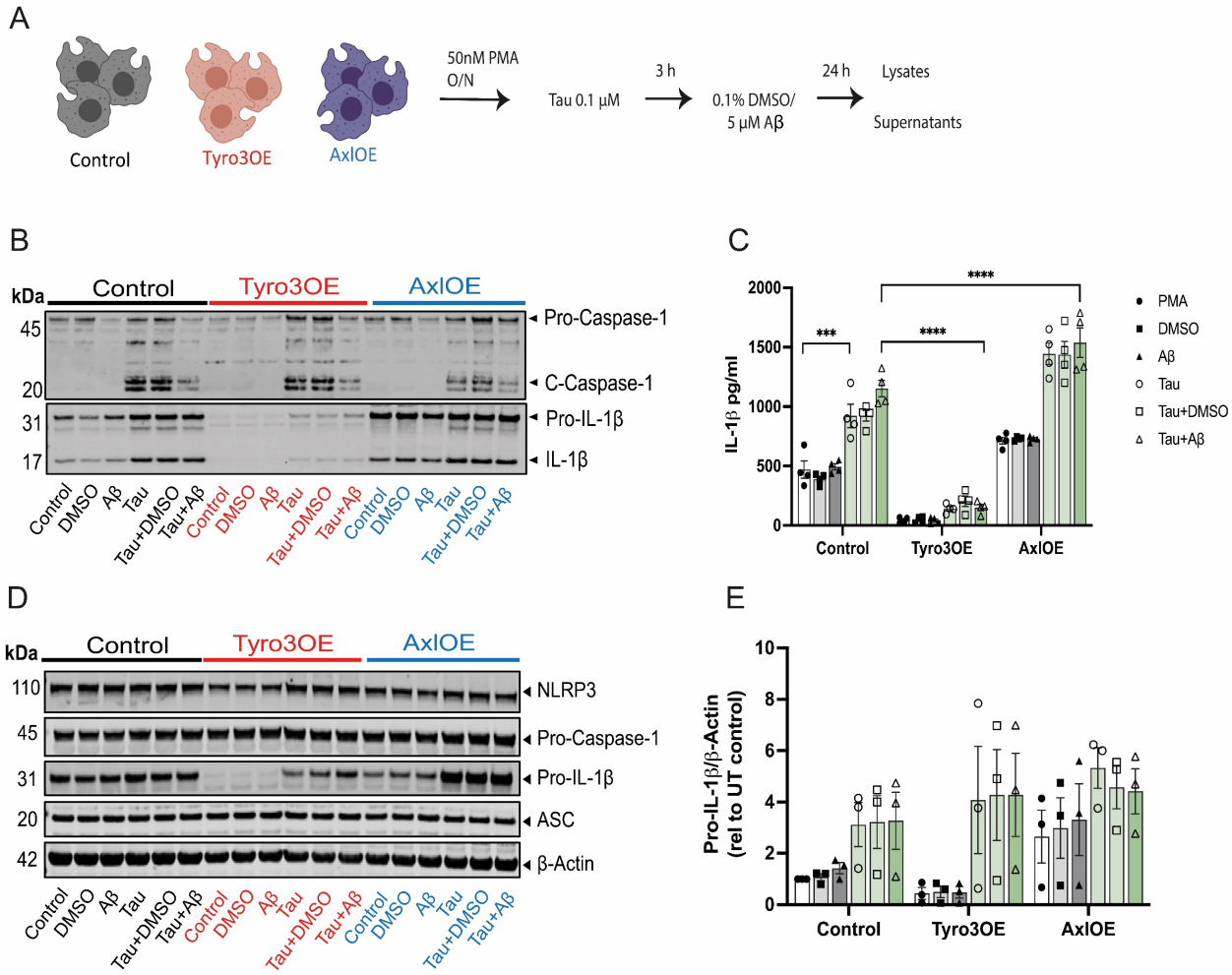

Figure 11: Tyro3-overexpression reduced IL-1β during tau + Aβ$_{42}$-induced NLRP3 inflammasome activation in THP-1 macrophages

(A) Schematic for tau + Aβ$_{42}$ induced NLRP3 inflammasome stimulation in Control, Tyro3OE, and AxlOE cells. **(B, C)** Representative western blots of pro-Caspase-1, cleaved Caspase-1, Pro-IL-1β, and mature IL-1β and (C) IL-1β ELISA measurements in the supernatants showing reduction of IL-1β release in Tyro3OE cells (N= 4 independent experiments, two-way ANOVA with Tukey's post-hoc analysis, * $p < 0.05$, ***$p < 0.001$, ****$p < 0.0001$). All data is presented as mean ± SEM. **(D, E)** Representative western blots of NLRP3, pro-Caspase-1, Pro-IL-1β, ASC, and the loading control β-Actin and (E) Pro-IL-1β analysis in the whole cell lysates showing decreased Pro-IL-1β in Tyro3OE cells (N= 3 independent experiments, two-way ANOVA with Tukey's post-hoc analysis). All data presented as mean ± SEM.

The only difference in the protein expression was found for the precursor form of IL-1β in the Tyro3OE. When quantified, there was a trend toward a decrease in the precursor form

of IL-1β in the Tyro3OE lysates [Two-way ANOVA with Tukey's post-hoc analysis, Cell type x Treatment $F_{(10, 36)}$ = 0.3575, p = 0.9569; Cell type $F_{(2, 36)}$ = 4.750, p = 0.0148; Treatment $F_{(5, 36)}$ = 5.232, p = 0.0010], (a. WT untreated: 1.0 ± 0, DMSO: 1.08 ± 0.12, $A\beta_{42}$: 1.42 ± 0.19, tau: 3.12 ± 0.75, tau + DMSO: 3.22 ± 0.89, tau + $A\beta_{42}$: 3.27 ± 0.96; b. Tyro3OE untreated: 0.44 ± 0.20, DMSO: 0.50 ± 0.20, $A\beta_{42}$: 0.48 ± 0.19, tau: 4.08 ± 1.81, tau + DMSO: 4.27 ± 1.53, tau + $A\beta_{42}$: 4.28 ± 1.40; c. AxlOE untreated: 2.65 ± 0.89, DMSO: 2.99 ± 1.02, $A\beta_{42}$: 3.31 ± 1.22, tau: 5.33 ± 0.69, tau + DMSO: 4.57 ± 0.73, tau + $A\beta_{42}$: 4.41 ± 0.76**, Figure 11 E**). Hence, Tyro3 overexpression suppressed IL-1β release from in the THP-1 cells and lead to a reduced inflammatory response upon tau and $A\beta_{42}$ stimulation.

3.2.4. Tyro3-overexpression reduced IL-1β during LPS + Nigericin-induced NLRP3 inflammasome activation in THP-1 macrophages

Next, in order to check if this effect was tau + $A\beta_{42}$ independent, the classical NLRP3 inflammasome activator, LPS + Nigericin, was used to re-establish the findings in a different model. The previous findings were completely reproducible in this model where there was a significant reduction in the release of IL-1β cytokine in the Tyro3OE cells when compared with control [Two-way ANOVA with Tukey's post-hoc analysis, Cell type x Treatment $F_{(6, 78)}$ = 10.19, p < 0.0001; Cell type $F_{(2, 78)}$ = 34.49, p < 0.0001; Treatment $F_{(3, 78)}$ = 48.03, p < 0.0001], (**Figure 12 C,** (i) WT untreated: 176.79 ± 66.41 pg/mL, LPS: 110.46 ± 31.06 pg/mL, Nig: 3363.17 ± 407.27 pg/mL, LPS + Nig: 3650.71 ± 488.96 pg/mL, Untreated vs. Nig: p < 0.0001, LPS vs. LPS + Nig: p < 0.0001, (ii) Tyro3OE untreated: 29.19 ± 7.15 pg/mL, LPS: 28.49 ± 15.20 pg/mL, Nig: 227.14 ± 51.11 pg/mL, LPS + Nig: 275.75 ± 47.83 pg/mL; (iii) AxlOE untreated: 113.25 ± 39.49 pg/mL, LPS: 56.37 ± 18.00 pg/mL, Nig: 2529.09 ± 563.23 pg/mL, LPS + Nig: 2694.18 ± 494.96 pg/mL, Untreated vs. Nig: p < 0.0001, LPS vs. LPS + Nig: p < 0.0001; WT Nig vs. Tyro3OE Nig: p < 0.0001, WT LPS + Nig vs. Tyro3OE LPS + Nig: p < 0.0001).

Similarly, normal levels of Caspase-1 and ASC were present in Tyro3OE lysates upon LPS + Nigericin stimulation, but there was a significant decrease in pro-IL-1β [Two-way ANOVA with Tukey's post-hoc analysis, Cell type x Treatment $F_{(6, 48)}$ = 1.657, p = 0.1522; Cell type $F_{(2, 48)}$ = 26.06, p < 0.0001; Treatment $F_{(3, 48)}$ = 7.678, p = 0.0003], (**Figure 12 E,** (i) WT untreated: 1.00 ± 0, LPS: 1.09 ± 0.12, Nig: 0.56 ± 0.08, LPS + Nig: 0.60 ± 0.11, (ii)

Tyro3OE untreated: 0.12 ± 0.05, LPS: 0.06 ± 0.08, Nig: 0.07 ± 0.02, LPS + Nig: 0.07 ± 0.02; (iii) AxlOE untreated: 1.14 ± 0.29, LPS: 1.16 ± 0.37, Nig: 0.37 ± 0.12, LPS + Nig: 0.41 ± 0.12; WT untreated vs. Tyro3OE untreated: $p = 0.0107$, WT LPS vs. Tyro3OE LPS: $p = 0.0053$). Hence, this regulation is not NLRP3-dependent, but due to a reduced pro-IL-1β.

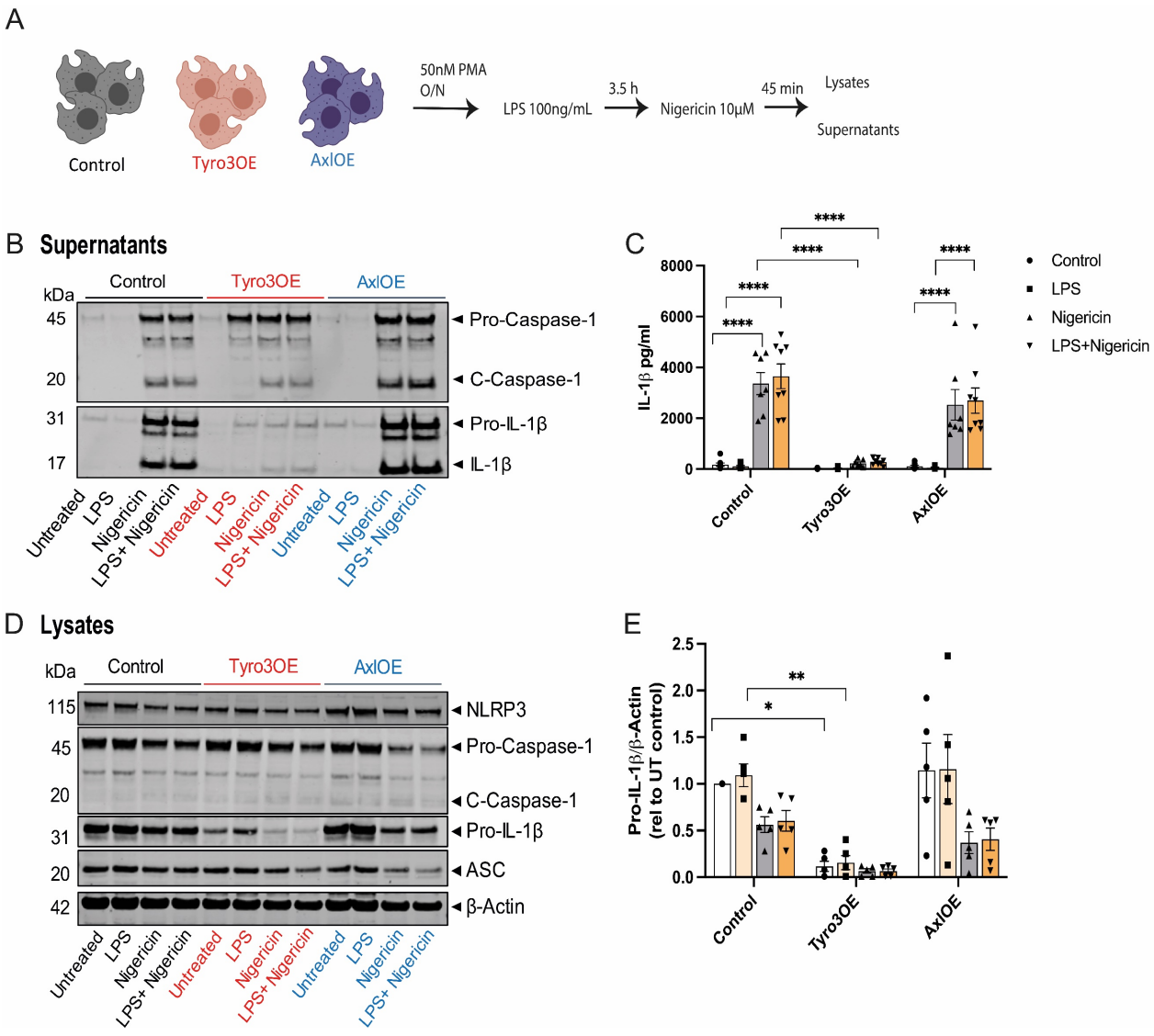

Figure 12: Tyro3-overexpression reduced IL-1β during LPS + Nigericin-induced NLRP3 inflammasome activation in THP-1 macrophages

(A) Schematic for LPS + Nigericin-induced NLRP3 inflammasome stimulation in WT Control, Tyro3OE, and AxlOE cells. **(B, C)** Representative western blots of pro-Caspase-1, cleaved Caspase-1, Pro-IL-1β, and mature IL-1β and (C) IL-1β ELISA measurements in the supernatants showing reduction of IL-1β release in Tyro3OE cells (N= 7-8 independent experiments, two-way ANOVA with Tukey's post-hoc analysis, * $p < 0.05$,

***p < 0.001, ****p < 0.0001). All data are presented as mean ± SEM. **(D, E)** Representative western blots of NLRP3, pro-Caspase-1, Pro-IL-1β, ASC, and the loading control β-Actin and (E) Pro-IL-1β analysis in the whole cell lysates showing decreased Pro-IL-1β in Tyro3OE cells (N= 5 independent experiments, two-way ANOVA with Tukey's post-hoc analysis). All data are presented as mean ± SEM.

3.2.5. Transcriptional regulation of IL-1β in Tyro3OE cells

To rule out that the decrease in IL-1β in the Tyro3OE cells was due to changes in the transcription, the mRNA levels of key pro-inflammatory cytokines along with inflammasome components were measured. The total mRNA from untreated WT control, Tyro3OE, and AxlOE cells were used for this quantification in order to check the baseline levels of the inflammatory components in these cells. There was a significant decrease in the levels of IL-1β and IL18 mRNA levels in the TAM overexpressing cells (**Figure 13 A**. *IL1B* : [one-way ANOVA with Dunnet's post-hoc analysis, $F_{(2, 13)} = 231.1$, $p < 0.0001$], WT: 1.0 ± 0, Tyro3OE: 0.19 ± 0.04, AxlOE: 0.23 ± 0.03, WT vs Tyro3OE: $p < 0.0001$, WT vs AxlOE: $p < 0.0001$, **Figure 13 B**. *IL18* : [one-way ANOVA with Dunnet's post-hoc analysis, $F_{(2, 13)} = 78.77$, $p < 0.0001$], WT: 1.0 ± 0, Tyro3OE: 0.39 ± 0.06, AxlOE: 0.31 ± 0.01, WT vs Tyro3OE: $p < 0.0001$, WT vs AxlOE: $p < 0.0001$).

Interestingly, Caspase-1 and ASC mRNA levels were significantly downregulated in these cells, although this was not completely reflected in the protein expression (**Figure 13 C**. *NLRP3* : [one-way ANOVA with Dunnet's post-hoc analysis, $F_{(2, 13)} = 17.59$, $p = 0.0002$], WT: 1.0 ± 0, Tyro3OE: 0.73 ± 0.04, AxlOE: 0.65 ± 0.06, WT vs Tyro3OE: $p < 0.0001$, WT vs AxlOE: $p = 0.0002$; **Figure 13 D**. *ASC* : [one-way ANOVA with Dunnet's post-hoc analysis, $F_{(2, 13)} = 22.13$, $p < 0.0001$], WT: 1.0 ± 0, Tyro3OE: 0.70 ± 0.06, AxlOE: 0.66 ± 0.03, WT vs Tyro3OE: $p = 0.0002$, WT vs AxlOE: $p < 0.0001$). These results point to a substantial regulation of inflammatory gene expression in the TAM over-expressing cells, especially in the Tyro3 over-expressing cells. Since NF-κB is essential for the transcription of these proteins, its translocation into the nucleus was examined in these cells. There was a significant reduction in the levels of nuclear NF-κB in the Tyro3OE cells when compared with untreated WT control [one-way ANOVA with Dunnet's post-hoc analysis, $F_{(2, 6)} = 34.44$, $p = 0.0005$], (WT: 1.0 ± 0, Tyro3OE: 0.44 ± 0.08, AxlOE: 0.93 ± 0.04, WT vs Tyro3OE: $p = 0.0005$, **Figure 13 F)**.

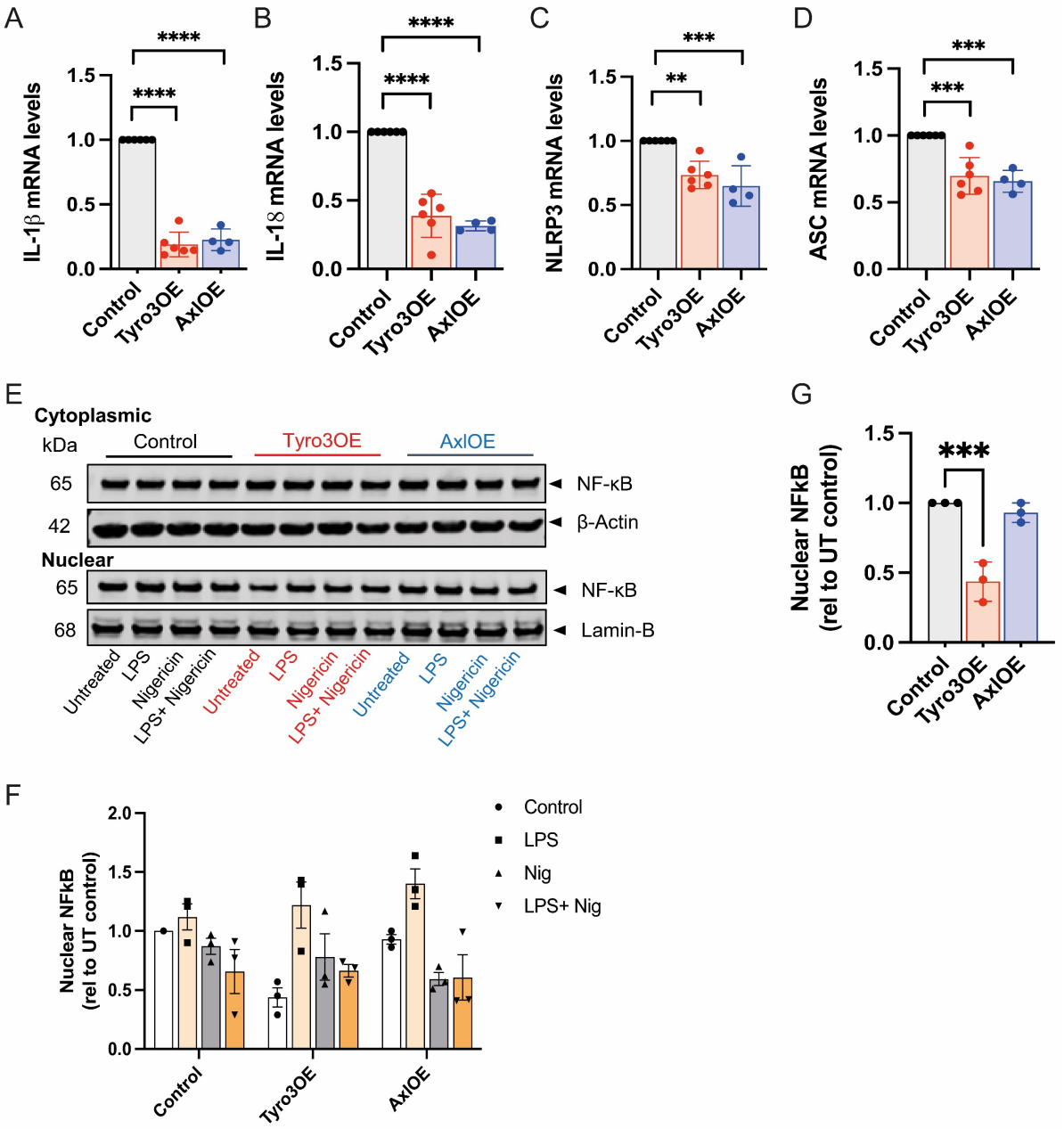

Figure 13: Transcriptional regulation of IL-1β in Tyro3OE cells

(A) Quantitative RT-PCR results showing decreased mRNA levels of IL-1β, **(B)** IL-18, **(C)** NLRP3, and **(D)** ASC in the TAM overexpressing cells. **(E)** Representative western blots of cytoplasmic and nuclear NF-κB normalized with loading controls β-actin and Lamin-B-1. **(F)** Analysis of nuclear NF-κB with inflammasome stimulation normalized with WT control untreated showed no difference (N= 3 independent experiments, two-way ANOVA with Tukey's post-hoc analysis, ***p < 0.001**). (G)** Selective analysis of baseline nuclear NF-κB in the untreated groups showed a significant reduction in nuclear NF-κB in the Tyro3OE cells (N= 3 independent experiments, one-way ANOVA with Dunnet's post-hoc analysis, ***p < 0.001). All data presented as mean ± SEM

3.2.6. STAT1 phosphorylation is increased in TAM-overexpressing THP-1 macrophages

Next, the influence of other transcription factors. STAT1 was checked since it is an important transcription factor downstream of Tyro3 signaling. Hence, the levels of STAT1 and its phosphorylation was measured after inflammasome stimulation using LPS+ Nigericin and Tau+ amyloid stimulations. There was an increase in the phosphorylation status of STAT1 (p-STAT1/ total STAT1) in the LPS + Nigericin stimulated TAM overexpressing cells, especially in the Tyro3OE cells [Two-way ANOVA with Tukey's post-hoc analysis, Cell type x Treatment $F_{(6, 24)} = 0.957$, $p = 0.4744$; Cell type $F_{(2, 24)} = 13.37$, $p = 0.0001$; Treatment $F_{(3, 24)} = 3.198$, $p = 0.0415$], (**Figure 14 B,** LPS + Nigericin, (i) WT untreated: 1.0 ± 0, LPS: 0.84 ± 0.11, Nigericin: 0.69± 0.11, LPS+ Nigericin: 0.58 ± 0.07, (ii) Tyro3OE untreated: 3.45 ± 1.05, LPS: 2.27 ± 0.43, Nigericin: 1.53 ± 0.23, LPS+ Nigericin: 1.76 ± 0.24, (iii) AxlOE untreated: 1.56 ± 0.36, LPS: 1.26 ± 0.37, Nigericin: 0.81 ± 0.27, LPS+ Nigericin: 1.37 ± 0.52, WT untreated vs Tyro3OE untreated : $p = 0.0129$).

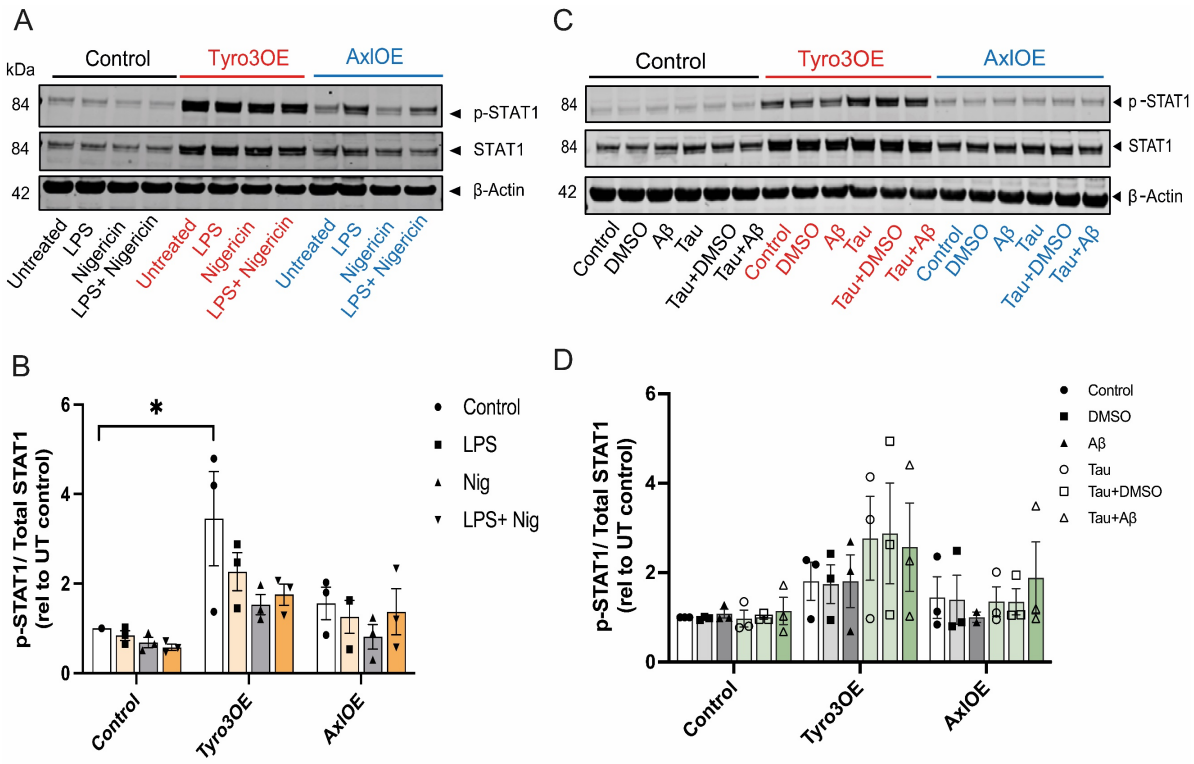

Figure 14: STAT1 phosphorylation is increased in TAM-overexpressing THP-1 macrophages

(A, C) Representative western blots of phospho-STAT1, total STAT1, and loading control β-Actin with **(A)** LPS + Nigericin stimulation and **(C)** tau + $A\beta_{42}$ stimulation. **(B, D)**

Corresponding p-STAT1/total STAT1 ratio showing increased STAT1 phosphorylation status in the TAM overexpressing cells with **(B)** LPS + Nigericin stimulation and **(D)** tau + $A\beta_{42}$ stimulation (N= 3 independent experiments, two-way ANOVA with Tukey's post-hoc analysis, * $p < 0.05$). All data is presented as mean ± SEM.

Similarly, there was a significant increase in the phosphorylation status of STAT1 (p-STAT1/ total STAT1) in the tau + $A\beta_{42}$ stimulated Tyro3OE cells [Two-way ANOVA with Tukey's post-hoc analysis, Cell type x Treatment $F_{(10, 35)} = 0.3311$, $p = 0.9666$; Cell type $F_{(2, 35)} = 7.804$, $p = 0.0016$; Treatment $F_{(5, 35)} = 0.5104$, $p = 0.7665$], (**Figure 14 D,** tau+ $A\beta_{42}$, (i) WT untreated: 1.0 ± 0, DMSO: 0.98 ± 0.02, $A\beta_{42}$: 1.08 ± 0.10, tau: 0.97 ± 0.19, tau + DMSO: 1.00 ± 0.04, tau + $A\beta_{42}$: 1.14 ± 0.31; (ii) Tyro3OE untreated: 1.81 ± 0.42, DMSO: 1.74 ± 0.43, $A\beta_{42}$: 1.81 ± 0.59, tau: 2.77 ± 0.97, tau + DMSO: 2.88 ± 1.13, tau + $A\beta_{42}$: 2.57 ± 0.99; (iii) AxlOE untreated: 1.44 ± 0.47, DMSO: 1.39 ± 0.55, $A\beta_{42}$: 1.01 ± 0.09, tau: 1.35 ± 0.33, tau + DMSO: 1.35 ± 0.30, tau + $A\beta_{42}$: 1.88 ± 0.81). This strongly suggests that STAT1 phosphorylation might be crucial for Tyro3-mediated immunosuppression during inflammasome activation.

3.2.7. JAK1/2 inhibition reduced STAT1 phosphorylation and restored IL-1β levels in Tyro3OE cells

It was inferred that STAT1 is strongly phosphorylated in the TAM overexpressing cells. To test whether the phosphorylation of STAT1 is key for the immunosuppression of IL-1β, the potential kinases that phosphorylates STAT1 could be inhibited. The first kinase to be tested would be the JAK1,2,3 since these initiate STAT1 phosphorylation during inflammation. The key question here was: Would inhibiting STAT1 and its phosphorylation impact the IL-1β levels in TAM overexpressing cells?

The JAK1/2 inhibitor Ruxolitinib (Rux) was used to inhibit STAT1 phosphorylation which was followed by LPS + Nigericin stimulation **(Figure 15 D)**. Firstly, Ruxolitinib (Rux) treatment at 10 µM for 24 h decreased the phosphorylation of STAT1 in all cell types **(Figure 15 B)**.

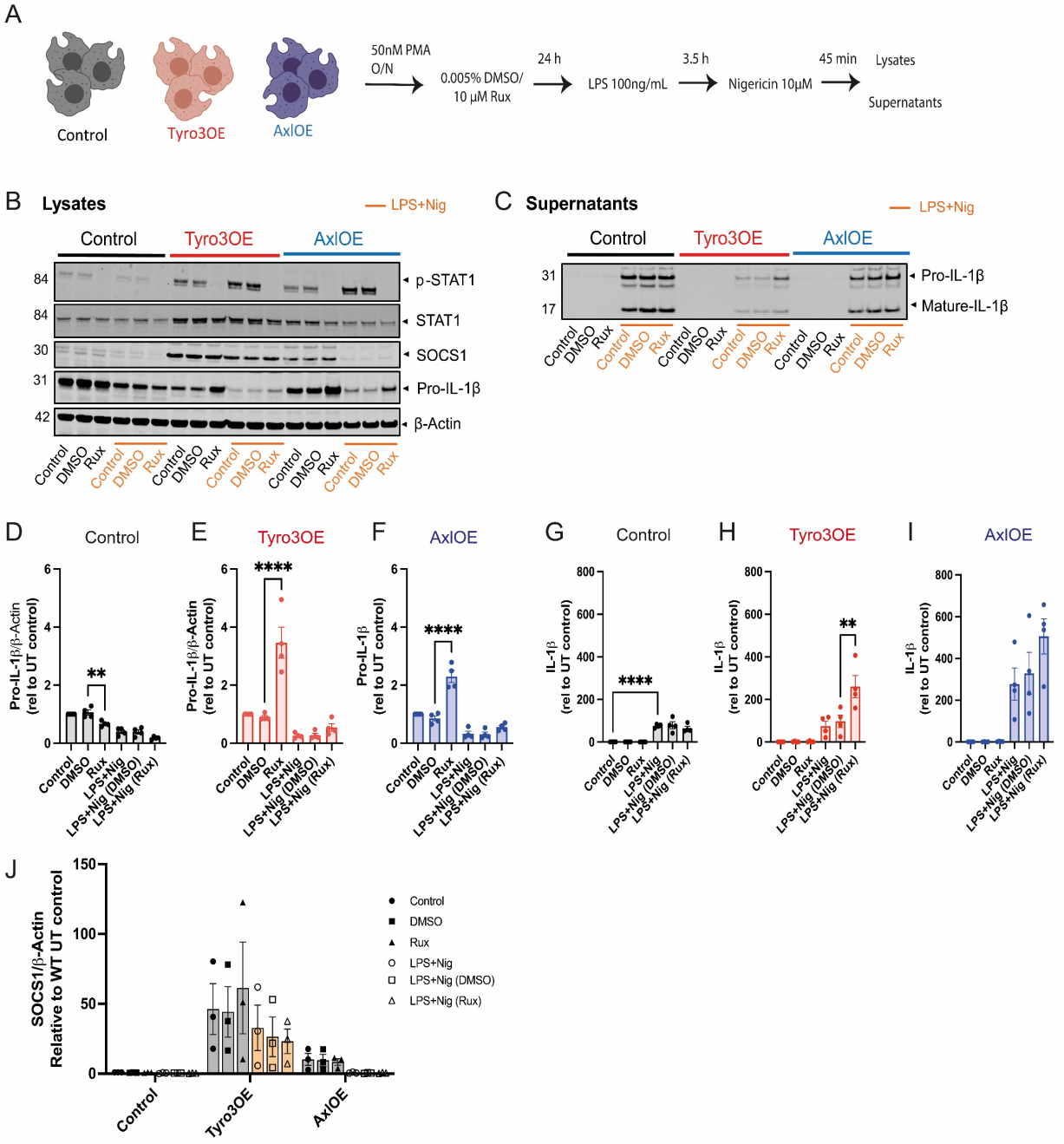

Figure 15: JAK1/2 inhibition reduced STAT1 phosphorylation and restored IL-1β levels in Tyro3OE cell

(A) Schematic for JAK1 inhibition and LPS + Nigericin-induced NLRP3 inflammasome stimulation in WT Control, Tyro3OE, and AxlOE cells. **(B, C)** Representative western blots of p-STAT1, total STAT1, SOCS1, Pro-IL-1β, and (C) mature IL-1β in the whole cell lysates and supernatants after JAK1 inhibition and inflammasome stimulation. (**D-F**) Analysis of the lysates of Rux-treated **(D)** WT-control, **(E)** Tyro3OE, and **(F)** AxlOE showed significantly increased pro-IL-1β in TAM overexpressing cells (N= 3 independent experiments, one-way ANOVA with Dunnet's post-hoc analysis, ** $p < 0.01$, ****$p < 0.0001$). All data are presented as mean ± SEM. (**G-I**) Analysis of the supernatants of

Rux-treated **(G)** WT-control, **(H)** Tyro3OE, and **(I)** AxlOE showed significantly increased mature-IL-1β in Tyro3OE cells (N= 3 independent experiments, one-way ANOVA with Dunnet's post-hoc analysis, ** p < 0.01, ****p < 0.0001). All data are presented as mean ± SEM. **(J)** Analysis of SOCS1 in the whole cell lysates of Rux-treated WT control, Tyro3OE, and AxlOE cells revealed a cell type-specific significant increase in SOCS1 (N= 3 independent experiments, two-way ANOVA with Tukey's post-hoc analysis, * p < 0.05). All data are presented as mean ± SEM.

Furthermore, Rux treatment significantly reduced pro-IL-1β in WT cells, whereas it increased pro-IL-1β in the TAM overexpressing cells Ruxolitinib treatment at 10 μM for 24 h decreased pro-IL-1β in WT cells, whereas it increased pro-IL-1β in the TAM overexpressing cells (**Figure 15 D.** WT: [one-way ANOVA with Dunnet's post-hoc analysis, $F_{(5, 18)} = 39.04$, $p < 0.0001$], WT untreated: 1.0 ± 0, DMSO: 1.06 ± 0.11, Rux: 0.67± 0.05, LPS + Nigericin: 0.40 ± 0.06, LPS + Nigericin + DMSO: 0.39 ± 0.07, LPS + Nigericin + Rux: 0.18 ± 0.02, DMSO vs. Rux: p =0.0019); (**Figure 15 E.** Tyro3OE: [one-way ANOVA with Dunnet's post-hoc analysis, $F_{(5, 18)} = 28.15$, $p < 0.0001$], Tyro3OE untreated: 1.0 ± 0, DMSO: 0.90 ± 0.06, Rux: 3.46± 0.53, LPS + Nigericin: 0.26 ± 0.04, LPS + Nigericin + DMSO: 0.28 ± 0.07, LPS + Nigericin + Rux: 0.54 ± 0.13, DMSO vs. Rux: $p < 0.0001$); (**Figure 15 F.** AxlOE: [one-way ANOVA with Dunnet's post-hoc analysis, $F_{(5, 18)} = 48.69$, $p < 0.0001$], AxlOE untreated: 1.0 ± 0, DMSO: 0.86 ± 0.09, Rux: 2.30 ± 0.21, LPS + Nigericin: 0.33 ± 0.08, LPS + Nigericin + DMSO: 0.31 ± 0.08, LPS + Nigericin + Rux: 0.55 ± 0.06, DMSO vs. Rux: $p < 0.0001$).

Consequently, Rux treatment in Tyro3OE showed a significant increase in the release of IL-1β proving that JAK-1 mediated STAT1 phosphorylation is responsible for reducing IL-1β in Tyro3OE cells (**Figure 15 G.** WT: [one-way ANOVA with Dunnet's post-hoc analysis, $F_{(5, 18)} = 26.68$, $p < 0.0001$], WT untreated: 1.0 ± 0, DMSO: 0.64 ± 0.09, Rux: 0.45 ± 0.13, LPS + Nigericin: 75.85 ± 4.13, LPS + Nigericin + DMSO: 79.08 ± 15.99, LPS + Nigericin + Rux: 64.13 ± 9.26, untreated vs. LPS + Nigericin : $p < 0.0001$); (**Figure 15 H.** Tyro3OE: [one-way ANOVA with Dunnet's post-hoc analysis, $F_{(5, 18)} = 14.79$, $p < 0.0001$], Tyro3OE untreated: 1.0 ± 0, DMSO: 1.38 ± 1.28, Rux: 1.88 ± 1.56, LPS + Nigericin: 74.93 ± 22.90, LPS + Nigericin + DMSO: 96.74 ± 29.39, LPS + Nigericin + Rux: 260.37 ± 52.43, LPS + Nigericin + DMSO vs. LPS + Nigericin + Rux: $p = 0.0039$); (**Figure 15 I.** AxlOE: [one-way ANOVA with Dunnet's post-hoc analysis, $F_{(5, 18)} = 12.08$, $p < 0.0001$], AxlOE untreated: 1.0 ± 0, DMSO: 0.60 ± 0.32, Rux: 2.15 ± 0.75, LPS + Nigericin: 276.71 ± 76.88, LPS +

Nigericin + DMSO: 328.78 ± 101.02, LPS + Nigericin+ Rux: 505.98 ± 84.27). This was further verified by Western blot analyses where the quantification revealed a significant upregulation of pro-IL-1β in the Tyro3OE cells and AxlOE cells **(Figure 15 C)**.

SOCS1, a downstream effector in TAM signaling, was also significantly upregulated in the TAM overexpressing cells [Two-way ANOVA with Tukey's post-hoc analysis, Cell type x Treatment $F_{(10, 36)} = 0.4228$, $p = 0.9228$; Cell type $F_{(2, 36)} = 20.51$, $p < 0.0001$; Treatment $F_{(5, 36)} = 0.9178$, $p = 0.4806$], (**Figure 15 J,** (i) WT untreated: 1.0 ± 0, DMSO: 0.79 ± 0.13, Rux: 0.87± 0.11, LPS + Nigericin: 0.37 ± 0.18, LPS + Nigericin + DMSO: 0.39 ± 0.04, LPS+ Nigericin + Rux: 0.41 ± 0.10; (ii) Tyro3OE untreated: 46.27 ± 18.27, DMSO: 44.15 ± 18.05, Rux: 61.38 ± 32.87, LPS + Nigericin: 32.75 ± 16.27, LPS + Nigericin + DMSO: 26.42 ± 14.26, LPS + Nigericin + Rux: 23.15 ± 8.80; (iii) AxlOE untreated: 10.24 ± 4.31, DMSO: 9.49 ± 4.27, Rux: 8.39 ± 2.34, LPS + Nigericin: 0.67 ± 0.28, LPS + Nigericin + DMSO: 0.40 ± 0.15, LPS + Nigericin + Rux: 0.56 ± 0.17). This strongly suggests that JAK1/2 meditated STAT1 phosphorylation is necessary for SOCS1, leading to IL-1β downregulation in the Tyro3OE cells.

3.2.8. Tyro3-overexpression in THP-1 macrophages may reduce NLRP3-mediated damage to SH-SY5Y neurons

Previous sections showed that LPS + Nigericin-induced NLRP3 inflammasome activation lead to an increased IL-1β release in the WT control supernatants, whereas a significantly decreased IL-1β release Tyro3OE supernatants. In order to check if this reduction translates into neuronal protection, the conditioned medium (CM) from these cells were exposed to differentiated SH-SY5Y human neuroblastoma cells for 45 min. Differentiation of the SH-SY5Y human neuroblastoma cells to human neurons was verified using the neuronal markers Tuj-1, and NeuN expression **(Figure 16 B)**. There was a high expression of Tuj-1 and NeuN in the differentiated neurons but not in the undifferentiated cells which verified complete differentiation **(Figure 16 B).** Percentage of healthy neurons were calculated by counting the cells that were positive for Tuj-1 after CM exposure from these cells. Interestingly, exposure to LPS + Nigericin stimulated Tyro3OE CM and AxlOE CM showed significantly increased percentage of healthy neurons when compared with the WT CM [Two-way ANOVA with Tukey's post-hoc analysis, Cell type x Treatment $F_{(2, 18)} = 70.94$, $p < 0.0001$; Cell type $F_{(1, 18)} = 135.9$, $p < 0.0001$; Treatment $F_{(2, 18)} = 16.66$, p

< 0.0001], (**Figure 16 A, D,** Control WT CM: 84.13 ± 0.90, Tyro3OE CM: 86.99 ± 1.89, AxlOE CM: 43.97 ± 3.22; LPS + Nigericin WT CM: 4.22 ± 1.49, Tyro3OE CM: 44.69 ± 5.51, AxlOE CM: 55.79 ± 6.54). Although, exposure to AxlOE control CM also significantly reduced the healthy neuron percentage, suggesting that only Tyro3OE CM is beneficial to the neurons **(Figure 16 A, D)**. Importantly, LPS + Nigericin in the neuronal medium was able to elicit neuronal damage after 45 min, even without conditioning it with the THP-1 cells **(Figure 16 C)**. Further experiments are required to properly utilize the TAM overexpressing system and reduced IL-1β in the context of neurodegeneration.

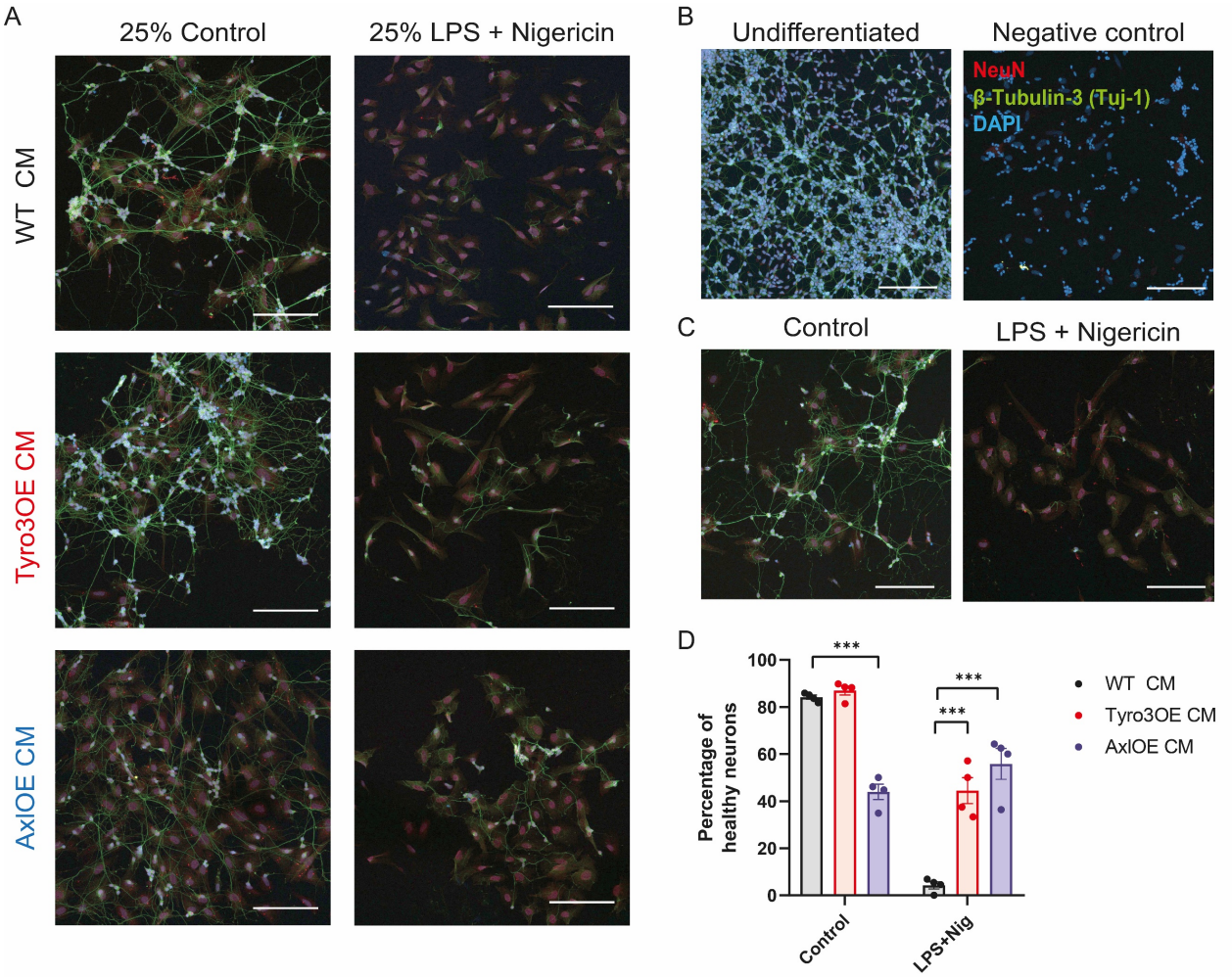

Figure 16: NLRP3-mediated damage to SH-SY5Y neurons is reduced by Tyro3-overexpression in THP-1 macrophages

(A) Representative confocal microscopy images of differentiated SH-SY5Y human neurons exposed to 25 % of LPS + Nigericin conditioned medium from WT control, Tyro3OE, and AxlOE cells for 45 min. The neurons were fixed and stained for neuronal markers Tuj-1 (green), NeuN (red), and the nuclear stain DAPI (blue). There was a heavy

loss of neurons in the WT control LPS + Nig group when compared with Tyro3OE and AxlOE LPS + Nig group. **(B)** Experimental and staining controls for the confocal microscopy in differentiated neurons. Representative confocal microscopy images of differentiated SH-SY5Y human neurons exposed to normal neuron medium and 25% of LPS + Nig in neuron medium for 45 min. Unconditioned neuron medium containing LPS + Nig inherently elicits neuronal damage. Other controls include undifferentiated neurons and the negative control for immunostaining which verifies differentiation.

3.2.9. Soluble MerTK and TAM receptor ligands Gas6 and Protein S are also increased in tau-positive subjects irrespective of Amyloid status and clinical diagnosis

Due to the availability of the extensive Olink® panel for the DELCODE cohort, the clinical analysis could be extended on the markers that are relevant to the *in vitro* findings. The other TAM receptor systems components like MerTK, Gas-6, and Protein-S survived the quality control pipeline and were used for the A/T scheme and Diagnosis/T scheme analyses. Firstly, the effects of pathological amyloid levels **(Table 12)** with pathological tau levels **(Table 12)** were examined in DELCODE Olink® (A/T scheme). All analyses were performed in R software. The detailed results containing ANCOVA analysis and significant covariates for the A/T scheme are listed separately for DELCODE Olink® **(Table 21).** Similarly, the effects of clinical diagnosis of cognitive staging with the pathological tau levels **(Table 12)** were examined in DELCODE Olink® (Diagnosis/T scheme). The detailed results containing ANCOVA analysis and significant covariates for the Diagnosis/T scheme are listed separately for DELCODE Olink® **(Table 22).** For the sake of simplicity, only the TAM ligands Gas-6, and Proteins S were stratified according to the A/T scheme and Diagnosis/T scheme and were visualized as boxplots using ggplot2 in R **(Figure 17)**.

In the A/T scheme, soluble MerTK, and TAM ligands Gas-6, and Protein-S were shown to be significantly upregulated in the Tau+ subjects **(Table 21)**. All markers were significant for covariate adjusted ANCOVA analysis. Although age and sex influenced only Gas-6 and protein-S, whereas BMI influenced only Protein S. *APOE4* showed no significant influence on these markers.

Similarly, in the Diagnosis/T scheme, soluble MerTK and TAM ligands Gas-6 and Protein-S were significantly upregulated in the Tau+ subjects **(Table 22)**. All markers were significant for covariate adjusted ANCOVA analysis in this analysis as well. Similar to the

A/T scheme, age, and sex were influencing only Gas-6 and protein-S, whereas BMI influenced only Protein S. *APOE4* showed no significant influence on these markers.

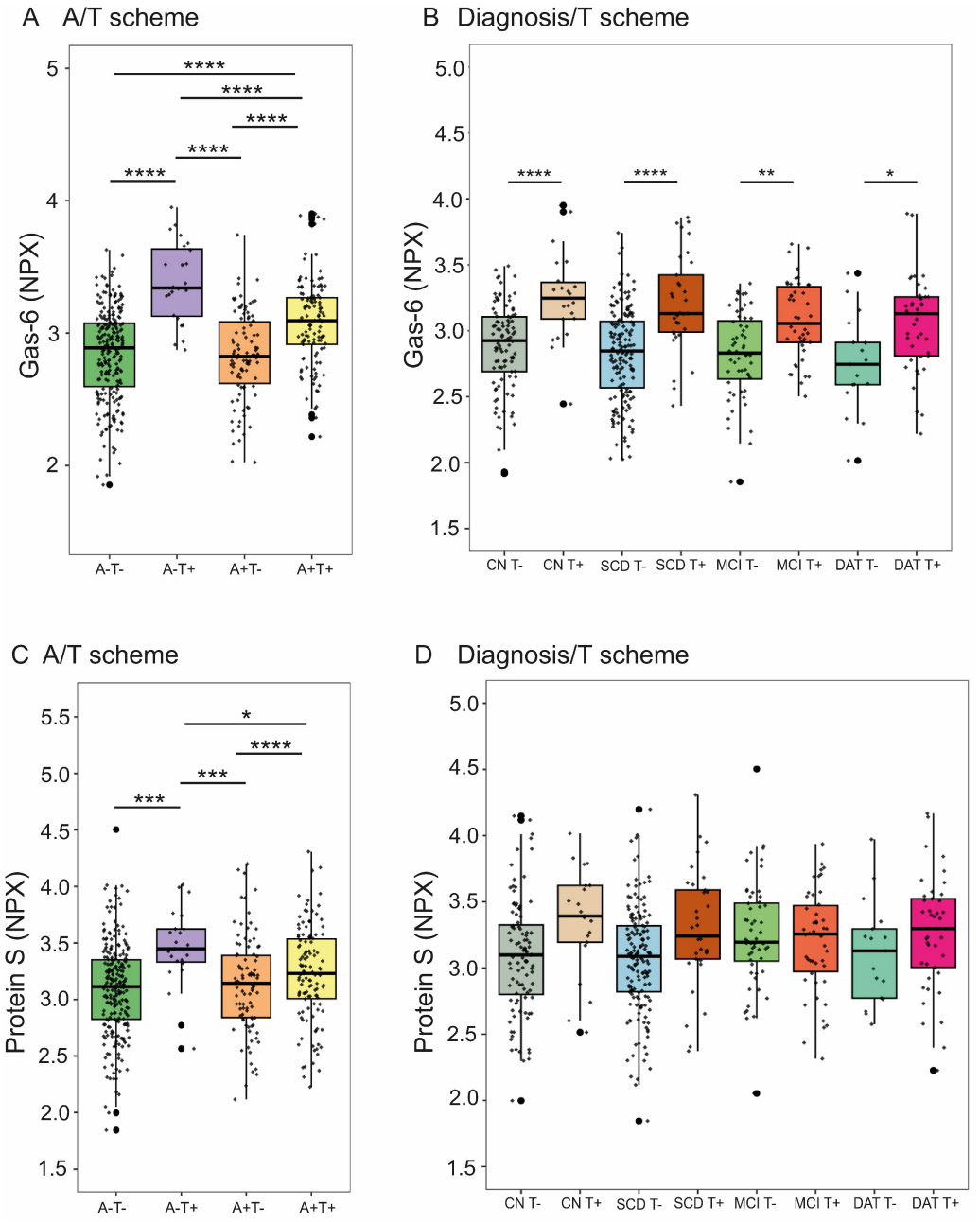

Figure 17: TAM receptor components on A/T and Diagnosis/T scheme
Gas-6 **(A,B)**, Protein-S **(C,D)** from DELCODE Olink® measurements A/T scheme (N= A-T- (216), A-T+ (21), A+T- (83), A+T+ (106), Kruskal-Wallis test, * $p < 0.05$, ** $p < 0.01$, *** $p < 0.001$, **** $p < 0.0001$), and Diagnosis/T scheme (N= CN T- (90), CN T+ (19), SCD T- (30), SCD T+ (30), MCI T- (47), MCI T+ (43), DAT T- (17), DAT T+ (35), Kruskal-Wallis test, * $p < 0.05$, ** $p < 0.01$, *** $p < 0.001$, **** $p < 0.0001$)

Table 21: DELCODE OLINK– A/T scheme: TAM system

Marker	A-T-	A-T+	A+T-	A+T+	Kruskal-Wallis	Covariates	ANCOVA
N	216	21	83	106	*p*-value	*p*-value	*p*-value
MerTK (NPX)	-4.7 ± 0.7 -3.4 - -6.8	-4.1 ± 0.7 -3.0 - -5.8	-4.9 ± 0.6 -3.3 - -6.6	-4.3 ± 0.6 -2.9 - -6.7	A- T+ > A- T- 0.0036991, A+ T+ > A- T- 0.0006638, A+ T- > A- T+ 0.0002599, A+ T+ > A+ T- 0.0000064	-	*p* < 0.0000001
Gas6 (NPX)	2.9 ± 0.3 3.6 - 1.8	3.3 ± 0.3 3.9 - 2.9	2.8 ± 0.3 3.7 – 2.0	3.1 ± 0.3 3.9 - 2.2	A- T+ > A- T- < 0.0000001, A+ T+ > A- T- 0.0000197, A+ T- > A- T+ < 0.0000001, A+ T+ > A- T+ 0.0000754, A+ T+ > A+ T- < 0.0000001	Age 0.0000095, sex 0.0000148	*p* < 0.0000001
Protein-S (NPX)	3.1 ± 0.4 4.5 - 1.8	3.4 ± 0.3 4.0 - 2.6	3.1 ± 0.4 4.2 - 2.1	3.2 ± 0.4 4.3 - 2.2	A- T+ > A- T- 0.0001607, A+ T- > A- T+ 0.0002654, A+T+ > A-T+ 0.0202224	Age 0.0005030, sex 0.0000006 BMI. 0.0016781	*p* = 0.0000713

Table 21: DELCODE OLINK– A/T scheme: TAM system

Molecules from the TAM system, soluble MerTK, Gas-6, and Protein-S measured in the OLINK panels were stratified with A/T ($A\beta_{42}$/ $A\beta_{40}$ ratio / t-tau) scheme groups of DELCODE subjects represented by median ± standard deviation maximum and minimum value. Differences between subject groups were tested by the non-parametric Kruskal-Wallis test, followed by ANCOVA with all 4 covariates (age, sex, BMI, and *APOE4*). Significant covariates that influence the biomarkers were identified, and a co-variate adjusted ANCOVA *p*-values for the group comparisons were reported for each biomarker.

Table 22: DELCODE OLINK- Diagnosis + Tau: TAM system

Marker	CN T-	CN T+	SCD T-	SCD T+	MCI T-	MCI T+	DAT T-	DAT T+	Kruskal-Wallis	Covariates	ANCOVA
N	90	19	145	30	47	43	17	35	*p*-value	*p*-value	*p*-value
MerTK (NPX)	-4.7 ± 0.7 -3.3 - -6.5	-4.2 ± 0.7 -2.9 - -5.8	-4.7 ± 0.6 -3.3 - -6.8	-4.3 ± 0.6 -3.3 - -5.6	-4.9 ± 0.6 -3.9 - -6.6	-4.3 ± 0.6 -3.2 - -5.9	-5.0 ± 0.5 -3.6 - -5.5	-4.2 ± 0.7 -3.0 - -6.7	CN T+ > CN T- 0.0473442 MCI T+ > MCI T- 0.0111576,	-	*p* = 0.0000024
Gas6 (NPX)	2.9 ± 0.3 3.5 - 1.9	3.2 ± 0.3 3.9 - 2.4	2.8 ± 0.3 3.7 - 2.0	3.1 ± 0.3 3.9 - 2.4	2.8 ± 0.3 3.4 – 1.9	3.0 ± 0.3 3.7 - 2.5	2.7 ± 0.4 3.4 - 2.0	3.1 ± 0.3 3.9 - 2.2	CN T+ > CN T- 0.0009413, SCD T+ > SCD T- 0.0000043 MCI T+ > MCI T- 0.0031135, DAT T+ > DAT T- 0.0127152,	Age 0.0.0000010, sex 0.0000656	*p* < 0.0000001
Protein-S (NPX)	3.1 ± 0.4 4.1 - 2.0	3.4 ± 0.4 4.0 - 2.5	3.0 ± 0.4 4.2 - 1.8	3.2 ± 0.4 4.3 - 2.4	3.2 ± 0.4 4.5 – 2.0	3.3 ± 0.4 3.9 - 2.3	3.1 ± 0.4 4.0 - 2.6	3.3 ± 0.4 4.2 - 2.2	-	Age 0.0005216 sex 0.0000011 BMI. 0.0029223	*p* = 0.0011063

Table 22: DELCODE OLINK- Diagnosis + Tau: TAM system

Molecules from the TAM system, soluble MerTK, Gas-6, and Protein-S measured in the OLINK panels were stratified with the cognitive staging of DELCODE subjects with pathological t-tau represented by median ± standard deviation, maximum and minimum. Differences between subject groups were tested by the non-parametric Kruskal-Wallis test, followed by ANCOVA with all 4 covariates (age, sex, BMI, and *APOE4*). Significant covariates that influence the biomarkers were identified, and a co-variate adjusted ANCOVA *p*-values for the group comparisons were reported for each biomarker

4. Discussion

4.1. Inflammatory biomarkers are elevated in the cerebrospinal fluid samples from dementia subjects

4.1.1. Olink® panels are a reliable measurement platform for unestablished biomarkers in the CSF

The 13 overlapping biomarkers that were measured in the Olink® and manual platforms were first correlated to check their reliability in detecting the differences between different groups. It is evident that there is a strong correlation between the markers measured on both panels **(Figure 7)**. Although, the targeting-antibodies used by both platforms might be entirely different, this analysis showed the reproducibility and the robustness of the results. There is an inherent hesitation in the scientific community to employ high-throughput biomarker platforms, which portrays a 'quantity-over-quality' situation. Such advertisements may be beyond the reality, which was also shown in this study. Out of the potential 3072 proteins, only 1340 proteins survived the quality control criteria. Although, the advertised biomarker measurements were validated only on human plasma samples, which is a much more robust biomaterial than the CSF. Hence, this discrepancy in the number of proteins that could be measured through Olink® in the CSF is justifiable. Especially, this is the pioneer study that investigates an extensive biomarker panel in the human CSF from dementia subjects, which merits a novel addition to the current knowledge about inflammatory biomarkers in the CSF.

4.1.2. Pathological tau in the CSF directly influences the inflammatory biomarkers present in Amyloid positive dementia subjects

The A/T scheme analysis was performed on three independent biomarker measurements: DELCODE manual, DELCODE Olink®, and F.ACE manual **(Table 16, 17, 18**). In all three analyses, there was a significant increase in the biomarkers in tau positive (T+) subjects. Of particular importance, the A-T+ subjects showed higher biomarker levels than A+T+ subjects. This suggests that amyloid pathology is prone to reduce inflammatory biomarkers in the CSF. This effect is contradictory to the amyloid hypothesis, however, a closer look at the classification of the subjects might explain this effect. As described

earlier in **Table 12**, a subject is classified as Amyloid positive (A+) when the ratio of $A\beta_{42}/A\beta_{40}$ in CSF drops below a set threshold (0.08). This classification relies on the fact that subjects with amyloid pathology have diminished $A\beta_{42}$ in the CSF since these are aggregated and trapped as amyloid plaques within the brain. Hence, amyloid pathology correlates with low $A\beta_{42}$ in the CSF. However, a subject is classified as tau positive (T+) when the phosphorylated-tau or the total tau levels are higher than a set threshold **(Table 12).** Here, tau pathology correlates with increased total Tau in the CSF. With this information combined with the clinical results that were obtained, it is inferred that those subjects with lower $A\beta_{42}$ (A+) showed reduced inflammatory biomarkers than subjects with higher total-Tau in CSF (T+). It is possible that the free-floating DAMPs in the CSF like Tau and $A\beta_{42}$ induce inflammation in the microglia. This might be the reason for a direct correlation between the levels of inflammatory biomarkers and the levels of Tau and $A\beta_{42}$.

Most of the proteins showed significant influence with the A/T scheme in all three independent measurements. This verifies that the secreted proteins and released soluble receptors were all significantly impacted by the levels of tau and $A\beta_{42}$. In the case of cytokines, these are direct measurements of the inflammatory response in the CSF of dementia subjects that aptly correlates with tau and $A\beta_{42}$ levels. However, two scenarios may be speculated in the case of increased soluble receptors in the CSF (Brosseron et al., 2022). Either the subjects express higher levels of these receptors that lead to their shedding (as a proxy for expression) or the subjects shed these receptors to reduce the downstream immune-signalling cascade (deactivation). It is difficult to infer the exact mechanism behind the shedding of these receptors, yet it is possible that both scenarios are true. For instance, soluble Axl found in human serum was directly correlated to the expression levels in hepatoma and melanoma cells suggesting that CSF soluble receptors might relate to their expression profile in the brain cells (Flem-Karlsen et al., 2020; Holstein et al., 2018).

Interestingly, out of the measured biomarkers, complement C3, Factor B, and CRP were not significantly impacted in the A/T scheme. CRP is a protein exclusively secreted in the liver and is observed in the CSF under inflammatory conditions. A recent injury or a surgical intervention is known to elevate CRP levels (Vasunilashorn et al., 2021). An irrelevant increase in the CRP levels might have dampened the effects of A+ and T+ in

these subjects. Similarly, complement C3 and Factor B were found to be unaffected in all three measurements suggesting that Amyloid and tau do not influence these specific complement factors. The effect observed in C3 may be diluted since an activated C3 only exists in its hydrolyzed forms (C3a and C3b) which may not be detected in these assays (Dunkelberger and Song, 2010). It is no surprise that effects on factor B were also diminished since factor B binds C3b for its activation.

In terms of influential co-variates, this study has identified key biomarkers that are impacted by age, sex, BMI, and *APOE4* status. It has been reproducibly shown that MIF, C1q, YKL-40, TREM2, and TNFR2 were significantly impacted by age in all three measurements for the A/T scheme. Multiple studies have already identified MIF, YKL40, and C1q as being strongly correlated with age (Brosseron et al., 2022; Llorens et al., 2017; van der Ende et al., 2022; S. Zhang et al., 2019). Only C1q was influenced by sex in all three measurements, suggesting that sex may not be the strongest co-variate determining the A/T effects. Similarly, Factor B and CRP were the only proteins influenced by BMI in all three measurements, which is in line with the fact that peripheral CRP is elevated in obese people (Aronson et al., 2004). This peripheral effect may be leaking into the CSF for the A/T scheme. Surprisingly, *APOE4* was not able to reproduce its effects on the A/T scheme in the three measurements. The presence of the *APOE4* allele increases the risk of Alzheimer's Disease by four-fold, yet this was not translated into the inflammatory biomarkers stratified with the A/T scheme (Blanchard et al., 2022). This *APOE4* variant impacts the $A\beta_{42}$ clearance through apolipoprotein E which worsens disease progression (Blanchard et al., 2022). $A\beta_{42}$-mediated effects on inflammatory biomarkers are minimal when compared with tau pathology in the A/T scheme. Hence, APOE4 may not affect these markers in the A/T scheme of these subjects.

4.1.3. Pathological tau in the CSF directly influence the inflammatory biomarkers present in cognitively categorized dementia subjects

It was inferred that tau pathology is more influential in driving inflammatory biomarkers in dementia subjects. To check if its influence could surpass the cognitive staging of dementia subjects, Diagnosis/T scheme analysis was performed. The measurements made from the two independent cohorts containing a diverse set of groups DELCODE Olink® (CN, SCD; MCI, DAT) and F.ACE manual (SCD, MCI) were analyzed. It is

important to note that the results from the F.ACE cohort were predominantly driven by MCI subjects (SCD (N=59); MCI (N=723)). Like the A/T scheme, Complement C3, Factor B, and CRP were unaffected in the Diagnosis/T scheme. The same reasoning that was proposed in the A/T scheme for these proteins that C3 and Factor B are inter-dependent and that hydrolyzed and active forms of C3 and Factor B may not be detected.

One of the key findings was that there was a significant reduction in the levels of Tyro3 in DAT T- subjects when compared with CN T- subjects in the DELCODE cohort **(Figure 9 A, Table 19)**. This suggests that a reduction in CSF Tyro3 levels is an indication of dementia progression. Since the F.ACE cohort contains SCD and MCI subjects, this finding could not be validated in an independent cohort. Yet, this data from DELCODE is in line with the recent findings where subjects with higher levels of Tyro3 performed cognitively better and showed reduced cortical atrophy (Brosseron et al., 2022). This approach further confirms an indication of neuroprotection in subjects with high Tyro3 in CSF.

Other key findings include the significant difference in the levels of major biomarkers within a clinical group depending on the tau pathology. This proposes that the cognitive staging of subjects is not entirely related to the inflammatory biomarkers in CSF, except Tyro3 which was discussed above. Healthy control subjects with pathological tau levels showed higher biomarkers than SCD, MCI, or DAT subjects without tau. Hence, tau pathology plays a pivotal role in determining the composition of the biomarkers in CSF, irrespective of the cognitive staging.

The influence of co-variates age, sex, BMI, and *APOE4* status with the Diagnosis/T scheme was similar to that observed in the A/T scheme. This was also expected since the dominant factor that determines these effects was tau in both schemes. In general, these results reiterate that inflammatory biomarkers in the CSF could be roughly claimed as a correlate of the total tau in the CSF.

4.2. Beneficial effects of Tyro3 overexpression *in vitro*

4.2.1. Tyro3 facilitates amyloid phagocytosis in macrophages

It is widely known that TAM receptors are involved in phagocytosis by macrophages (Lemke and Rothlin, 2008; Myers et al., 2019). A recent study showed that microglia use MerTK and Axl to engulf amyloid plaques in a mouse model of AD (Huang et al., 2021). The expression of Tyro3 in microglia is not as prominent as compared to that of its expression in the neurons (Prieto et al., 2000). Hence, phagocytosis of $A\beta_{42}$ plaques by microglia could be predominantly executed via the Axl receptor. This study paints a different picture regarding the role of $A\beta_{42}$ phagocytosis by TAM receptors. Here, it was shown that Tyro3 overexpression, but not Axl, increased phagocytosis of $A\beta_{42}$ in THP-1 macrophages. Altering the microglial expression to higher Tyro3 on its surface may promote increased $A\beta_{42}$ phagocytosis as compared to the existing Axl/MerTK – mediated $A\beta_{42}$ phagocytosis. However, this claim is certainly bound to limitations because these results were obtained in a monocyte cell line and future studies could be designed in human microglia.

Another key observation was that pre-treatment with tau impaired the phagocytosis of macrophages. Tau may initiate the TLR signaling that occupies most of the cellular machinery to process the inflammatory cascade. Hence, subsequent exposure to the amyloid beta fibrils impaired the ability of the cell to channel its resources for actin rearrangement and phagocytosis. Studies have shown that tau could both prime and activate the NLRP3 inflammasome which leads to the release of IL-1β during the tau pre-treatment before $A\beta_{42}$ exposure (Jiang et al., 2021, Meng et al., 2022). Hence, the dampening effect of $A\beta_{42}$ phagocytosis in the WT cells may be due to the chronic release of IL-1β after tau exposure. Interestingly, this dampening of phagocytosis with tau was absent in the Tyro3OE cells. Since, Tyro3OE cells release lower levels of IL-1β, $A\beta_{42}$ phagocytosis may not be impaired in these cells with tau exposure. Although, the best way to confirm the role of IL-1β in phagocytosis would be to block IL-1 receptors using anakinra and investigate if the phagocytic ability is restored in the WT cells. This paves the way for future studies to understand and dissect the exact mechanisms that mutually regulate neuroinflammation and $A\beta_{42}$ phagocytosis in AD brains.

4.2.2. Tyro3 overexpression regulates the NLRP3 inflammasome byproducts

A novel phenomenon was identified *in vitro*: Tyro3 overexpression was able to reduce NLRP3 inflammasome byproducts in two activation models. To simulate the AD patient's micro-environment, the tau + $A\beta_{42}$ model was used. Here, tau alone can activate the NLRP3 inflammasome leading to the release of IL-1β in the WT controls THP-1 cells. Partly, this might be due to the PMA-induced differentiation of the THP-1 cells into macrophages, which involve the activation of NF-κB thereby priming the cells. In particular, there was an increase in caspase-1 cleavage in the tau-treated cells suggesting that the NLRP3 inflammasome machinery is successfully assembled leading to the proteolytic cleavage of caspase-1. However, the effect of $A\beta_{42}$ fibrils was minimal in these cells. This is unsurprising since it is already established that tau is a predominant factor driving inflammation in clinical datasets. The tau-induced inflammasome activation may saturate the capacity of the THP-1 cells to generate pro-IL-1β level, which remained unchanged with $A\beta_{42}$ exposure. Similarly, fibril preparation is a crucial step to generate fibrils that bind to TLR2/4. Subtle differences in the aggregation environment including the pH of the buffer and temperature might impact the size and potency of the generated $A\beta_{42}$ fibrils.

Caution must be emphasized on the involvement of recombinant bacteria in the generation of tau protein. The inflammatory effects of tau stimulation might be enhanced due to the presence of trace amounts of endotoxins. Although the protocol for tau production ensures the removal of bacterial content, it is impossible to completely eradicate all the endotoxins in the preparation. As a side note, even the commercially available recombinant tau protein involves bacteria in its production phase. Hence, despite the limitations concerning the endotoxin levels, it was logical to generate recombinant Tau that costs five times less than when bought commercially. The striking finding in this study was that even the strongest inflammasome activators were ineffective in inducing IL-1β release by the Tyro3OE cells.

Both tau and Nigericin showed strong NLRP3 inflammasome activation in the WT control cells. Reduced precursor of IL-1β in the Tyro3OE cells prevents it from generating excessive IL-1β even with the influence of strong NLRP3 activators. Although, these

effects were only observed in the Tyro3OE cells not in AxlOE **(Figure 11, 12).** This is a novel finding since, previous studies have only shown the protective effects of Axl and MerTK in the brain, but not Tyro3 (Huang et al., 2021). This is primarily due to the pre-existing notion that Tyro3 is not expressed in the microglia and may not contribute to the regulation of neuroinflammation (Prieto et al., 2000). Here, it is proposed that microglia with an increases Tyro3 expression might be efficient in phagocytosing $A\beta_{42}$ and regulating NLRP3 inflammasome-mediated IL-1β release.

Another interesting phenomenon was that only IL-1β protein is regulated in the Tyro3OE. All other pro-inflammatory components like NLRP3, Caspase-1, and ASC in the Tyro3OE were not regulated **(Figure 11, 12).** However, this was not reflected in their mRNA levels, since there was a downregulation of NLRP3 and ASC in the Tyro3OE cells. Additionally, IL-1β, IL-18, NLRP3, and ASC were not only downregulated in Tyro3OE cells but also the AxlOE cells **(Figure 13)**. This contradicts the western blots that showed similar or increased profiles in AxlOE when compared with the WT cells. It is speculated that there might be a strong post-transcriptional and post-translational regulation of these proteins in the TAM overexpressing cells which accounts for these discrepancies in the mRNA and protein content of inflammatory molecules.

Particularly, there was a reduction in NF-κB translocation into the nucleus of the Tyro3OE cells. This justifies the reduction of IL-1β, IL-18, NLRP3, and ASC mRNA levels in the Tyro3OE cells, but fails to support the AxlOE results. NF-κB translocation into the nucleus is a time-sensitive phenomenon and the exact effects for AxlOE may be lost due to a different translocation speed. Nevertheless, it is also emphasized here that all the cells were transformed into macrophages using PMA, which is a well-known NF-κB activator that mediates this transformation. Hence, there may be a residual impact of PMA on the NF-κB levels in these cells which could account for these discrepancies. The residual PMA effect may also answer the unaltered NLRP3 and ASC protein levels of Tyro3OE in the western blots **(Figure 11, 12).**

Since, the effect of NF-κB is not completely reliant on the cells, instead influenced by PMA exposure, it is speculated that other mechanisms are involved in the regulation of IL-1β in the Tyro3OE cells. Specifically, it is suggested that the promoter regions of IL-1β in these cells might be modified to accommodate the transcription factor for binding and initiation

of transcription. It is known that other cytokines like IL-37 and TGF-β play a role in regulating IL-1β through its promoter region (Brosseron et al., 2022; Rudloff et al., 2020). However, there was no significant difference in the levels of IL-37 and TGF-β in Tyro3OE thereby ruling out these possibilities (Data not presented). Hence, the effects of NF-κB and other known anti-inflammatory may not be the primary factor causing these effects in Tyro3OE.

4.2.3. Excessive STAT1 phosphorylation mediates IL-1β suppression

A striking finding in this thesis was that STAT1 was strongly phosphorylated in the Tyro3OE cells **(Figure 14)**. The reason for this phosphorylation in the TAM overexpressing cells might be due to the TAM overexpression in itself. It is known that any tyrosine kinase receptor is activated by the ligand followed by dimerization. It brings the receptors in proximity leading to the phosphorylation of the adjacent receptors. Phosphorylated tyrosine domains in the activated TAM receptors attract and phosphorylate proteins with Src homology-2 (SH2) and phospho-tyrosine binding (PTB) domains (Wium et al., 2018). One of the key proteins is JAK1/2 kinase which phosphorylates STAT1 for pro-inflammatory signaling. Hence, there is an inherent STAT1 phosphorylation in the TAM-overexpressing cells without the TAM ligands Gas-6 and Protein-S exposure.

These results are in line with the existing literature which claims STAT1 as a regulator of inflammation. In particular, STAT1 binds and induces the interferon-sensitive responsive element (ISRE) leading to antiviral mechanisms that are both pro- and anti-inflammatory (Schneider et al., 2014). However, in the case of TAM-overexpression, STAT1 might be more anti-inflammatory. Chronically activated TAM signaling ensures prolonged p-STAT1 levels in the cytosol. Excessive STAT1 induces the expression of SOCS1, which is an endogenous inhibitor of STAT1 phosphorylation (Bai et al., 2018). Incidentally, we. have also identified the upregulation of SOCS1 in TAM overexpressing cells, possibly enhanced through the excessive levels of p-STAT1 in the cytosol. It is speculated that excessive STAT1 triggers a critical threshold beyond which the SOCS1 expression is activated leading to the suppression of inflammation. This system is part of the negative feedback loop to regulate the pro-inflammatory downstream signaling cascade.

This study reveals that SOCS1 is increased in Tyro3OE, but the link between SOCS1 and IL-1β transcription was not explored in detail. The exact mechanism through which SOCS1 reduces inflammation is unknown, although, several anti-inflammatory functions were proposed. SOCS1 is an endogenous inhibitor of unphosphorylated JAK1 to regulate the downstream STAT1 phosphorylation in the cells (Ha et al., 2016). In addition, it promotes the ubiquitination and proteasomal degradation of transcription enhancers like CCAAT/enhancer-binding proteins (C/EBPs) (Ha et al., 2016). PAMPs/DAMPs-mediated transcription of IL-1β requires these enhancers for the upstream inducible sequence (UIS) to interact with the promoter sequence. For instance, C/EBPs-bound NF-κB, CREB, and ATF1 increased the transcription of IL-1β which strongly suggests the role of C/EBPs in modulating the concentration of IL-1β protein expression (Bent et al., 2018; Listman et al., 2008). It is inferred that Tyro3OE increased STAT1 phosphorylation which induced SOCS1 expression to regulate STAT1. SOCS1 in turn degrades C/EBPs, which are essential for IL-1β transcription leading to the marked decline of IL-1β in the Tyro3OE cells. Although, the involvement of C/EBPs must be verified through SOCS1 inhibitors or C/EBP overexpression that restores IL-1β levels in Tyro3OE.

Interestingly, reducing the p-STAT1 levels through the JAK1 inhibitor Ruxolitinib was able to restore the levels of IL-1β in Tyro3OE cells **(Figure 15)**. This narrows down the IL-1β suppression effect in Tyro3OE to a JAK1-mediated pathway. If SOCS1 is instrumental in dampening IL-1β transcription, Rux treatment must have diminished SOCS1 in Tyro3OE owing to the increased IL-1β. Yet, no significant effect was observed of SOCS1 with Rux treatment suggesting that SOCS1 may not be the only player in regulating IL-1β transcription. Further studies are needed to dissect the exact pathway involved in the regulation of Il-1β transcription under the Tyro3 overexpression system.

Not only in the *in vitro* THP-1 TAM overexpression model, but TAM ligand activation has also been shown to reduce IL-1β in vivo (Jung et al., 2022). Injection of a Gas-6-$A\beta_{42}$ targeting fusion protein in AD mice decreased the Amyloid plaques. TAM activation increased STAT1 phosphorylation and reduced IL-1β in microglia which contributed to this protective effect in AD mice, which completely validates the key *in vitro* findings of this thesis in a preclinical model of AD (Jung et al., 2022).

Taken together, Tyro3 overexpression in THP-1 cells is a model for chronically TAM-activated macrophages, that exhibit higher p-STAT1 in the cytosol. This might lead to a SOCS1-mediated depletion of C/EBPs thereby dampening the transcription of IL-1β in macrophages. In fact, this could be a novel pathway to regulate the IL-1β release in not just NLRP3, but also AIM2, NLRP1, NLRC4 and other inflammasome activation. In this way, Tyro3OE cells show anti-inflammatory effects that may be employed for devising therapeutic strategies against Alzheimer's disease.

4.2.4. TAM signaling pathway offers protection in the tau-positive subjects with high Tyro3

The neuron experiment with the inflammasome-activated conditioned medium was not the best model to study beneficial effects since the neurons themselves were activated due to the residual Nigericin present in the conditioned medium. Few studies have documented the presence of NLRP3 in neurons, which might account for this effect that was observed (von Herrmann et al., 2018; P. Zhang et al., 2016). Hence, a direct link between the TAM receptor system and neuroprotection was not established *in vitro.* However, having access to the extensive Olink® panel for the DELCODE cohort, other TAM components apart from Tyro3 and Axl were checked if they were impacted in the A/T and Diagnosis/T schemes.

As hypothesized, there was a significant impact on the levels of MerTK, and the TAM ligands Gas-6 and Protein-S in the tau-positive subjects **(Table 21, 21)**. These results resemble the preliminary results that were obtained for Tyro3 and Axl. In addition, subjects with higher levels of Tyro3 and Axl showed neuroprotection leading to a reduced cognitive decline and increased cortical mass (Brosseron et al., 2022). These results combined, it is proposed that subjects with higher levels of Tyro3 might also have higher TAM ligands Gas6 and Protein-S that activates the TAM signaling. This might lead to p-STAT1-SOCS1- C/EBP-mediated dampening of IL-1β transcription resulting in diminished neuroinflammation in these subjects. Although, this claim is with several limitations since these results were derived from a cell line that is of non-CNS origin. Similarly, a causal effect between the TAM ligands and receptors was not explored. Nevertheless, this study emphasizes a novel role of the TAM receptors, particularly Tyro3 in downregulating IL-1β, which could be employed as an anti-inflammatory strategy to target several

neurodegenerative diseases. Specifically, Tyro3-activating ligands or nanobodies might pave the way for a new field in therapeutic strategies against AD.

4.3. Conclusion

In this thesis, we have validated the upregulation of selected biomarkers in the CSF of T+ subjects, irrespective of their amyloid and diagnosis. The results from this thesis were partially published where it was shown that subjects with higher levels of the soluble receptors Tyro3 and Axl in their CSF showed a reduced cortical atrophy with age and increased cognitive protection (Brosseron et al., 2022). This suggests that higher levels of Tyro3 and Axl in the CSF could be a protective factor for the disease progression. In this thesis, a novel anti-inflammatory role of Tyro3 receptor was identified. Here, overexpression of Tyro3 in human macrophages resulted in diminished IL-1β release upon Tau and $A\beta_{42}$-induced inflammasome activation. This effect was due to an increased phosphorylation of the transcription factor STAT1 in Tyro3-overexpressing cells that impair IL-1β transcription, irrespective of the pro-inflammatory transcription factor NF-κB. Furthermore, Tyro3 ligands Gas6 and Protein S were upregulated in the tau positive (T+) subjects suggesting an active TAM signalling cascade in these individuals. It is proposed that subjects with increased Tyro3 and Axl have higher levels of the ligands Gas6 and Protein S that activate the TAM signalling **(Figure 18)**. This leads to STAT1 phosphorylation-mediated reduction in the IL-1β levels in these subjects, owing to the cognitive protection that was observed. Currently, monoclonal antibodies against $A\beta_{42}$ and NLPR3 inhibitors are proposed as therapeutic strategies against AD to ameliorate $A\beta_{42}$ plaque burden and IL-1β-mediated neuroinflammation. Tyro3 overexpressing or activating strategies might enhance $A\beta_{42}$ phagocytosis and reduce not only NLRP3-mediated, but also other inflammasome-mediated IL-1β release and neuroinflammation in the brains. Future studies are required to test the therapeutic function of Tyro3 overexpression *in vivo* in AD mouse models.

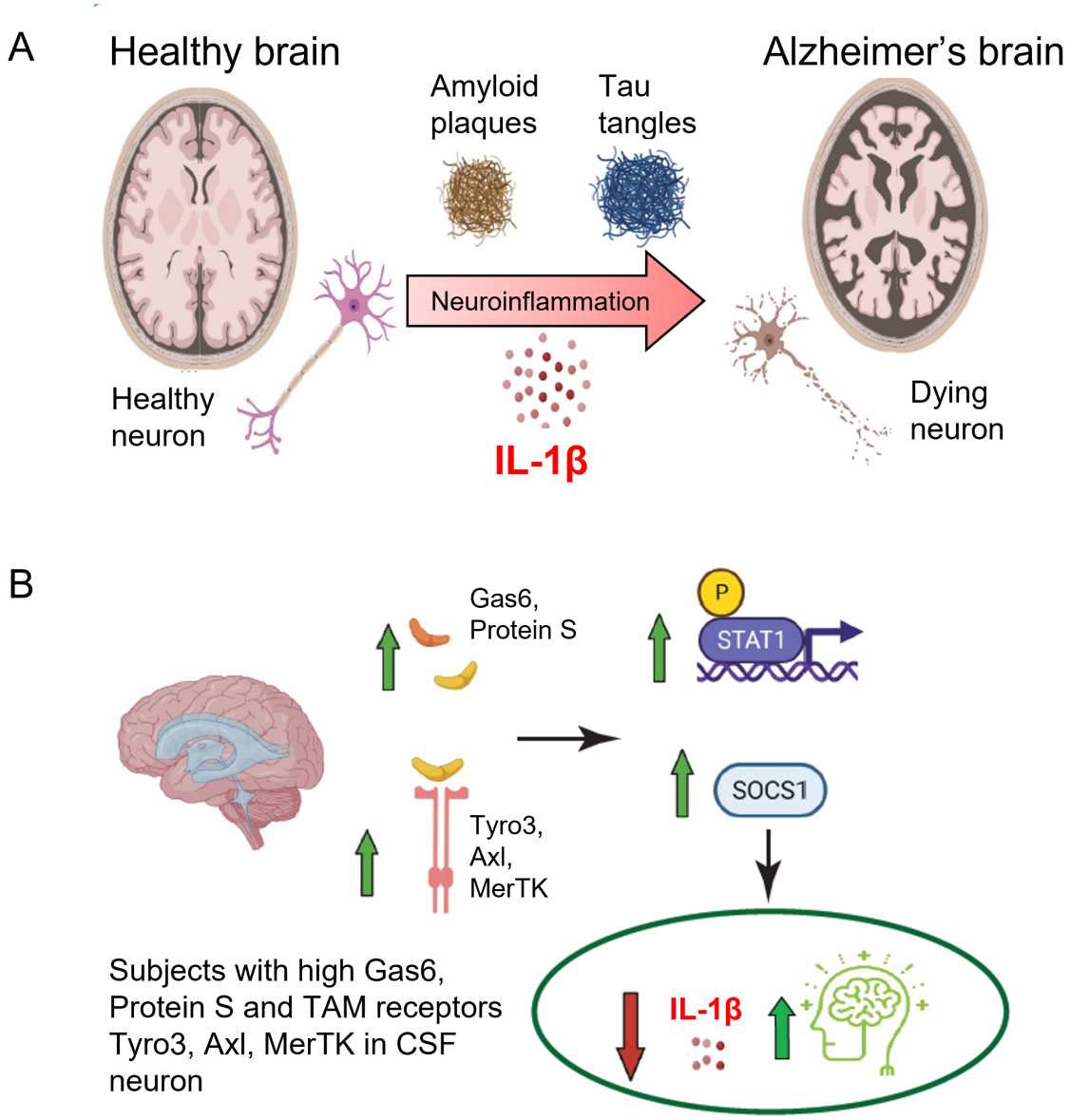

Figure 18: Increased Tyro3 in CSF indicates protective mechanism in Alzheimer's disease (AD)
(A) In AD brain, amyloid plaques and tau tangles activate the NLRP3 inflammasome leading to the production of IL-1β leading to neuroinflammation. This results in the death of neurons, cortical atrophy, and cognitive impairment in AD. **(B)** Subjects with high Gas6 and Protein S ligands and TAM receptors Tyro3, Axl, and MerTK in their CSF might have increased TAM signalling leading to STAT1-SOCS1- mediated reduction of IL-1β in the brains. This might protect the brain from neuroinflammation and subsequently reduce the cognitive deficits. This could be the underlying mechanism behind the protective effects that were observed in high CSF Tyro3 individuals (Brosseron et al., 2022).

5. Abstract

Inflammation plays a key role in Alzheimer's disease (AD) progression. Microglia in the AD brain are exposed to pathological amyloid β ($A\beta_{42}$) and tau peptide aggregates, resulting in the NLRP3 inflammasome activation within these cells. Activated microglia release pro-inflammatory cytokines IL-1β and IL-18 resulting in the acceleration of neuronal death in AD brain. Besides AD, an aging brain also underlies neuroinflammation due to senescent cells that generate reactive oxygen species and NLPR3 activation. Hence, aging and AD brain have inflammatory byproducts and factors within the brain parenchyma, which might be detected in the cerebrospinal fluid (CSF) as a biomarker. In this study, the primary aim was to measure the pre-selected 15 biomarkers namely YKL40, MIF, Tyro3, Axl, TREM2, VCAM1, ICAM1, TNFR1, TNFR2, C1q, C3, C4, Factor B, Factor H, and CRP in the CSF from different European dementia cohorts (DELCODE and F.ACE). It was shown that most of the biomarkers were significantly increased in the tau positive (T+) subjects, implying that tau pathology plays a crucial role in inflammatory byproduct release in the CSF in two independent cohorts. Applying these results in the PREADAPT data analysis workflow showed that subjects with elevated soluble TAM receptors, Tyro3 and Axl, in their CSF had larger cortical volume and were more stable in cognition at follow-up (Brosseron et. al., 2022).

In order to determine the functional relevance of our clinical findings, an *in vitro* setup was used that consists of three human monocytic leukemia (THP-1) cell lines: Wild-type (Control), Tyro3-overexpressing (Tyro3OE), and Axl-overexpressing (AxlOE). Since TAM receptors facilitate phagocytosis, it was hypothesized that their overexpression in THP-1 cells might enhance tau and $A\beta_{42}$ phagocytosis. There was a significant increase in $A\beta_{42}$ phagocytosis by the Tyro3OE cells. Also, $A\beta_{42}$ phagocytosis was reduced when the control THP-1 cells were pre-treated with tau, but this effect was absent in Tyro3OE cells. It was speculated that this beneficial role of Tyro3OE might be supported by an anti-inflammatory effect. The NLRP3 inflammasome activity was examined in these cells using two models: the AD microenvironment model (tau + $A\beta_{42}$) and classical NLRP3 inflammasome model (LPS + Nigericin). A significant reduction in IL-1β release was found in the Tyro3OE when compared with control THP-1 cells. This was supported by a reduced IL-1β mRNA expression in Tyro3OE cells. STAT1 phosphorylation in Tyro3OE

cells was significantly increased in western blot analysis, which when inhibited by JAK1/2 inhibitor Ruxolitinib, partially restored IL-1β release in Tyro3OE. Hence, STAT1 phosphorylation is key for Tyro3OE-mediated immunosuppression in models of AD. Lastly, novel biomarkers MerTK receptor and the TAM ligands Gas6, Protein S were also found to be elevated in the tau positive subjects in the DELCODE cohort. In summary, these results suggest that subjects with elevated TAM receptors, also have increased ligands Gas6 and Protein S which activate the TAM signalling in their brain. Activated TAM signalling leads to the Tyro3-STAT1-IL-1β pathway that was described in order to suppress inflammation and enhance $A\beta_{42}$ phagocytosis. It is proposed that subjects with increased Tyro3 in their CSF might employ this mechanism that confers subtle protection against AD. Results from this thesis show promising effects for Tyro3 overexpression and activation that could disarm inflammatory cells against not only NLPR3, but also AIM2, NLRP1, and NLRC4-mediated IL-1β release and henceforth ameliorate pathogenesis in AD. Future studies are required to verify these beneficial functions of Tyro3 in AD mouse models.

6. List of figures

7. List of Tables

8. References

Aehnlich P, Powell RM, Peeters MJW, Rahbech A, Thor Straten P. TAM Receptor Inhibition-Implications for Cancer and the Immune System. Cancers (Basel) 2021; 13(6): 1195

Andronie-Cioara FL, Ardelean AI, Nistor-Cseppento CD, Jurcau A, Jurcau MC, Pascalau N, Marcu F. Molecular Mechanisms of Neuroinflammation in Aging and Alzheimer's Disease Progression. Int J Mol Sci 2023; 24(3): 1869

Aronson D, Bartha P, Zinder O, Kerner A, Markiewicz W, Avizohar O, Brook GJ, Levy Y. Obesity is the major determinant of elevated C-reactive protein in subjects with the metabolic syndrome. Int J Obes 2004; 28(5): 674–679

Bai J, Wu L, Chen X, Wang L, Li Q, Zhang Y, Wu J, Cai G, Chen X. Suppressor of Cytokine Signaling-1/STAT1 Regulates Renal Inflammation in Mesangial Proliferative Glomerulonephritis Models. Front Immunol 2018; 9

Barbier P, Zejneli O, Martinho M, Lasorsa A, Belle V, Smet-Nocca C, Tsvetkov PO, Devred F, Landrieu I. Role of Tau as a Microtubule-Associated Protein: Structural and Functional Aspects. Front Aging Neurosci 2019; 11: 204

Bent R, Moll L, Grabbe S, Bros M. Interleukin-1 Beta-A Friend or Foe in Malignancies? Int J Mol Sci 2018; 19(8): 2155

Blanchard JW, Akay LA, Davila-Velderrain J, von Maydell D, Mathys H, Davidson SM, Effenberger A, Chen C-Y, Maner-Smith K, Hajjar I, Ortlund EA, Bula M, Agbas E, Ng A, Jiang X, Kahn M, Blanco-Duque C, Lavoie N, Liu L, … Tsai L-H. APOE4 impairs myelination via cholesterol dysregulation in oligodendrocytes. Nature 2022; 611(7937): 769–779

Boada M, Tárraga L, Hernández I, Valero S, Alegret M, Ruiz A, Lopez OL, Becker JT. Design of a comprehensive Alzheimer's disease clinic and research center in Spain to meet critical patient and family needs. Alzheimer's & Dementia 2014; 10(3): 409–415

Boucher D, Monteleone M, Coll RC, Chen KW, Ross CM, Teo JL, Gomez GA, Holley CL, Bierschenk D, Stacey KJ, Yap AS, Bezbradica JS, Schroder K. Caspase-1 self-cleavage

is an intrinsic mechanism to terminate inflammasome activity. J Exp Med 2018; 215(3): 827–840

Brosseron F, Kolbe C-C, Santarelli F, Carvalho S, Antonell A, Castro-Gomez S, Tacik P, Namasivayam AA, Mangone G, Schneider R, Latz E, Wüllner U, Svenningsson P, Sánchez-Valle R, Molinuevo JL, Corvol J-C, Heneka MT, group on behalf of the A study. Multicenter Alzheimer's and Parkinson's disease immune biomarker verification study. Alzheimer's & Dementia 2020; 16(2): 292–304

Brosseron F, Maass A, Kleineidam L, Ravichandran KA, González PG, McManus RM, Ising C, Santarelli F, Kolbe C-C, Häsler LM, Wolfsgruber S, Marquié M, Boada M, Orellana A, de Rojas I, Röske S, Peters O, Cosma N-C, Cetindag A, … Heneka MT. Soluble TAM receptors sAXL and sTyro3 predict structural and functional protection in Alzheimer's disease. Neuron 2022; 110(6): 1009-1022

Brosseron F, Traschütz A, Widmann CN, Kummer MP, Tacik P, Santarelli F, Jessen F, Heneka MT. Characterization and clinical use of inflammatory cerebrospinal fluid protein markers in Alzheimer's disease. Alzheimers Res Ther 2018; 10(1): 25

Broz P, Dixit VM. Inflammasomes: mechanism of assembly, regulation and signalling. Nat Rev Immunol 2016; 16(7): 407–420

Busche MA, Hyman BT. Synergy between amyloid-β and tau in Alzheimer's disease. Nat Neurosci 2020; 23(10): 1183–1193

Caberoy NB, Alvarado G, Bigcas J-L, Li W. Galectin-3 is a new MerTK-specific eat-me signal. J Cell Physiol 2012; 227(2): 401–407

Caberoy NB, Zhou Y, Li W. Tubby and tubby-like protein 1 are new MerTK ligands for phagocytosis. EMBO J 2010; 29(23): 3898–3910

Chatterjee M, Özdemir S, Kunadt M, Koel-Simmelink M, Boiten W, Piepkorn L, Pham T V., Chiasserini D, Piersma SR, Knol JC, Möbius W, Mollenhauer B, van der Flier WM, Jimenez CR, Teunissen CE, Jahn O, Schneider A. C1q is increased in cerebrospinal fluid-derived extracellular vesicles in Alzheimer's disease: A multi-cohort proteomics and immuno-assay validation study. Alzheimer's & Dementia 2023

Chen W, Abud EA, Yeung ST, Lakatos A, Nassi T, Wang J, Blum D, Buée L, Poon WW, Blurton-Jones M. Increased tauopathy drives microglia-mediated clearance of beta-amyloid. Acta Neuropathol Commun 2016; 4(1): 63

Couturier J, Stancu I-C, Schakman O, Pierrot N, Huaux F, Kienlen-Campard P, Dewachter I, Octave J-N. Activation of phagocytic activity in astrocytes by reduced expression of the inflammasome component ASC and its implication in a mouse model of Alzheimer disease. J Neuroinflammation 2016; 13 20

Davis BK, Wen H, Ting JP-Y. The inflammasome NLRs in immunity, inflammation, and associated diseases. Annu Rev Immunol 2011; 29 707–735

De S, Wirthensohn DC, Flagmeier P, Hughes C, Aprile FA, Ruggeri FS, Whiten DR, Emin D, Xia Z, Varela JA, Sormanni P, Kundel F, Knowles TPJ, Dobson CM, Bryant C, Vendruscolo M, Klenerman D. Different soluble aggregates of Aβ42 can give rise to cellular toxicity through different mechanisms. Nat Commun 2019; 10(1): 1541

Duncan JA, Bergstralh DT, Wang Y, Willingham SB, Ye Z, Zimmermann AG, Ting JP-Y. Cryopyrin/NALP3 binds ATP/dATP, is an ATPase, and requires ATP binding to mediate inflammatory signaling. Proceedings of the National Academy of Sciences 2007; 104(19): 8041 – 8046

Dunkelberger JR, Song W-C. Complement and its role in innate and adaptive immune responses. Cell Res 2010; 20(1): 34–50

Felsky D, Roostaei T, Nho K, Risacher SL, Bradshaw EM, Petyuk V, Schneider JA, Saykin A, Bennett DA, De Jager PL. Neuropathological correlates and genetic architecture of microglial activation in elderly human brain. Nat Commun 2019; 10(1): 409

Flem-Karlsen K, Nyakas M, Farstad IN, McFadden E, Wernhoff P, Jacobsen KD, Fløother VA, Mælandsmo GM. Soluble AXL as a marker of disease progression and survival in melanoma. PLoS One 2020; 15(1): e0227187

Flores J, Fillion M-L, LeBlanc AC. Caspase-1 inhibition improves cognition without significantly altering amyloid and inflammation in aged Alzheimer disease mice. Cell Death Dis 2022; 13(10): 864

Gustavsson A, Norton N, Fast T, Frölich L, Georges J, Holzapfel D, Kirabali T, Krolak-Salmon P, Rossini PM, Ferretti MT, Lanman L, Chadha AS, van der Flier WM. Global estimates on the number of persons across the Alzheimer's disease continuum. Alzheimer's & Dementia 2023; 19(2): 658–670

Ha Y-J, Choi YS, Kang EH, Shin K, Kim TK, Song YW, Lee YJ. SOCS1 suppresses IL-1β-induced C/EBPβ expression via transcriptional regulation in human chondrocytes. Exp Mol Med 2016; 48(6): e241–e241

Halle A, Hornung V, Petzold GC, Stewart CR, Monks BG, Reinheckel T, Fitzgerald KA, Latz E, Moore KJ, Golenbock DT. The NALP3 inflammasome is involved in the innate immune response to amyloid-β. Nat Immunol 2008; 9(8): 857–865

Han C, Sheng Y, Wang J, Zhou X, Li W, Zhang C, Guo L, Yang Y. Double-negative T cells mediate M1 polarization of microglial cells via TNF-α-NLRP3 to aggravate neuroinflammation and cognitive impairment in Alzheimer's disease mice. J Cell Physiol 2022; 237(10): 3860–3871

Hanslik KL, Ulland TK. The Role of Microglia and the Nlrp3 Inflammasome in Alzheimer's Disease. Front Neurol 2020; 11

Haseeb M, Javaid N, Yasmeen F, Jeong U, Han JH, Yoon J, Seo JY, Heo JK, Shin HC, Kim MS, Kim W, Choi S. Novel Small-Molecule Inhibitor of NLRP3 Inflammasome Reverses Cognitive Impairment in an Alzheimer's Disease Model. ACS Chem Neurosci 2022; 13(6): 818–833

He X, Xu J, Li G, Li M, Li L, Pei Z, Zhang L, Hu X. NLRP3-dependent microglial training impaired the clearance of amyloid-beta and aggravated the cognitive decline in Alzheimer's disease. Cell Death Dis 2020; 11(10): 849

He Y, Zeng MY, Yang D, Motro B, Núñez G. NEK7 is an essential mediator of NLRP3 activation downstream of potassium efflux. Nature 2016; 530(7590): 354–357

Heneka MT, Carson MJ, El Khoury J, Landreth GE, Brosseron F, Feinstein DL, Jacobs AH, Wyss-Coray T, Vitorica J, Ransohoff RM, Herrup K, Frautschy SA, Finsen B, Brown

GC, Verkhratsky A, Yamanaka K, Koistinaho J, Latz E, Halle A, … Kummer MP. Neuroinflammation in Alzheimer's disease. Lancet Neurol 2015; 14(4): 388–405

Heneka MT, Kummer MP, Stutz A, Delekate A, Schwartz S, Vieira-Saecker A, Griep A, Axt D, Remus A, Tzeng T-C, Gelpi E, Halle A, Korte M, Latz E, Golenbock DT. NLRP3 is activated in Alzheimer's disease and contributes to pathology in APP/PS1 mice. Nature 2013; 493(7434): 674–678

Herrera-Rivero M, Santarelli F, Brosseron F, Kummer MP, Heneka MT. Dysregulation of TLR5 and TAM Ligands in the Alzheimer's Brain as Contributors to Disease Progression. Mol Neurobiol 2019; 56(9): 6539–6550

Hoffman HM, Mueller JL, Broide DH, Wanderer AA, Kolodner RD. Mutation of a new gene encoding a putative pyrin-like protein causes familial cold autoinflammatory syndrome and Muckle-Wells syndrome. Nat Genet 2001; 29(3): 301–305

Holstein E, Binder M, Mikulits W. Dynamics of Axl Receptor Shedding in Hepatocellular Carcinoma and Its Implication for Theranostics. Int J Mol Sci 2018; 19(12): 4111

Hu WT, Ozturk T, Kollhoff A, Wharton W, Christina Howell J, Weiner M, Aisen P, Petersen R, Jack CR, Jagust W, Trojanowki JQ, Toga AW, Beckett L, Green RC, Saykin AJ, Morris J, Perrin RJ, Shaw LM, Kachaturian Z, … Chiang G. Higher CSF sTNFR1-related proteins associate with better prognosis in very early Alzheimer's disease. Nat Commun 2021; 12(1): 4001

Huang Y, Happonen KE, Burrola PG, O'Connor C, Hah N, Huang L, Nimmerjahn A, Lemke G. Microglia use TAM receptors to detect and engulf amyloid β plaques. Nat Immunol 2021; 22(5): 586–594

Hughes C, Choi ML, Yi J-H, Kim S-C, Drews A, George-Hyslop P St., Bryant C, Gandhi S, Cho K, Klenerman D. Beta amyloid aggregates induce sensitised TLR4 signalling causing long-term potentiation deficit and rat neuronal cell death. Commun Biol 2020; 3(1): 79

Ising C, Venegas C, Zhang S, Scheiblich H, Schmidt S V, Vieira-Saecker A, Schwartz S, Albasset S, McManus RM, Tejera D, Griep A, Santarelli F, Brosseron F, Opitz S, Stunden

J, Merten M, Kayed R, Golenbock DT, Blum D, … Heneka MT. NLRP3 inflammasome activation drives tau pathology. Nature 2019; 575(7784): 669–673

Jessen F, Spottke A, Boecker H, Brosseron F, Buerger K, Catak C, Fliessbach K, Franke C, Fuentes M, Heneka MT, Janowitz D, Kilimann I, Laske C, Menne F, Nestor P, Peters O, Priller J, Pross V, Ramirez A, … Düzel E. Design and first baseline data of the DZNE multicenter observational study on predementia Alzheimer's disease (DELCODE). Alzheimers Res Ther 2018; 10(1): 15

Jiang S, Maphis NM, Binder J, Chisholm D, Weston L, Duran W, Peterson C, Zimmerman A, Mandell MA, Jett SD, Bigio E, Geula C, Mellios N, Weick JP, Rosenberg GA, Latz E, Heneka MT, Bhaskar K. Proteopathic tau primes and activates interleukin-1β via myeloid-cell-specific MyD88- and NLRP3-ASC-inflammasome pathway. Cell Rep 2021; 36(12): 109720

Jung H, Lee SY, Lim S, Choi HR, Choi Y, Kim M, Kim S, Lee Y, Han KH, Chung WS, Kim CH. Anti-inflammatory clearance of amyloid-β by a chimeric Gas6 fusion protein. Nature Medicine 2022 28:9 2022; 28(9): 1802–1812

Kasikara C, Kumar S, Kimani S, Tsou W-I, Geng K, Davra V, Sriram G, Devoe C, Nguyen K-QN, Antes A, Krantz A, Rymarczyk G, Wilczynski A, Empig C, Freimark B, Gray M, Schlunegger K, Hutchins J, Kotenko S V., Birge RB. Phosphatidylserine Sensing by TAM Receptors Regulates AKT-Dependent Chemoresistance and PD-L1 Expression. Molecular Cancer Research 2017; 15(6): 753–764

Knopman DS, Amieva H, Petersen RC, Chételat G, Holtzman DM, Hyman BT, Nixon RA, Jones DT. Alzheimer disease. Nat Rev Dis Primers 2021; 7(1): 33

Latz E, Xiao TS, Stutz A. Activation and regulation of the inflammasomes. Nat Rev Immunol 2013; 13(6): 397–411

Lemke G, Rothlin C V. Immunobiology of the TAM receptors. Nat Rev Immunol 2008; 8(5): 327–336

Leng F, Edison P. Neuroinflammation and microglial activation in Alzheimer disease: where do we go from here? Nat Rev Neurol 2021; 17(3): 157–172

Lew ED, Oh J, Burrola PG, Lax I, Zagórska A, Través PG, Schlessinger J, Lemke G. Differential TAM receptor–ligand–phospholipid interactions delimit differential TAM bioactivities. Elife 2014; 3

Listman JA, Race JE, Walker-Kopp N, Unlu S, Auron PE. Inhibition of IL-1β transcription by peptides derived from the hCMV IE2 transactivator. Mol Immunol 2008; 45(9): 2667–2677

Llorens F, Thüne K, Tahir W, Kanata E, Diaz-Lucena D, Xanthopoulos K, Kovatsi E, Pleschka C, Garcia-Esparcia P, Schmitz M, Ozbay D, Correia S, Correia Â, Milosevic I, Andréoletti O, Fernández-Borges N, Vorberg IM, Glatzel M, Sklaviadis T, … Zerr I. YKL-40 in the brain and cerebrospinal fluid of neurodegenerative dementias. Mol Neurodegener 2017; 12(1): 83

Lonnemann N, Hosseini S, Marchetti C, Skouras DB, Stefanoni D, D'Alessandro A, Dinarello CA, Korte M. The NLRP3 inflammasome inhibitor OLT1177 rescues cognitive impairment in a mouse model of Alzheimer's disease. Proceedings of the National Academy of Sciences 2020; 117(50): 32145 – 32154

Manfioletti G, Brancolini C, Avanzi G, Schneider C. The Protein Encoded by a Growth Arrest-Specific Gene (Gas6) Is a New Member of the Vitamin K-Dependent Proteins Related to Protein S, a Negative Coregulator in the Blood Coagulation Cascade. Mol Cell Biol 1993; 13(8): 4976–4985

Martinon F, Burns K, Tschopp J. The Inflammasome: A Molecular Platform Triggering Activation of Inflammatory Caspases and Processing of proIL-β. Mol Cell 2002; 10(2): 417–426

Meng JX, Zhang Y, Saman D, Haider AM, De S, Sang JC, Brown K, Jiang K, Humphrey J, Julian L, Hidari E, Lee SF, Balmus G, Floto RA, Bryant CE, Benesch JLP, Ye Y, Klenerman D. Hyperphosphorylated tau self-assembles into amorphous aggregates eliciting TLR4-dependent responses. Nat Commun 2022; 13(1): 2692

Moonen S, Koper MJ, Van Schoor E, Schaeverbeke JM, Vandenberghe R, von Arnim CAF, Tousseyn T, De Strooper B, Thal DR. Pyroptosis in Alzheimer's disease: cell type-

specific activation in microglia, astrocytes and neurons. Acta Neuropathol 2023; 145(2): 175–195

Müller UC, Deller T, Korte M. Not just amyloid: physiological functions of the amyloid precursor protein family. Nat Rev Neurosci 2017; 18(5): 281–298

Muñoz-Planillo R, Kuffa P, Martínez-Colón G, Smith BL, Rajendiran TM, Núñez G. K+ efflux is the common trigger of NLRP3 inflammasome activation by bacterial toxins and particulate matter. Immunity 2013; 38(6): 1142–1153

Myers K V, Amend SR, Pienta KJ. Targeting Tyro3, Axl and MerTK (TAM receptors): implications for macrophages in the tumor microenvironment. Mol Cancer 2019; 18(1): 94

Nakanishi H. Microglial cathepsin B as a key driver of inflammatory brain diseases and brain aging. Neural Regen Res 2020; 15(1): 25–29

Oroz J, Barrera-Vilarmau S, Alfonso C, Rivas G, de Alba E. ASC Pyrin Domain Self-associates and Binds NLRP3 Protein Using Equivalent Binding Interfaces*. Journal of Biological Chemistry 2016; 291(37): 19487–19501

Parajuli B, Sonobe Y, Horiuchi H, Takeuchi H, Mizuno T, Suzumura A. Oligomeric amyloid β induces IL-1β processing via production of ROS: implication in Alzheimer's disease. Cell Death Dis 2013; 4(12): e975–e975

Prieto AL , Weber JL , Lai C . Expression of the receptor protein-tyrosine kinases Tyro-3, Axl, and Mer in the developing rat central nervous system. J Comp Neurol. 2000; 425 (2): 295–314

Rauchmann B-S, Sadlon A, Perneczky R. Soluble TREM2 and Inflammatory Proteins in Alzheimer's Disease Cerebrospinal Fluid. Journal of Alzheimer's Disease 2020; 73(4): 1615–1626

Ravichandran KA, Heneka MT. Inflammasome activation in neurodegenerative diseases. Essays Biochem 2021; 65(7): 885–904

Ravichandran KA, Heneka MT. Inflammasome and neurodegenerative diseases. Elsevier Inflammasome Biology 2023: 291–326

Reed-Geaghan EG, Savage JC, Hise AG, Landreth GE. CD14 and Toll-Like Receptors 2 and 4 Are Required for Fibrillar Aβ-Stimulated Microglial Activation. The Journal of Neuroscience 2009; 29(38): 11982 – 11992

Rudloff I, Ung HK, Dowling JK, Mansell A, D'Andrea L, Ellisdon AM, Whisstock JC, Berger PJ, Nold-Petry CA, Nold MF. Parsing the IL-37-Mediated Suppression of Inflammasome Function. Cells 2020; 9(1): 178

Rui W, Xiao H, Fan Y, Ma Z, Xiao M, Li S, Shi J. Systemic inflammasome activation and pyroptosis associate with the progression of amnestic mild cognitive impairment and Alzheimer's disease. J Neuroinflammation 2021; 18(1): 280

Santa Cruz Garcia AB, Schnur KP, Malik AB, Mo GCH. Gasdermin D pores are dynamically regulated by local phosphoinositide circuitry. Nat Commun 2022; 13(1): 52

Schneider WM, Chevillotte MD, Rice CM. Interferon-Stimulated Genes: A Complex Web of Host Defenses. Annu Rev Immunol 2014; 32(1): 513–545

Schroder K, Tschopp J. The inflammasomes. Cell 2010; 140(6): 821–832

Shi H, Wang Y, Li X, Zhan X, Tang M, Fina M, Su L, Pratt D, Bu CH, Hildebrand S, Lyon S, Scott L, Quan J, Sun Q, Russell J, Arnett S, Jurek P, Chen D, Kravchenko V V, … Beutler B. NLRP3 activation and mitosis are mutually exclusive events coordinated by NEK7, a new inflammasome component. Nat Immunol 2016; 17(3): 250–258

Stancu IC, Lodder C, Botella Lucena P, Vanherle S, Gutiérrez de Ravé M, Terwel D, Bottelbergs A, Dewachter I. The NLRP3 inflammasome modulates tau pathology and neurodegeneration in a tauopathy model. Glia 2022; 70(6): 1117–1132

Suárez-Calvet M, Kleinberger G, Araque Caballero MÁ, Brendel M, Rominger A, Alcolea D, Fortea J, Lleó A, Blesa R, Gispert JD, Sánchez-Valle R, Antonell A, Rami L, Molinuevo JL, Brosseron F, Traschütz A, Heneka MT, Struyfs H, Engelborghs S, … Haass C. sTREM 2 cerebrospinal fluid levels are a potential biomarker for microglia activity in early-stage Alzheimer's disease and associate with neuronal injury markers . EMBO Mol Med 2016; 8(5): 466–476

Swanson K V, Deng M, Ting JP-Y. The NLRP3 inflammasome: molecular activation and regulation to therapeutics. Nat Rev Immunol 2019; 19(8): 477–489

Tahara K, Kim H-D, Jin J-J, Maxwell JA, Li L, Fukuchi K -i. Role of toll-like receptor signalling in A uptake and clearance. Brain 2006; 129(11): 3006–3019

Tan M-S, Liu Y, Hu H, Tan C-C, Tan L. Inhibition of caspase-1 ameliorates tauopathy and rescues cognitive impairment in SAMP8 mice. Metab Brain Dis 2022; 37(4): 1197–1205

van der Ende EL, Heller C, Sogorb-Esteve A, Swift IJ, McFall D, Peakman G, Bouzigues A, Poos JM, Jiskoot LC, Panman JL, Papma JM, Meeter LH, Dopper EGP, Bocchetta M, Todd E, Cash D, Graff C, Synofzik M, Moreno F, … (GENFI) the GFDI. Elevated CSF and plasma complement proteins in genetic frontotemporal dementia: results from the GENFI study. J Neuroinflammation 2022; 19(1): 217

Vasunilashorn SM, Ngo LH, Dillon ST, Fong TG, Carlyle BC, Kivisäkk P, Trombetta BA, Vlassakov K V, Kunze LJ, Arnold SE, Xie Z, Inouye SK, Libermann TA, Marcantonio ER, Inouye SK, Arnold S, Dickerson B, Fong T, Jones R, … Group RS. Plasma and cerebrospinal fluid inflammation and the blood-brain barrier in older surgical patients: the Role of Inflammation after Surgery for Elders (RISE) study. J Neuroinflammation 2021; 18(1): 103

Venegas C, Kumar S, Franklin BS, Dierkes T, Brinkschulte R, Tejera D, Vieira-Saecker A, Schwartz S, Santarelli F, Kummer MP, Griep A, Gelpi E, Beilharz M, Riedel D, Golenbock DT, Geyer M, Walter J, Latz E, Heneka MT. Microglia-derived ASC specks cross-seed amyloid-β in Alzheimer’s disease. Nature 2017; 552(7685): 355–361

von Herrmann KM, Salas LA, Martinez EM, Young AL, Howard JM, Feldman MS, Christensen BC, Wilkins OM, Lee SL, Hickey WF, Havrda MC. NLRP3 expression in mesencephalic neurons and characterization of a rare NLRP3 polymorphism associated with decreased risk of Parkinson’s disease. NPJ Parkinsons Dis 2018; 4: 24.

Wang X, Chi J, Huang D, Ding L, Zhao X, Jiang L, Yu Y, Gao F. α-synuclein promotes progression of Parkinson’s disease by upregulating autophagy signaling pathway to activate NLRP3 inflammasome. Exp Ther Med 2020; 19(2): 931–938

Wium M, Paccez J, Zerbini L. The Dual Role of TAM Receptors in Autoimmune Diseases and Cancer: An Overview. Cells 2018; 7(10): 166

Won J-H, Park S, Hong S, Son S, Yu J-W. Rotenone-induced Impairment of Mitochondrial Electron Transport Chain Confers a Selective Priming Signal for NLRP3 Inflammasome Activation*. Journal of Biological Chemistry 2015; 290(45): 27425–27437

Xia Y, Prokop S, Gorion K-MM, Kim JD, Sorrentino ZA, Bell BM, Manaois AN, Chakrabarty P, Davies P, Giasson BI. Tau Ser208 phosphorylation promotes aggregation and reveals neuropathologic diversity in Alzheimer's disease and other tauopathies. Acta Neuropathol Commun 2020; 8(1): 88

Xiao L, Magupalli VG, Wu H. Cryo-EM structures of the active NLRP3 inflammasome disc. Nature 2023; 613(7944): 595–600

Xing Y, Yao X, Li H, Xue G, Guo Q, Yang G, An L, Zhang Y, Meng G. Cutting Edge: TRAF6 Mediates TLR/IL-1R Signaling-Induced Nontranscriptional Priming of the NLRP3 Inflammasome. J Immunol 2017; 199(5): 1561–1566

Yin J, Zhao F, Chojnacki JE, Fulp J, Klein WL, Zhang S, Zhu X. NLRP3 Inflammasome Inhibitor Ameliorates Amyloid Pathology in a Mouse Model of Alzheimer's Disease. Mol Neurobiol 2018; 55(3): 1977–1987

Zhang P, Shao X-Y, Qi G-J, Chen Q, Bu L-L, Chen L-J, Shi J, Ming J, Tian B. Cdk5-Dependent Activation of Neuronal Inflammasomes in Parkinson's Disease. Movement Disorders 2016; 31(3): 366–376

Zhang S, Zhao J, Zhang Y, Zhang Y, Cai F, Wang L, Song W. Upregulation of MIF as a defense mechanism and a biomarker of Alzheimer's disease. Alzheimers Res Ther 2019; 11(1): 54

Zhang Y, Rong H, Zhang F-X, Wu K, Mu L, Meng J, Xiao B, Zamponi GW, Shi Y. A Membrane Potential- and Calpain-Dependent Reversal of Caspase-1 Inhibition Regulates Canonical NLRP3 Inflammasome. Cell Rep 2018; 24(9): 2356-2369

Zhao Y, Tan S-W, Huang Z-Z, Shan F-B, Li P, Ning Y-L, Ye S-Y, Zhao Z-A, Du H, Xiong R-P, Yang N, Peng Y, Chen X, Zhou Y-G. NLRP3 Inflammasome-Dependent Increases

in High Mobility Group Box 1 Involved in the Cognitive Dysfunction Caused by Tau-Overexpression. Front Aging Neurosci 2021; 13

Zheng D, Liwinski T, Elinav E. Inflammasome activation and regulation: toward a better understanding of complex mechanisms. Cell Discov 2020; 6(1): 36

9. Acknowledgements

Words cannot describe my gratitude towards everyone who were significant in supporting me throughout this thesis. First of all, I would like to thank Prof. Dr. Michael Heneka for giving me the opportunity to work with his excellent team and for providing constant encouragement, support, and constructive criticism throughout my PhD. I would also like to thank Prof. Dr. Michael Pankratz, Prof. Dr. Jochen Walter, and Prof. Dr. Mathias Geyer for being part of my doctoral committee and monitoring my progress in the PhD.

My PhD is impossible without the guidance of Dr. Frederic Brosseron, who mentored me for this PhD thesis. Thanks to his perfect planning and execution of the clinical project that allowed me to gather data in such a short span of time. His calmness under stressful situations and his meticulous efforts towards science were some of the notable values that I take with me for life.

An equally important support was provided by Dr. Róisín McManus. Although, I was not her official PhD student, she accepted to guide me for the *in vitro* study due to her generous nature. She has patiently taught me and allowed me to grow independent in formulating my own ideas. She was more than a mentor; she was my friend, critic, and a great scientist to learn from.

Special thanks go to Dr. Christina Ising for helping me with the Tau preparation and experiments which added more value to our findings. She was kind-hearted and has shared her extensive knowledge on the field which further boosted my PhD research.

The enormous amount of clinical sample processing for nearly 1000 samples was not possible without the help of the extremely skilled technician, Mr. Francesco Santarelli. His curiosity-driven approach to work is something to learn from and I really enjoyed our lively discussion about science and life.

I would like to thank Prof. Dr. Alfredo Ramirez, Prof. Dr. Augustin Ruiz for supporting me in the PREADAPT project and Dr. Pamela Martina-Adami for teaching me to write R scripts.

I am indebted to Dr. Susanne Schmidt and Dr. Simone Görgens from the institute of innate immunity and Prof. Dr. Eicke Latz for providing the crucial cell culture models. I would also like to thank them for their suggestions and feedback to improve my study.

Additionally, I thank Dr. Hannah Scheiblich for her support with setting up neuronal experiments and sharing scientific knowledge for efficient results. Similarly, I would like to thank Ms. Paula Martorell, Mr. Tao Li, Mr. Frederik Eikens, Dr. Sergio-Castro Gomez for their moral support that helped me feel comfortable during my stay in the lab.

I owe my mental sanity to the support I received from my friends Mr. Deniz Karabag, Ms. Bolanle Fatimat Olabiyi, Dr. rer. nat. Dilek Mercan, Ms. Hira Akmal. They were all significant in making my PhD a painless and enjoyable one!

Special thanks once again for Dr. Frederic Brosseron, Dr. Roisin McManus, Dr. Christina Ising, and Dr. Joanna Komorrowska-Muller for reading my thesis and giving valuable suggestions to make it better.

And finally, I got to this point of my life because of the constant support and encouragement from my family. They were crucial in helping me revive from my down-points, make hard life choices, and celebrate with me any minimal accomplishment. Me and my achievements are a win to our community and particularly my family: my mother Kalaiselvi, my father Ravichandran, my sister Priyadharshini, and last but not the least, my Abi, who all showed unconditional support during my PhD.

10. List of Publications

1. **Ravichandran KA**, Heneka MT. Inflammasome activation in neurodegenerative diseases. Essays Biochem. 2021 Dec 22;65(7):885-904. doi: 10.1042/EBC20210021. PMID: 34846519.
2. Brosseron F, Maass A, Kleineidam L, **Ravichandran KA**, González PG, McManus RM, Ising C, Santarelli F, Kolbe CC, Häsler LM, Wolfsgruber S, Marquié M, Boada M, Orellana A, de Rojas I, Röske S, Peters O, Cosma NC, Cetindag A, Wang X, Priller J, Spruth EJ, Altenstein S, Schneider A, Fliessbach K, Wiltfang J, Schott BH, Bürger K, Janowitz D, Dichgans M, Perneczky R, Rauchmann BS, Teipel S, Kilimann I, Goerss D, Laske C, Munk MH, Düzel E, Yakupov R, Dobisch L, Metzger CD, Glanz W, Ewers M, Dechent P, Haynes JD, Scheffler K, Roy N, Rostamzadeh A, Teunissen CE, Marchant NL, Spottke A, Jucker M, Latz E, Wagner M, Mengel D, Synofzik M, Jessen F, Ramirez A, Ruiz A, Heneka MT; DELCODE study group. Soluble TAM receptors sAXL and sTyro3 predict structural and functional protection in Alzheimer's disease. Neuron. 2022 Mar 16;110(6):1009-1022.e4. doi: 10.1016/j.neuron.2021.12.016. PMID: 34995486.

3. Brosseron F, Maass A, Kleineidam L, **Ravichandran KA**, Kolbe CC, Wolfsgruber S, Santarelli F, Häsler LM, McManus R, Ising C, Röske S, Peters O, Cosma NC, Schneider LS, Wang X, Priller J, Spruth EJ, Altenstein S, Schneider A, Fliessbach K, Wiltfang J, Schott BH, Buerger K, Janowitz D, Dichgans M, Perneczky R, Rauchmann BS, Teipel S, Kilimann I, Görß D, Laske C, Munk MH, Düzel E, Yakupow R, Dobisch L, Metzger CD, Glanz W, Ewers M, Dechent P, Haynes JD, Scheffler K, Roy N, Rostamzadeh A, Spottke A, Ramirez A, Mengel D, Synofzik M, Jucker M, Latz E, Jessen F, Wagner M, Heneka MT; DELCODE study group. Serum IL-6, sAXL, and YKL-40 as systemic correlates of reduced brain structure and function in Alzheimer's disease: results from the DELCODE study. Alzheimers Res Ther. 2023 Jan 12;15(1):13. doi: 10.1186/s13195-022-01118-0. PMID: 36631909.

4. Braatz C, Komes MP, **Ravichandran KA**, de Fragas MG, Griep A, Schwartz S, McManus RM, Heneka MT. NLRP3-directed antisense oligonucleotides reduce

microglial immunoactivities in vitro. J Neurochem. 2023 Feb 17. doi: 10.1111/jnc.15778. PMID: 36799439.

5. **Ravichandran KA** & Heneka MT. Inflammasomes and neurodegenerative diseases. Inflammasome Biology 2023: 291 - 326.

6. **Ravichandran KA** & Heneka MT. Inflammasomes in neurological disease – mechanisms and therapeutic potential. Nat Rev Neurol 20, 67–83 (2024). https://doi.org/10.1038/s41582-023-00915-x. PMID: 38195712

Conferences

1. **Ravichandran KA,** McManus RM, Brosseron F, Ising, C, Görgen S, Schmidt SV, Santarelli F, Martino-Adami P, Cano A, García Gonzalez P, Marqué M, Boada M, Orellan A, de Rojas I, Ramirez A, Ruiz Laza A, Latz E, Heneka MT (2021). Firing without bullets in Alzheimer's disease: The potential of Tyoro3 receptors. Cluster Science Days, Bonn, Germany. (Selected Talk)
2. **Ravichandran KA,** Brosseron F, McManus RM, Ising, C, Görgens S, Schmidt SV, Santarelli F, Martino-Adami P, Cano A, García Gonzalez P, Peters OH, Priller J, Schneider A, Fliessbach K, Wiltfang J, Jessen F, Düzel E, Bürger K, Perneczky R, Teipel S, Laske C, Spottke A, Wagner M, Ruiz Laza A, Ramirez A, Latz E, Heneka MT. Increased TAM receptors in CSF: Protection against Alzheimer's disease? (2022). Society for Neuroscience (SFN) 2022, San Diego, United States of America. (Poster presentation)